AERODYNAMIC LOADING ON THE BLADES OF A HELICOPTER ROTOR IN STEADY TRANSLATIONAL FLIGHT

AERODYNAMIC LOADING ON THE BLADES OF A HELICOPTER ROTOR IN STEADY TRANSLATIONAL FLIGHT

by

SURESH K. GUPTA, M.E.

A Thesis

Submitted to the Faculty of Graduate Studies

in Partial Fulfilment of the Requirements

for the Degree

Doctor of Philosophy

McMaster University

September 1972

ACKNOWLEDGEMENTS

The author expresses his sincere appreciation for the guidance and assistance given by Professor J.H.T. Wade of McMaster University. Help given by Mr. V. K. Jha of the Department of Electrical Engineering in using the optimisation subroutine "GRADMIN" is gratefully acknowledged.

DOCTOR OF PHILOSOPHY (1972)
(Mechanical Engineering)

McMASTER UNIVERSITY
Hamilton, Ontario

TITLE: Aerodynamic Loading on the Blades of a Helicopter Rotor in Steady Translational Flight

AUTHOR: Suresh K. Gupta, B.E. (Delhi University)
M.E. (Indian Institute of Science)
M.Eng. (McMaster University)

SUPERVISOR: Professor J.H.T. Wade

NUMBER OF PAGES: v, 129

SCOPE AND CONTENTS:

One of the most important and complex problems in the design of helicopters is the estimation of aerodynamic loading on the blades of the lifting rotor in steady translational flight. It is essential for the designer to have a fairly good knowledge of this blade loading, especially its harmonic content. Such information is necessary in order to successfully evaluate and solve problems such as: the structural integrity of the rotor hub and the blades; the oscillatory forces in the control systems; and the vibrations of the entire aircraft. Many analytical and computational methods have been developed to predict the blade loading in forward flight. These methods invariably demand a knowledge of the rotor wake details and the sectional airfoil data. The trailing wake of the rotor is extremely complex and it has not yet been possible to include in the analysis all its details. Nor has it yet been possible to obtain the sectional airfoil data in a manner which is compatible with the

unsteady three dimensional and compressible aerodynamic environment of the rotating blades. We are presenting, in this thesis, a new technique to calculate the blade loading in forward flight. The proposed technique does not require a knowledge of the rotor wake or the sectional airfoil data. We have used our proposed model to calculate the blade loading for a full scale NASA model rotor at an advance ratio of 0.29. Our results compare very well with those obtained experimentally by NASA. In fact, our results show better agreement with the experimental results than those obtained by using currently available computational models for rotor blade loading in forward flight.

"Probably one of the most difficult problems facing the designer of rotary wing aircraft at the present time is that of determining the blade aerodynamic loading, and in particular the oscillatory content of this loading. The magnitude of the problem may be appreciated if it is realized that an equivalent ignorance on the part of fixed wing designer would mean that no method existed for predicting the spanwise load and distribution on a conventional wing and consequently no rational design of the wing structure could be effected until the aircraft has flown, and extensive test data obtained which would permit substantiation of the structure for all anticipated flight conditions."

R. H. Millar (1962)

TABLE OF CONTENTS

SECTION 1

INTRODUCTION

INTRODUCTION

The design of helicopter rotors is a difficult and complicated job. Numerous complex problems must be solved. Satisfactory solutions have not yet been developed for many of these problems. Evaluation of aerodynamic loading on rotating blades in forward flight is one such problem. It has been long recognized that this aerodynamic loading contains large harmonic content. Even the higher order harmonics are of significant magnitude. There are three primary reasons. These are:

(a) The blades encounter a periodic inflow as they rotate.

(b) A continuously distorting and complex wake below and behind the rotor results in periodic and varying induced velocities in the plane of the rotor. Evaluation of these induced velocities is, perhaps, the most difficult problem in rotor analysis.

(c) The blades usually are very flexible. They twist and bend along the span as they rotate. The exact distortion of the blades is a function of aerodynamic excitation and their dynamic and structural characteristics. The aerodynamic loading, in turn, is influenced by the motion and distortion of the blades. Clearly, the blade aerodynamic loading problem, therefore, requires the solution of the complete aeroelastic problem. We, however, concentrated our efforts in solving the aerodynamic part of this aeroelastic problem. We realized it to be the more basic and the more difficult part of the complete problem. The blade

motions and the distortions are thus assumed to be given quantities.

It is essential that we have a fairly good knowledge of the aerodynamic loading on rotating blades in forward flight, especially its harmonic content. Such knowledge is vital in properly evaluating the dynamic stresses and fatigue lives of the rotor blades, the hub assembly, and the control system components. In addition to the all important problem of rotor blade structural integrity, control of vibrations is another major problem in helicopter design. Vibrations have constantly plagued the helicopters. A flexible rotor coupled to a flexible fuselage through a hub assembly constitutes a dynamic system of extreme complexity. The harmonic airloads within the rotor act as excitation input to the system. In order that we successfully combat the problem of vibrations in helicopters, we would need a detailed knowledge of the harmonic content of the blade aerodynamic loading. Dynamic instability of the rotating blades is another problem which confronts the designer. In addition to the classical fixed wing flutter, we can encounter many other modes of divergent blade motions. Here again, we need a detailed knowledge of the blade aerodynamic loading.

Considerable effort has now been devoted to obtain solutions for the blade loading problem in forward flight. All the analytical work done so far, however, assumes the validity of the 'Independence Principle', i.e. a sufficiently thin section

of the rotating blade can be considered as a two dimensional airfoil, operating independently from the rest of the blade. Knowing the relative airflow and the sectional aerodynamic data, we can thus calculate the aerodynamic loading for this section of the blade. Two major problems are encountered. The aerodynamic environment of the rotating blade is unsteady, three dimensional and compressible. The use of steady two dimensional airfoil data, is, therefore, questionable. Modifications, empirical or semi empirical, are then devised to improve upon this data. Such an approach, hopefully, makes it possible to include in the analysis the first order effects of the complex aerodynamics prevailing at the blade. Complete and satisfactory solutions are however, still lacking. The second problem is that of knowing the relative airflow at the blade section. Even if the blade motions are assumed to be known, we still need a detailed knowledge of the induced velocity distribution over the rotor disc. Induced velocity is a complex and non-linear function of time and space coordinates. It is a function of the trailing rotor wake, which in turn is the product of varying blade loading. The geometry of the wake and the vorticity distribution in it are extremly difficult to include into the theoretical analysis. It has not yet been done. The exact wake is idealized by simple theoretical models which can be handled in calculations. The modern high speed computing

machines of today have made it possible to account for much more details of the wake than has been possible in the past. It is clear that there is a lot of empiricism and simplification involved in the existing analytical solutions for the blade loading problem.

In this thesis, we are suggesting a new technique to calculate the aerodynamic loading on the rotating blades of a helicopter rotor in steady translation flight. The earlier mentioned 'Principle of Independence' is not used. The rotating blade is not considered as a series of thin, two dimensional strips. It is treated as one complete unit. It is no longer necessary to know the relative airflow at the blade sections. Nor is it necessary to know the proper sectional aerodynamic data. Considerations of wake do not enter into the analysis. We therefore do not have to perform calculations for rotor wake details. Chordwise loading distribution of loading over the blade, moreover, poses no additional problems. The technique makes use, as its basis, of the lifting surface theories, which have been developed for the fixed wing analysis. To our knowledge, this is the first time this technique has been used. We have, therefore, restricted ourselves to a rather simple rotor model. Every mathematical model constitutes a compromise between the complexity of the live configuration it is to describe, and the requirement that the computations be manageable. Assumptions

have been made not only for the purpose of simplifying the model, but also to limit the computer time used to a reasonable value. It has not been our aim to solve a particular problem and obtain results as accurately as possible. Rather, we have aimed to develop the technique, obtain reasonable results, and isolate problems which should be solved in future work.

SECTION 2

ROTOR BLADE AERODYNAMIC LOADING - A REVIEW

2. ROTOR BLADE AERODYNAMIC LOADING - A REVIEW

Rotor blade aerodynamic loading in steady translation flight is obtained by assuming that each thin strip of the blade acts as an independent two dimensional airfoil. Knowing the relative wind in the plane of the airfoil, we can obtain the aerodynamic loading using airfoil sectional data. The component of flow along the blade span is ignored. The two dimensional sectional data obtained in a wind tunnel is mostly used, as such or with suitable modifications. The relative airflow at the blade section has three components: (a) free stream flow, which is known; (b) the velocity induced by the rotor wake and the bound vorticity of other blades. (The component normal to the rotor disc is most significant. We will refer to this component as the induced velocity); and (c) the relative blade motion. For the present discussion, we assume it to be known.

The blade loading problem is, therefore, reduced to that of finding the induced velocity at the rotor blade, and that of obtaining the sectional data which is compatible with the prevailing aerodynamic environment of the blade.

The distribution of time-varying induced velocity over the rotor disc is basically a function of the rotor wake details. Unlike the wake of a fixed wing, the wake of a lifting rotor remains near the disc for a considerable time, strongly influencing the blade loading in a complex and non-linear manner. The

wake is shed as a thin sheet of vorticity from the blade trailing edge. Vorticity is shed normal to the blade trailing edge as a consequence of spanwise variation of circulation over the blade. Vorticity is also shed parallel to the blade trailing edge as a consequence of the temporal variation of circulation around the blade. Each of these vortices vary in time and hence, along the wake. Once shed, the wake convects with local airflow velocity, forming roughly a skewed, non-planar distorted spiral wake below the rotor. The exact configuration of the wake is a function of blade loading. The blade loading, in turn, strongly depends on the wake configuration. Any solution of the blade loading problem thus requires a simultaneous solution for the wake. Considerable difficulties arise in obtaining such a coupled solution. Only recently have such solutions been developed, though still within the framework of certain simplifying assumptions.

SECTION 2.1

The early attempts, say during the nineteen fifties and sixties, solved the problem of rotor blade loading in two independent steps. In step one, the induced velocity over the rotor disc was calculated on the basis of the overall thrust developed by the rotor. The blade loading was then obtained in step two using the induced velocity calculated in step one. With the advent of digital computers, this procedure underwent much development and sophistication. We could thus deal with any arbitrary blade geometry, induced velocity distribution , airfoil data etc. The equations of motion for the blade could also be integrated into the analysis. These procedures have been widely used in the design office for many years. They are still extremely useful for performance calculations, but their use for the solution of the aeroelastic problem is of somewhat limited value. The effects of compressible, unsteady and the three dimensional nature of the flow were included in the analysis by suitably modifying the two dimensional static airfoil data.

Induced Velocity: Froude first obtained a uniform value of induced velocity over the rotor disc for a helicopter in hover or vertical climb, using purely momentum considerations. Glauert (References 1,2) later, extended his formula, though without any theoretical justification, for

forward flight. He proposed that the induced velocity v_i can be given as

$$v_i = \frac{p}{2\rho V},$$

where V is the average flow velocity through the rotor disc, and p is the disc loading. (The meaning of the various symbols used is given in Section 7). In spite of its simplicity, it does give at least a first approximation for the average value of induced velocity over the rotor disc. It has, therefore, been extensively used in design offices for performance calculations. However, it ignores the variation of the induced velocity in space and time, and is therefore, totally inadequate to obtain blade loading. It was soon realised that the skewness of the wake caused the induced velocity to continuously increase towards the downstream side of the rotor disc. Glauert (Reference 2) suggested a linear variation for the induced velocity and proposed,

$$v_i = v_o(1 + Kx \cos\psi)$$

where K is a constant to be determined from flight conditions, x is the non-dimension radius and ψ is the azimuth angle. Various empirical relations were proposed for calculating K, for example, see Reference 3. Coleman and others (Reference 4) calculated the value of K analytically by directly considering the skewness of wake. They obtained the induced velocity along the fore and aft dia of the rotor in closed form in which K was shown to be equal to $\nu/2\lambda_o$. They, however, con-

sidered a very simple model for the rotor and its wake. A lightly loaded disc having an infinite number of blades with a constant circulation was considered. The trailing wake could then be idealised by a series of successive circular rings parallel to the rotor plane and lying along the surface of a skewed elliptical cylinder. Though still greatly restricted in its use to predict realistically the blade loadings, the model did evaluate the effect of the skewness of wake in forward flight. Using basically the same model, Castles and DeLeew (Reference 5) in 1953 calculated numerically the induced velocity at all points in the longitudinal plane of symmetry, and along the lateral axis of the rotor disc. The results were presented in the form of charts, which have been extensively used in design calculations since that time. The results enabled one to calculate the interference effects of one rotor on another rotor, such as occur in tandem and side by side configurations; but it did not take the designer any nearer to the solution of the blade loading problem.

Sectional Airfoil Data: The two dimensional airfoil data obtained in a wind tunnel under steady flow conditions has generally been used in helicopter analysis for years. The use of such data for rotor blade analysis has been under question for some time. The aerodynamic environment of a rotating blade is very complex. The flow is unsteady, compressible and three dimensional. The problem is further complicated by the presence

of retreating blade stall, advancing blade stall, reverse flow, shock formation, etc. Attempts have now been made to evaluate the effect of these factors on the airfoil aerodynamic data. Each factor, however, is considered in isolation. Based on these studies, the airfoil data is then suitably modified to account for the various complexities of the airflow over the rotating blade.

A large amount of work has been published dealing with the behaviour of the two dimensional airfoil in unsteady flow. Most of this is either not comprehensive in nature or deals with a limited range of parameters. Of particular interest to us is the work reported by Rainey in Reference 6, by Ham in Reference 7, by Carta and Ham in Reference 8, and by Liiva in Reference 9. Liiva obtained the data for sectional lift and Pitching Moment versus angle of attack for a two dimensional pitching and plunging model of an NACA 23010 airfoil. Figures 2.1 and 2.2 summarize the results respectively. The data was obtained at full scale Reynolds number and up to a Mach number of 0.6. Consider the results as presented in Figure 2.3 for the case of the pitching airfoil. Below stall, the characteristic elliptic shape is obtained, in accordance with the theory (Reference 10). Unsteady flow seems to have little effect on steady rotor performance below stall. Of particular interest to us is the behaviour at and near stall. The most typical feature is the presence of hysteresis. A substantial increase in the maximum normal force can be observed. This partly explains

the stall delay which has been observed on helicopter rotor blades. The Moment curve (Figure 2.1) shows that for certain angles of attack, the damping can even become negative. Beyond the immediate vicinity of stall, the hysteresis effect persists, though on a reduced scale. The frequency of pitching (and plunging) and the Mach number of flow have appreciable influence on the nature of the hysteresis loops and stall characteristics of the airfoil. A complete description of the pitching and plunging airfoil characteristics is given in Reference 9. An empirical method was suggested in Reference 11 to account for the unsteadiness of the flow. This has resulted in a better evaluation of rotor performance. Figure 2.3, which is taken from Reference 11, clearly demonstrates the improvement obtained in the prediction of rotor performance as a result of including the unsteady flow effects in the analysis.

The rotating blades experience a considerable amount of radial flow in forward flight. Attempts have been made to evaluate the effect of radial flow on the rotor performance and on the blade loadings (References 11,12). Figure 2.4, which is extracted from Reference 12 and is based on the wind tunnel tests for yawed wings as reported in Reference 13, shows the effect of radial flow on the two dimensional sectional lift coefficient. At angles of attack below stall, the effect of radial flow is minimal. For angles of attack at or near stall, the radial flow significantly alters the lift.

characteristics. An increase in the maximum lift can be observed. Considerable stall delay is also present, which further explains the stall delay which has been observed in helicopter rotors. An engineering approximation was suggested in Reference 12 to account for the radial flow effects. The maximum lift coefficient was increased by a factor of $1.0/\cos\Lambda$ for laminar flows, and by a factor of $1.0/\cos^{3/4}\Lambda$ for turbulent flows. These factors resulted in an improved prediction of rotor performance as can be seen in Figure 2.3.

Mach number effects are generally accounted for by suitably increasing the lift curve slope. The problems associated with the transonic and sonic Mach numbers on the advancing blade, however, have not been successfully solved. Some experimental work has been recently done in this area (Reference 14). Another problem which has only recently attracted attention is the behaviour of the airfoil in reversed flow (Reference 15).

SECTION 2.2

The solution for the rotor blade loading problem for a rotor with a finite number of blades was first obtained by Willmer (Reference 16) in 1959. Unlike the previous attempts, he treated the blade loading and the details of the wake in a coupled manner, as it should really be done. The strength of the trailing vortices was made compatible with the blade loading, and a fixed wake geometry was used. The model used, however, was very simple and thus much restricted in its use. Various simplifications adopted in the model are briefly discussed here. The blades were replaced by lifting lines with associated trailing vorticity forming an undistorted spiral wake below the rotor. The problem was treated in a quasi-static sense, making it possible to ignore the shed vorticity in the wake. The geometry of the wake was simplified by a process of 'rectangularisation', i.e., having found the important part of the wake with respect to the position of the blade, the vortex elements are extended to infinity ignoring the curvature of the wake. Thus a stack of infinite vortex sheets was considered. Clearly the model cannot be used to predict higher harmonics in blade loading. The method essentially gives a first approximation for the blade loading. It also ignores advancing blade compressibility, retreating blade stall, radial flow, etc.

The procedure developed by Pizialli (References 17 and 18) seems the most satisfactory method for obtaining blade loadings and more or less represents the current state of art. The represen-

tation of the blade and its wake was quite realistic. Chordwise loading distribution on the blade was also computed. Blade spanwise bending was also accounted for in the analysis. The analysis could be extended to include other elastic deformations of the blade. It thus brings one closer to the solution of the complete problem. Each blade was divided into n spanwise segments, each with a constant but unknown circulation. Blade loading was determined for m azimuth positions. Thus there were n×m unknown circulations to be determined. The blade was moved from one azimuth position to another in a stepwise manner. With each azimuth increment, it deposited in the wake the trailing and shed vorticity - straight vortex filaments of constant circulation. The circulation of a wake vortex filament was calculated as a function of unknown circulations around blade segments. The induced velocity at a blade segment was also, therefore, represented in terms of the unknown circulations around the blade segments. Each vortex filament was given an individual transport velocity at the start, with which it travelled for a specified but arbitrary time. Beyond this, all filaments were made to travel with the same velocity. This grid representation of the wake could be discontinued after a certain specified but arbitrary time. The wake was then continued as tip vortex only. The radial location of the tip vortex was arbitrary to allow for the wake contraction. Figure 2.5 shows the idealised wake of a rotor blade. Even though the geometry of the wake was to be prescribed, a wide variety of wake configurations could be accommodated. The boundary condition was satisfied at the mid chord of each blade segment. It was required that there was no

airflow across the blade section. Unsteady, two dimensional airfoil theory was used for the chordwise circulation distribution. The blade sectional pitching moment could thus also be calculated. A set of linear algebraic equations was obtained, which was solved to give the circulation, and hence the loading distribution on the blade.

It was necessary to use a constant value of the lift curve slope. This was rather an important limitation. It became difficult, for example, to properly account for compressibility, unsteady flow, radial flow, retreating blade stall, etc. The lift curve slope was adjusted to include the effects of compressibility and Reynolds number, though only for first order effects. The retreating blade stall was considered. For angles of attack greater than the stalling angle, the circulation was limited to the stalled value. Effects of unsteady flow or of radial flow at or near stall were not accounted for. In the region of reverse flow, the lift was made negative, and therefore the exact behaviour of the airfoil in reverse flow was not considered. The most serious limitation, however, is the fact that a rigid wake geometry was used. The wake geometry was not calculated within the program but was supplied to the program as an input parameter. The computed load distributions, especially the higher harmonics, are sensitive to the wake details (Reference 18). Each element of the wake convects with the local flow velocity, which has three components: (a) free stream velocity; (b) blade induced velocity; (c) wake induced

or self induced velocity. A theoretical prediction of the wake geometry is thus extremely difficult and has not yet been achieved. The general approach to the problem has so far been to gain as much physical understanding of the wake as possible by flow visualisation studies. The insight thus obtained is then used to idealise the shape of the wake as closely as possible to the real wake. Considerable research effort has thus been devoted to the experimental techniques for wake visualization (Reference 20). It has been clearly demonstrated that the wake vortex sheet leaving the blade quickly rolls itself into tip and root vortices within a few chord lengths. The root vortex quickly dissipates itself, and has little or no effect on the blade loading. The tip vortex, however, is observed to be quite stable, and experiences little or no diffusion due to viscous effects for several rotor revolutions. It has also been demonstrated that the wake contracts as it moves downstream due to self induced effects. This contraction of the wake can have a significant effect on the blade loadings. The phenomenon of blade-vortex interaction has also come under much discussion recently. At low advance ratios, the induced velocity at the upstream side of the rotor disc is very small. Occasionally it may even be upwards. The vorticity sheet leaving the blade would, therefore, remain very near the rotor disc or perhaps move up through it. The successive blades would then be very near the vortex sheet or actually cut through it. If this occurs

then large local distortions in the blade loading can be expected.

An attempt has been made to establish the time varying periodic wake for a lifting rotor using a digital computer. In the method developed by Peter Crimi (Reference 19) each element of the wake was allowed to convect freely under the influence of the blades and the associated wake. The blades were replaced by vortex lines with constant spanwise circulation. The circulation was varied sinusoidally in azimuth. The blade loading was treated as a given quantity and was not allowed to depend on the wake details. The wake consisted of only the tip vortices. Figure 2.6 shows the geometry of the wake for a two bladed rotor obtained using the above model. It is easy to observe that it significantly differs from the observed helical wake, generally assumed. The method was actually developed to obtain the time varying induced velocity in the vicinity of a lifting rotor, so that the aerodynamic forces on auxiliary surfaces such as the fuselage could be calculated. Because of the simplified nature of the blade and wake representation, one cannot expect accurate computation of induced velocity at or near the blades. It is then of little use as such to calculate the blade loadings. An improved model can be obtained by combining the work of Crimi (Reference 19) with that of Pizialli (Reference 18). This, of course, would greatly increase the computational effort.

R. H. Miller (References 21, 22, 23) has paid considerable attention to the harmonic content of the blade aerodynamic loading. An excellent account of the various aerodynamic problems associated with lifting rotors is also given in References 24 and 25.

SECTION 3

THE MATHEMATICAL MODEL

3 THE MATHEMATICAL MODEL

We considered a lifting rotor translating with a steady velocity, U. The oncoming wind was assumed to be deflected by a small amount in passing through the rotor. The perturbation quantities in the flow were, therefore, assumed small as compared to the steady quantities. This allowed us to linearise the fluid motion equations. The problem was treated in a quasi-static sense. The perturbation quantities in the flow, corresponding to a given azimuthal position of rotor blades, were calculated assuming steady flow conditions. Viscous effects were, of course, neglected.

A non-rotating right-handed co-ordinate system, oxyz, was defined, with 'o' at the center of the rotor hub and 'ox' along the flight path. The Continuity and the Momentum equations for the flow were linearised. The linearised flow equations thus obtained were identical to those given in Reference 29. These can be written as,

$$\frac{U}{\rho}\frac{\partial \rho^*}{\partial x} + \frac{\partial u^*}{dx} + \frac{\partial v^*}{\partial y} + \frac{\partial w^*}{\partial z} = 0 \qquad (3\text{-}1a)$$

$$\frac{U\partial u^*}{\partial x} + \frac{1}{\rho}\frac{\partial p^*}{\partial x} = 0 \qquad (3\text{-}1b)$$

$$\frac{U\partial v^*}{\partial x} + \frac{1}{\rho}\frac{\partial p^*}{\partial y} = 0 \qquad (3\text{-}1c)$$

$$\frac{U\partial w^*}{\partial x} + \frac{1}{\rho}\frac{\partial p^*}{\partial z} = 0 \qquad (3\text{-}1d)$$

Differentiating (3-1a) w.r.t x, (3-1b) w.r.t x, (3-1c) w.r.t y and (3-1d) w.r.t z we obtained the following equation.

$$\beta^2\frac{\partial^2 \phi}{\partial x^2} + \frac{\partial^2 \phi}{\partial y^2} + \frac{\partial^2 \phi}{\partial x^2} = 0 \qquad (3\text{-}2)$$

where $\beta^2 = 1-M^2$, and Φ, the acceleration potential was (p^*/ρ). Performing an axis transformation

$$y' = \beta^2 y$$

$$z' = \beta^2 z$$

equation (3-2) was reduced to

$$\frac{\partial^2 \Phi}{\partial x^2} + \frac{\partial^2 \Phi}{\partial^2 y'} + \frac{\partial^2 \Phi}{\partial z'^2} = 0 \quad . \qquad (3-3)$$

Equation (3-3) shows that the acceleration potential satisfies the Laplace equation. A discontinuity surface in this field can be thought of as a sheet of doublets with their axis normal to it. The only such discontinuity surfaces in the Φ-field are the blades of the rotor. Being sufficiently thin, they are replaced by doublet sheets occupying the projected area of the blades on the x-y' plane. If $\Delta\Phi$ is the difference of potential between the lower and upper surface of the blade at any point (x,y'), then the aerodynamic loading $\ell(x,y')$ at this point can be given by an equation of the form

$$\ell(x,y') = (\Delta\Phi)\rho \qquad (3-4)$$

Since Φ is a solution of the Laplace equation in three dimensions, we can write down the equation of the $\Phi(x,y',z')$-field by integrating over the elementary fields of doublets. For a unit doublet at $x = \xi$, $y' = \eta$, $z' = 0$, with its axis in z-direction this elementary field is given as

$$- \frac{1}{4\pi} \frac{\partial}{\partial z'} \frac{1}{[(x-\xi)^2 + (y'-\eta') + z'^2]^{1/2}}$$

We could, therefore, express the acceleration potential as follows.

$$\Phi(x,y',z') = - \frac{1}{4\pi} \frac{\partial}{\partial z'} \iint_S \frac{\Delta\Phi(\xi,\eta')}{[(x-\xi)^2+(y'-\eta')^2+z'^2]^{1/2}} \, d\xi d\eta'$$

or using equation (3-4)

$$= - \frac{1}{4\pi} \frac{1}{\rho} \frac{\partial}{\partial z'} \iint_S \frac{\ell(\xi,\eta')d\xi d\eta'}{[(x-\xi)^2+(y'-\eta')^2+z'^2]^{1/2}} \qquad (3\text{-}5)$$

It is interesting to note that the integration is to be performed only over the surface of the blades. Considerations of the rotor wake do not enter the analysis. Equation (3-1d) and (3-5) were combined to give

$$U \frac{\partial \omega}{\partial x} (x,y',z') = \frac{1}{4\pi\rho} \frac{\partial^2}{\partial z'^2} \iint_S \frac{\ell(\xi,\eta')d\xi d\eta'}{[(x-\xi^2)+(y'-\eta')^2+z'^2]^{1/2}} .$$

Transforming y', z' and η' back to x,z and η coordinates, we obtained

$$U \frac{\partial \omega}{\partial x} (x,y,z) = \frac{1}{4\pi\rho} \frac{\partial^2}{\partial z^2} \iint_S \frac{\ell(\xi,\eta)d\xi d\eta}{[(x-\xi)^2+\beta^2(y-\eta)^2+\beta^2 z^2]^{1/2}} .$$

We were, however, interested in obtaining downwash only for $z = 0$. Thus

$$U \frac{\partial \omega}{\partial x} (x,y,o) = \frac{1}{4\pi\rho} \operatorname*{Lt}_{z\to o} \frac{\partial^2}{\partial z^2} \iint_S \frac{\ell(\xi,\eta)\, d\xi d\eta}{[(x-\xi)^2+\beta^2(y-\eta)^2+\beta^2 z^2]^{1/2}} .$$

or

$$U \frac{\partial \omega}{\partial x}(x,y,o) = \frac{\partial \omega}{\partial t}(x,y,o)$$

$$= \omega_x(x,y,o,t), \quad \text{say}$$

$$= \frac{1}{4\pi\rho} \operatorname*{Lt}_{z \to o} \frac{\partial^2}{\partial z^2} \iint_S \frac{\ell(\xi,\eta,t)\,d\xi d\eta}{[(x-\xi)^2+\beta^2(y-\eta)^2+\beta^2 z^2]^{1/2}} \quad (3\text{-}6)$$

$$= \frac{1}{4\pi\rho} \iint_S \ell(\xi,\eta,t)\ K(x,\xi;y,\eta;z)\,d\xi d\eta$$

where K is the kernel of the integral equations (3-6). Equations (3-6) can be integrated to give downwash ω at any point (x,y,o) on the rotor blade. Thus

$$\omega(x,y,o) = \frac{1}{4\pi\rho} \frac{1}{U} \int_{-\infty}^{x} \omega_x(x,y,o,x_o)\,dx_o$$

or,

$$= \frac{1}{4\pi\rho} \int_o^t \omega_x(x,y,o,t)\,dt. \quad (3\text{-}7)$$

The downwash, ω, is also prescribed on the blades as boundary condition. The loading ℓ is to be calculated using equations (3-6). Equation (3-6) is thus a Fredholm's singular integral equation of the second kind. An analytical solution of this equation is difficult and has not been achieved. A numerical procedure was, therefore, developed to solve this equation. It is presented in the next section.

SECTION 4

THE NUMERICAL SOLUTION

4. THE NUMERICAL SOLUTION

The blade loading was expressed as an arbitrary superposition of elementary loading distributions, thus introducing a certain number of unknown constants. Using equation (3-6) we then evaluated ω_x, the potential, at pre-selected points in the plane of the blade. This was to be done only once, and outside the main program. Moving the blades in small steps, the integral in equation (3-7) was then evaluated numerically to yield the downwash at the selected pivot points. We, therefore, obtained the downwash of certain pre-selected points on the blades, as a function of the unknown loading coefficients. The downwash could, however, be exactly calculated at these points, since there could be no flow through the blade and the orientation of the blade surface to the free stream was known for the given blade geometry and flight conditions. These known values of downwash were used as boundary conditions for the problem. The original integral equation was thus reduced to a set of linear algebraic equations. These were solved numerically to obtain the aerodynamic loading on the rotating blades of the rotor.

4.1 The Aerodynamic Load Distribution on the Blade

Wind tunnel and flight measurements (Reference 30) of the aerodynamic loading distribution on a rotating blade indicate that the chordwise loading distribution is basically of the same form as that obtained on a two dimensional thin airfoil. We, therefore, assumed that the chordwise loading distribution on the rotating blade could be given by the Birnbaum-Glauert series. Having defined $\cos\phi$ as $(1-2x_b/\text{chord})$ and θ as $(2y_b/\text{span})$, we expressed the chordwise loading as follows.

$$\ell(\phi,\theta,\psi) = a_o(\theta,\psi)\cot\phi/2 - \sum_{n_c=1}^{N_c} a_{n_c}(\theta,\psi)\sin n_c\phi. \quad (4\text{-}1)$$

The spanwise distribution of each chordwise loading was assumed to be represented by first N_s terms of a sine series in θ. Thus

$$\ell(\phi,\theta,\psi) = \sum_{n_s=1}^{N_s} a_{o_{ns}}(\psi)\sin(n_s\theta)\cot\phi/2 - \sum_{n_s=1}^{N_s}\sum_{n_c=1}^{N_c} a_{n_c n_s}\sin n_s\theta \sin n_c\phi \quad (4\text{-}2)$$

Each of these $(N_c \times N_s)$ loading distributions was assumed to have N_a harmonics with the angular rotation of the blade. Thus the final loading was given by

$$\ell(\phi,\theta,\psi) = \sum_{n_a=1}^{N_a}\left[\sum_{n_s=1}^{N_s} a_{on_s n_a}\sin n_s\theta\cot\phi/2 - \sum_{n_s=1}^{N_s}\sum_{n_c=1}^{N_c} a_{n_c n_s n_a}\sin n_s\theta \sin n_c\phi\right] f_{n_a}(\psi) \quad (4\text{-}3)$$

or

$$= \sum_{n_a=1}^{N_a} \sum_{n_s=1}^{N_s} \sum_{n_c=1}^{N_c} \ell_{n_a n_s n_c}$$

where

$$f_1 = 1$$

$$f_2 = \sin\psi$$

$$f_3 = \cos\psi$$

$$f_4 = \sin 2\psi$$

$$f_5 = \cos 2\psi$$

and so on.

4.2 Evaluation of 'ω_x' (Equation (3-6))

The double integral in equation (3-6) has a strong singularity as $\xi \to x$ and $\eta \to y$. The region of integration 'S' was divided into two separate regions. The first, region R, was a small area surrounding the point (x,y,o). The other region was the remaining area (S-R). We shall deal with two regions separately in the following sections.

4.2A Evaluation of 'ω_x' (Non-singular part)

We have to evaluate

$$\omega_x(x,y,o,t) = \frac{1}{4\pi\rho} \lim_{z\to o} \frac{\partial^2}{\partial z^2} \iint_{S-R} \frac{\ell(\xi,\eta',t)\, d\xi d\eta}{[(x-\xi)^2+\beta^2(y-\eta)^2+\beta^2 z^2]^{1/2}}$$

$$= \frac{-1}{4\pi\rho} \iint_{S-R} \frac{\ell(\xi,\eta,t)\, d\xi d\eta}{[(x-\xi)^2+\beta^2(y-\eta)^2]^{3/2}}$$

$$= -\frac{1}{4\pi\rho}\sum_{n_a=1}^{N_a}\sum_{n_s=1}^{N_s}\sum_{n_c=1}^{N_c}\iint_{S-R}\frac{\ell_{n_a n_s n_c}(\xi,\eta,t)\,d\xi d\eta}{[(x-\xi)^2+\beta^2(y-\eta)^2]^{3/2}} \quad (4\text{-}4)$$

The numerical procedure developed in following pages is identical for all loading modes. We will, therefore, drop the summation sign in equation (4-4) and consider a general loading mode $\ell_{n_a n_s n_c}$. A similar procedure was also used in Reference (26).

The plane $z_b=0$ was divided into a network of squares with sides 2Δ (see figure 4-1). 'ω_x' was to be evaluated at the centre of each square. Each square is referred to by a set of integers $(\bar{\mu},\mu)$. If the square lies on the blade it is referred to by $(\bar{\nu},\nu)$.

Consider one square $(\bar{\nu},\nu)$ on the blade surface. Let us evaluate its contribution in 'ω_x' at $(\bar{\mu},\mu)$. A new axis system $o_{\bar{\nu},\nu}$ u,v was defined with $o_{\bar{\nu},\nu}$ at the centre of box $(\bar{\nu},\nu)$ (Figure 4.1), u and v are defined as

$$u = [\xi - \xi_{\bar{\nu}}]/\Delta$$

Therefore, $$du = d\xi/\Delta$$

$$v = [\eta - \eta_{\bar{\nu}}]/\Delta$$

Therefore, $$dv = d\eta/\Delta.$$

'ω_x' at $(\bar{\mu},\mu)$, due to all squares $(\bar{\nu},\nu)$ on the blade could thus be written as,

$$(\omega_x)_{NS}(x_{\bar{\mu}}, y_\mu, o, t) = -\frac{1}{4\pi\rho} \sum_{\bar{\nu}\nu \neq \bar{\mu}\mu} \int_{-1}^{+1}\int_{-1}^{+1} \ell_{n_a n_s m_c}(u,v,t)\Delta^2$$

$$K(u,v,x_{\bar{\mu}}, y_{\bar{\mu}}, t)\,dudv \quad . \quad (4\text{-}5)$$

The kernel K is always regular and was thus expanded in Legendre polynomials in u and v. If $\bar{n}$ and n represent the degree of polynomial in the u and v direction respectively, equation (4-5) reduces to

$$(\omega_x)_{NS}(x_{\bar{\mu}}, y_\mu, o, t) = -\frac{1}{4\pi\rho}\left(\bar{n} - \frac{1}{2}\right)\left(n - \frac{1}{2}\right) \sum_{\bar{\nu}\nu \neq \mu\mu} \sum_{\bar{n}n}$$

$$\int_{-1}^{+1}\int_{-1}^{+1} P_{\bar{n}}(u) P_n(v) \ell_{n_a n_s m_c}(u,v,t)$$

$$\left\{ \int_{-1}^{+1}\int_{-1}^{+1} P_{\bar{n}}(u) P_n(v) K(u,v,x_{\bar{\mu}}, y_\mu, t)\, dudv \right\} \Delta^2 dudv$$

$$= -\frac{1}{4\pi\rho} \sum_{\bar{\nu}\nu \neq \bar{\mu}\mu} \sum_{\bar{n}n} a_{\bar{n}n} I_{\bar{n}n} \qquad (4\text{-}6)$$

where '$a_{\bar{n}n}$', the generalised Fourier coefficient, and '$I_{\bar{n}n}$', the influence function, were evaluated easily by numerical quadrature.

4.2B Evaluation of 'ω_x' (Singular Part)

Because the loading on the blade was regular, we could expand it in double Legendre polynomials. We observed that equation (3-6) consequently reduced to a relation similar to equation (4-4). Thus

$$(\omega_x)_s(x,y,o,t) = \frac{1}{4\pi\rho} \sum_{\bar{\nu}\nu=\mu\mu} \sum_{\bar{n}n} \alpha_{\bar{n}n} I_{\bar{n}n} \qquad (4\text{-}5)$$

where

$$I_{\bar{n}n} = \underset{z\to 0}{Lt} \frac{1}{\Delta^3} \frac{\partial^2}{\partial z^2} \int_{-1}^{+1}\int_{-1}^{+1} P_{\bar{n}}(u)P_n(v) \left\{ \frac{1}{(u^2+\beta^2v^2+\beta^2\omega^2)^{1/2}} \right\} dudv \qquad (4\text{-}6)$$

At $u = 0$ and $v = 0$, $I_{\bar{n}n}$ has a singularity. A special procedure was, therefore, adopted for its evaluation. The procedure was somewhat similar to the one adopted in Reference (27). We had

$$I_{\bar{n}n}(o,o,o) = \frac{1}{\Delta^3} \underset{z\to 0}{Lt} \frac{\partial^2}{\partial z^2} \int_{-1}^{+1}\int_{-1}^{+1} \frac{P_{\bar{n}}(u)P_n(v)}{(u^2+\beta^2v^2+\beta^2\omega^2)^{1/2}} dudv$$

$$= \frac{1}{\Delta^3} \underset{z\to 0}{Lt} \int_{-1}^{+1}\int_{-1}^{+1} P_{\bar{n}}(u)P_n(v) \left\{ -\frac{\beta^2\partial^2}{\partial u^2} - \frac{\partial^2}{\partial v^2} \right\} \frac{dudv}{r}$$

where,

$$r^2 = u^2 + \beta^2v^2 + \beta^2\omega^2 \quad . \qquad (4\text{-}7)$$

Let

$$A_u = P_{\bar{n}}(u)P_n(v) \frac{\partial}{\partial v} \frac{1}{r}$$

$$A_v = -\beta^2 P_{\bar{n}}(u)P_n(v) \frac{\partial}{\partial u} \frac{1}{r}$$

Using Stokes' theorem,

$$\int_{-1}^{+1}\int_{-1}^{+1} \left(\frac{\partial A_v}{\partial u} - \frac{\partial A_u}{\partial v}\right) du\,dv = \oint A_u\,du + A_v\,dv$$

$$= \int_{-1}^{+1}\int_{-1}^{+1} P_{\bar{n}}(u) P_n(v) \left\{ -\frac{\beta^2\partial^2}{\partial u^2} - \frac{\partial^2}{\partial v^2} \right\} \frac{du\,dv}{r}$$

$$- \int_{-1}^{+1}\int_{-1}^{+1} \left\{ \frac{\beta^2}{\partial u} \frac{1}{r} \frac{\partial}{\partial u} \left(P_{\bar{n}}(u) P_n(v)\right) \right.$$

$$\left. + \frac{\partial}{\partial v} \frac{1}{r} \frac{\partial}{\partial v} \left(P_{\bar{n}}(u) P_n(v)\right) \right\} du\,dv$$

$\oint$ is the counter integral taken anticlockwise around the area (S-R).

Rearranging,

$$\Delta^3 I_{\bar{n}n}(o,o,o) = \oint A_u\,du + \oint A_v\,dv - \int_{-1}^{+1}\int_{-1}^{+1} \left(u\beta^2 P_n(v) \frac{\partial}{\partial u} P_{\bar{n}}(u) + v\beta^2 P_{\bar{n}}(u) \frac{\partial}{\partial v} P_n(v)\right) \frac{du\,dv}{r^3}$$

$$= -\oint P_{\bar{n}}(u) P_n(v) \beta^2 v \frac{du}{r^3} + \oint P_{\bar{n}}(u) P_n(v) \beta^2 u \frac{dv}{r^3}$$

$$-\beta^2 \int_{-1}^{+1}\int_{-1}^{+1} \left\{ uP_n(v) \frac{\partial}{\partial u} P_{\bar{n}}(u) + vP_{\bar{n}}(u) \frac{\partial}{\partial v} P_n(v) \right\} \frac{du\,dv}{r^3}$$

or,

$$\frac{\Delta^3}{\beta^2} I_{\bar{n}n}(o,o,o) = + \int_{-1}^{1} P_{\bar{n}}(u)P_n(-1)\,\frac{du}{r^3} - \int_{+1}^{-1} P_{\bar{n}}(u)P_n(+1)\,\frac{du}{r^3}$$

$$+ \int_{-1}^{+1} P_{\bar{n}}(1)P_n(v)\,\frac{dv}{r^3} - \int_{+1}^{-1} P_{\bar{n}}(-1)P_n(v)\,\frac{dv}{r^3}$$

$$- I_{\bar{n}n}^{3}$$

or,

$$\frac{\Delta^3}{\beta^2} I_{\bar{n}n}(o,o,o) = I_{\bar{n}n}^{1} + I_{\bar{n}n}^{2} - I_{\bar{n}n}^{3}$$

where,

$$I_{\bar{n}n}^{1} = \int_{-1}^{1} \left\{P_n(1)P_{\bar{n}}(-u)+P_n(-1)P_{\bar{n}}(u)\right\} \frac{du}{(u^2+\beta^2)^{3/2}} \qquad (4\text{-}8a)$$

$$I_{\bar{n}n}^{2} = \int_{-1}^{1} \left\{P_{\bar{n}}(1)P_n(v)+P_{\bar{n}}(-1)P_n(-v)\right\} \frac{dv}{(1+\beta^2v^2)^{3/2}} \qquad (4\text{-}8b)$$

$$I_{\bar{n}n}^{3} = \int_{-1}^{+1}\int_{-1}^{+1} \left(uP_n(v)\,\frac{\partial}{\partial u}P_{\bar{n}}(u)+vP_{\bar{n}}(u)\,\frac{\partial}{\partial v}P_n(v)\right) \frac{dudv}{r^3} \qquad (4\text{-}8c)$$

Equations (4-8) are evaluated in Appendix 1. In particular, for $\beta^2 = 1.0$ i.e. for incompressible flow, we obtained the following relations.

$$\Delta^3 I_{11}(o,o,o) = 2\sqrt{2} + 2\sqrt{2} - 0.0$$

$$= 4\sqrt{2} \qquad (4\text{-}9a)$$

$$\Delta^3 I_{21}(o,o,o) = 0.0 \qquad (4\text{-}9b)$$

$$\Delta^3 I_{31}(o,o,o) = (3 \log_e(3+2\sqrt{2}) - 4\sqrt{2}) + 2\sqrt{2} - (6 \log_e(3+2\sqrt{2}))$$

$$= -3 \log_e(3+2\sqrt{2}) - 2\sqrt{2} \qquad (4\text{-}9c)$$

$$\Delta^3 I_{12} = \Delta^3 I_{22} = \Delta^3 I_{32} = 0.0 \qquad (4\text{-}9d)$$

$$\Delta^3 I_{13}(o,o,o) = (3 \log_e(3+2\sqrt{2}) - 4\sqrt{2}) - 6 \log_e(3+2\sqrt{2}) + 2\sqrt{2} \qquad (4\text{-}9e)$$

$$= -3 \log_e(3+2\sqrt{2}) - 2\sqrt{2}$$

$$\Delta^3 I_{23}(o,o,o) = 0.0 \qquad (4\text{-}9f)$$

$$\Delta^3 I_{33}(o,o,o) = (3 \log_e(3+2\sqrt{2}) - 4\sqrt{2}) \qquad (4\text{-}9g)$$

$$+ (3 \log_e(3+2\sqrt{2}) - 4\sqrt{2})$$

$$- 6 \log_e(3+2\sqrt{2}) + 2\sqrt{2} = -6\sqrt{2}$$

SECTION 5

NASA MODEL ROTOR - AERODYNAMIC LOADING IN STEADY TRANSLATIONAL FLIGHT

SECTION 5

NASA MODEL ROTOR - AERODYNAMIC LOADING IN STEADY TRANSLATIONAL FLIGHT

Based on the theory developed in Section 3 and Section 4, we developed a series of computer programs, which enabled us to calculate the aerodynamic loading on the rotating blades of a translating rotor. The results thus obtained were then compared to those obtained in wind tunnel experiments. This, we hoped, would validate our mathematical model and establish the philosophy we have advanced in this thesis. We also thought it desirable, in addition, to compare our results with those obtained by using refined wake models and strip theory (Reference 17).

We selected the full scale NASA model for our calculations (Reference 30). The computer programs are, however, quite general in scope and can easily be adopted to any other rotor. The NASA model rotor, under consideration, was a two bladed teetering rotor with no coning angle. The blades were of rectangular platform, untwisted and had an NACA 0012 airfoil section. The rotor diameter was about 15 feet and the rotor solidity was 0.097. This gave a chord of 14 inches. The rotor tip speed was 460 feet per second. The calculations were made for an advance ratio of 0.29. The translational velocity of the rotor was thus approximately equal to 150 feet per second. The

rotor blade stiffness both in bending and in torsion was very high. The bending stiffness varied from a maximum of about 900,000 psia at the root to a constant value of 2,850,000 psia for the outboard 40% of the blade span. The overall torsional stiffness, measured between the blade root and the blade tip was 278 inch pounds per degree of twist. Our reasons for choosing this particular rotor for calculations were as follows.

(a) NASA obtained the loading on the blades of this rotor in forward flight in full scale wind tunnel tests. The results were available in Reference 30.

(b) The blade distortions and the dynamic response were not included in our analysis. The blades of the selected NASA rotor were very stiff in bending and in torsion. They were therefore, not expected to have large distortions during flight, and hence agreed with our assumption fairly well.

(c) Results based on the strip theory and refined wake models were available (Reference 17).

(d) For the flight conditions we were interested in, there was no retreating or advancing blade stall.

(e) Mach numbers encountered were low. Compressibility effects were, therefore, not expected to be very large.

(f) The coning angle was zero.

4.1 The Numerical Calculations and the Computer Programs

The various steps involved in the numerical calculations are shown in the diagram below.

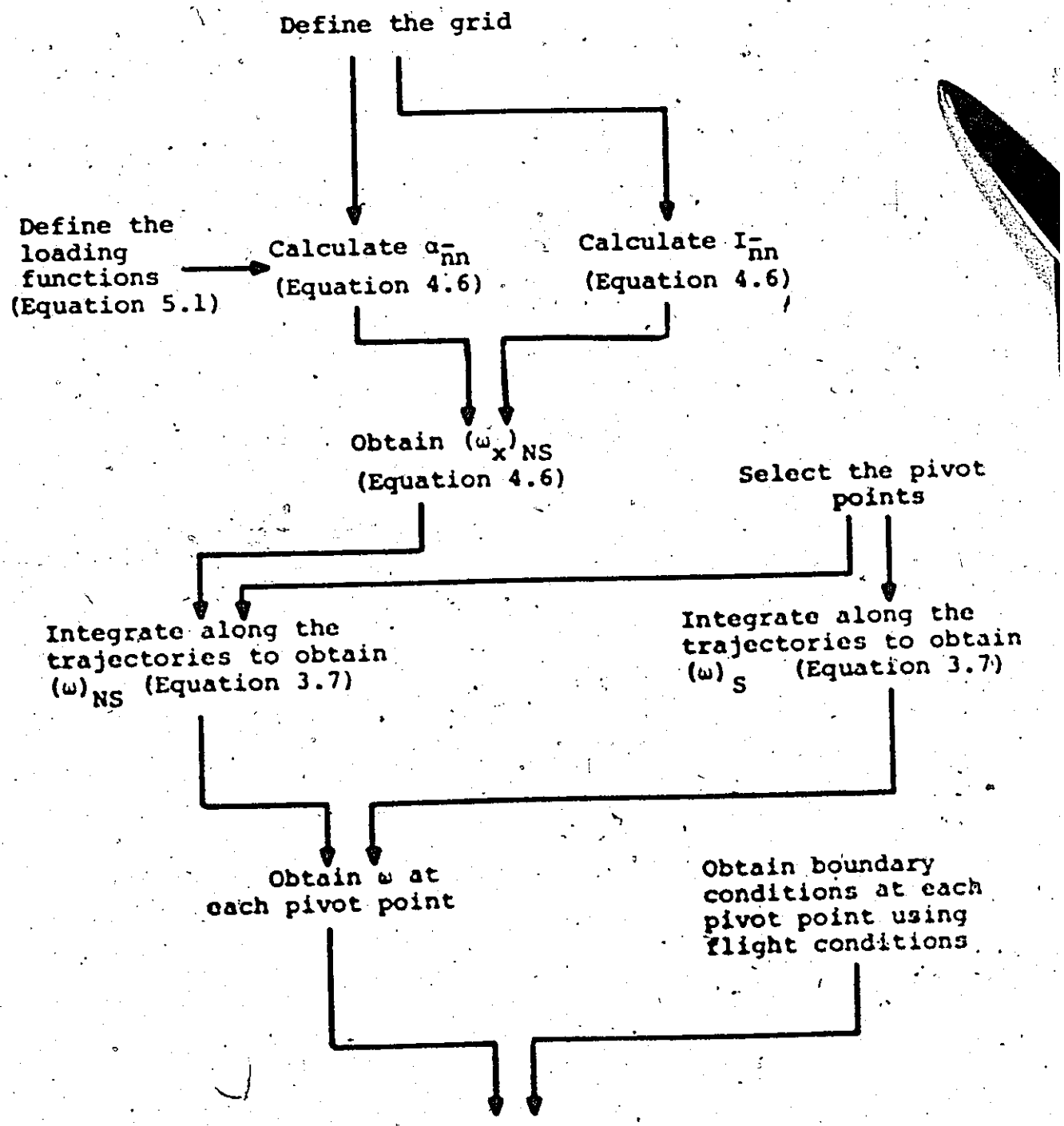

Solve to obtain loading coefficients, and hence the loading on the blade.

The Grid: A grid of identical squares was defined in the plane of the blade. Each side of the square was 3.5 inches (Figure 4.1). At the centre of each square of this 16×33 inner grid, $(\omega_x)_{NS}$ was to be evaluated. In addition, a larger grid was also defined. Each side of the squares of this outer grid was 14 inches. This grid was used to evaluate $(\omega_x)_{NS}$ at points which were distant from the blade.

The Loading Functions: We restricted our work to include only the spanwise and the azimuthwise variation of loading on the rotating blade. The chordwise distribution of loading, though not included in our analysis, can be easily handled in the computer programs we developed. We, therefore, considered only the first term of the chordwise loading distribution (Equation 4.1). For spanwise loading distribution, we considered the first five sine harmonics. For azimuthwise loading distribution, we considered first three sine and cosine harmonics. These 35 elementary loading functions, we felt, could adequately represent the prevailing blade loading. The number of elementary loading functions considered had to be restricted to a minimum to limit the computer time used. The blade loading considered could, therefore, be written as

$$\ell(\phi,\theta,\psi) = \cot\phi/2[\{a_{111} + a_{112}\sin\psi + a_{113}\cos\psi + \ldots. + \{a_{116}\sin3\psi + a_{117}\cos3\psi\}\sin\theta + \{a_{121} + \ldots\ldots + a_{127}\cos3\psi\}\sin2\theta + \ldots\ldots + \{a_{151} + \ldots. + a_{157}\cos3\psi\}\sin5\theta]. \quad (5\text{-}1)$$

Number and Location of Pivot Points: There were 35 unknown loading coefficients to be determined. Ideally, we had, therefore, to satisfy the boundary conditions only at 35 pivot points. We, however, used 72 pivot points in our analysis. There were no guidelines available to suitably select the spanwise and the azimuthwise location of the pivot points. We, therefore, took a rather larger set of pivot points and obtained an optimum solution by minimising the total mean root square error. Though such an approach used up some extra computer time, we nevertheless found it useful and reliable. The azimuthwise and the spanwise location of the pivot points is shown in Figure 5.1. The chordwise location of the pivot points was at three quarter chord line. This location was, of course, necessary since we included only the first term of chordwise loading distribution in our analysis. A detailed discussion of this point is given in References 28 and 29.

The Fourier Coefficient $a_{\bar{n}n}$ and the Influence Function $I_{\bar{n}n}$: $a_{\bar{n}n}$ and $I_{\bar{n}n}$ were calculated using Equation 4.6. We admitted only the first value of $\bar{n}$ and n in our analysis, i.e. $\bar{n} = 1$,

and n = 1. Considerable computer time was consequently saved. The errors thus introduced were not expected to be large. The approximation effectively reduced the continuous chordwise loading distribution, the cotangent function, to a staircase function with four steps. Let us first consider the evaluation of α_{nn}^{-}. It had to be calculated for each square of the grid which carried the load. The square for which α_{nn}^{-} was to be evaluated was further divided into a finer 7×7 grid. At the centre of each square of this finer 7×7 grid, $P_n^{-}(u)P_n(v)\ell(u,v)$ was evaluated. α_{nn}^{-} was then obtained simply by a trapezoidal integration formula. For squares along the leading edge, a finer 19×19 grid was necessary to yield acceptable accuracies. A similar procedure was used for I_{nn}^{-}. For points close to the square under consideration a finer 9×9 grid was used. For points relatively away from the square, a 5×5 grid was used. I_{nn}^{-} was to be calculated at each point of the grid, separately for each load carrying square of the grid. This represented a very large amount of computational effort, and hence computer time. Most of these pairings for I_{nn}^{-}, however, became identical if the compressibility effect was ignored. The calculations could then be made for only a relatively small number of pairs. We therefore ignored the effects of compressibility in our calculations.

The Downwash w_n Non-singular Contribution: Assume that at a given time, an air particle was at a point in the plane of the

rotor. With each increment in time, this particle moved with a velocity U along the wind direction, i.e. along the positive x-direction. At the same time the blade rotated counter clockwise with the angular velocity Ω. If the air particle was observed in a reference system fixed in the rotating blade, it would have appeared to move along a trajectory. A few of these trajectories are shown in Figures 5.2a and 5.2b. In order to obtain the downwash at a selected pivot point, we therefore performed the integration (Equation 3-7) along one such trajectory which ended at the selected pivot point. Actually we started the integration at the pivot point, continued backwards along the trajectory until the trajectory moved out of the outer grid. $(\omega_x)_{NS}$ was obtained by simple interpolation. The integration itself was performed using a 14-point Gaussian quadrature formula. For parts of the trajectories which were relatively away from the blade surface, a six point Gaussian quadrature formula or simple trapezoidal formula was used. The contribution of each blade was calculated separately. Each contribution was then added to yield the final value of ω_{NS}.

The Downwash ω_s Singular Contribution: We considered a load carying square of the inner grid, with the dimensions of 2Δ. We assumed that the average value of aerodynamic loading in this square was a. The singular influence function of this square was therefore $4\sqrt{2}/\Delta^3$ (Equation 4.9a, $\bar{n} = n = 1$). $(\omega_x)_{singular}$ for this square hence equalled $(4\Delta^2 \cdot a)(4\sqrt{2}/\Delta^3)4\pi\rho$ or $(16\sqrt{2}/4\pi\rho\Delta)a$. If a particle moved a distance dx within this square, the increase

in downwash due to this singular contribution was therefore, equal to $(16\sqrt{2}/\Delta\pi\rho\Delta)\alpha\, dx$. We, therefore, calculated the singular contribution to the downwash by performing the integration $(16\sqrt{2}/4\pi\rho\Delta)\int \alpha dx$ along the trajectories. Clearly only those parts of the trajectories which were on any one of the two blades yielded a non-zero contribution. The integration itself was performed using Gaussian quadrature formula. We would, however, like to mention that this rather simple procedure was possible because we admitted only one value for $\bar{n}$ and n.

SECTION 6

RESULTS AND DISCUSSION

SECTION 6 RESULTS AND DISCUSSION

For the full scale NASA model rotor blades described earlier in Section 5, we obtained the aerodynamic loading for three different flight conditions. Two of these were arbitrary, and involved rather simple boundary conditions. Calculations were initially made for these two conditions. Our aim was to get some preliminary results which could be easily compared with those obtained by simple theoretical analysis. This helped us to isolate and remove problems in the computer programming, the numerical procedure and the mathematical model. A satisfactory agreement, we hoped, would validate our mathematical model and the numerical procedure as outlined in Sections 3, 4 and 5. Once this was successfully done, we then proceeded to calculate the blade loadings for the flight condition for which NASA had obtained experimental results in the wind tunnel (Reference 30).

We first considered a single non-rotating blade set at a fixed azimuth angle of 90 degrees. The blade was thus equivalent to an unyawed fixed wing. Further, the blade was given a geometric angle of incidence of 5 degrees. Using our mathematical model, we calculated the spanwise distribution

of sectional lift coefficient. This distribution is shown by the solid line in Figure 6.1. The two dotted lines in the same figure show the theoretical values of the lift coefficient obtained with and without the aspect ratio correction. Our results were clearly in excellent agreement with the theory, and this fact allowed us to proceed to the case of a rotating blade. We considered a lifting rotor translating with a steady velocity of 150 feet per second. The advance ratio was 0.29. A fixed geometric pitch setting of five degrees was given to the blades. No flapping or feathering of the blades was, however, included in the analysis. The plane of the rotor, consequently, was aligned in the direction of the oncoming wind. Calculations were made first for a one bladed rotor and then for a two bladed rotor. In addition, we calculated the blade loadings, for identical flight conditions, using the simple strip theory assuming a uniform downwash in the plane of the rotor. Because of the simplicity of the model used for such theoretical analysis, the resultant blade loadings could only be very approximate in nature. We aimed to compare the two results only for general features. Speculations could, however, be made to see how the general features of the theoretically calculated blade loadings would undergo modifications under the actual flight conditions. For example, the actual downwash could be expected to be larger at rear of the rotor disc than that at the front of the rotor disc. It could

similarly be expected to be larger in a region near $\psi = 90°$ than that in a region near $\psi = 270°$. An increase in downwash means a decrease in the blade loading. We could, therefore, expect reduced blade loadings in those regions of the rotor disc where higher downwash was expected. The calculated values for the blade loadings are shown by the solid lines in Figure 6.2 and Figure 6.3. The dotted lines in the same figures give the theoretical results. The same dotted line represents the results for the one bladed rotor, and the two bladed rotor. Our calculations showed that difference in the blade loading for the two cases was quite small, say 5 to 10 percent. Figure 6.2 shows the variation of total blade loading in azimuth. Our calculated results reproduce very nicely the general features in the blade loadings as shown by the theoretical curves. Out results clearly show a lower blade loading at the rear of the rotor disc, and a higher blade loading at the front of the rotor disc. Similarly, we observe that the blade loading is generally higher in a region around $\psi = 270°$, and is lower in a region around $\psi = 90°$. The spanwise variation of the blade loading at a specified azimuth location is shown in Figures 6.3. We notice that at all the azimuth locations considered, our results exhibit all the characteristics of the theoretical strip theory results, except near the blade tip. In our model the blade loading was made equal to zero at the blade tip, while no such attempt was made in the strip theory. The blade loading, of course, actually vanishes at the blade tip during flight.

Having satisfied ourselves with the preliminary results as outlined in the preceeding paragraph, we proceeded to analyse the lifting rotor for the flight conditions for which NASA experimental results were available. The blade loadings so obtained are presented in various ways by the solid lines in Figures 6.4, 6.5 and 6.6. Experimental results are also given in the same figures by the chained lines in Figures 6.4 and 6.5, and by the dotted line in Figure 6.6. The results obtained using sophisticated strip theories with refined wake models (i.e. by Pizialli and others in Reference 17) are also shown in Figures 6.4 by the dotted lines. Let us first examine the results shown in Figure 6.4. We recall that in Section 5, we restricted our analysis to include only the first seven terms of the Fourier series which represented the expansion of the blade loading in azimuth . We calculated the blade loadings by considering first only the initial three terms (Figure 6.4a), then the initial five terms (Figure 6.4b), and finally the initial seven terms. In each of these three cases our results compare very well with the experimental results. The agreement is in fact excellent for the first few harmonics, for example: the zeroth, the first and the second harmonics in Figure 6.4b; the zeroth and first cosine harmonics in Figure 6.4c. We further notice that the agreement is very good in Figures 6.4a and 6.4b but deteriorates somewhat (though it is acceptable in our opinion) in Figure

6.4c where the largest number of loading functions were considered. It would seem that a larger set of pivot points is perhaps required. Our results, furthermore, show better agreement with experimental results than those of Reference 17, which were obtained, we recall, by refined strip theory analysis. The improvement is particularly distinct for the lower harmonics, for example the zeroth harmonic. Only for a few isolated azimuth terms, say first harmonic sine and third harmonic sine and cosine terms (Figure 6.4c), do their results show better agreement. We also calculated the spanwise variation of the aerodynamic loading on the blades at various fixed azimuth locations. The results are presented in Figure 6.5. Except for the characteristic peak near the blade tip noticeable in the experimental curves, our results show good agreement with the experimental results. In developing our model, we assumed that the spanwise loading distribution could be replaced by a Fourier sine series, and then included only the first five terms of this series. A larger number of terms, it seems, would be necessary to represent the shape of the experimental curves near the blade tip. In addition, the aerodynamics near the blade tip is very complex. There is some spillage of flow from the lower surface to the upper surface around the blade tip. These effects are very difficult to include in the analysis. Figure 6.6 reproduces the same results in another manner. The variation of total blade loading in azimuth is shown.

Our calculated results show satisfactory agreement with the experimental results given by the dotted line. The agreement is particularly good for the case where we considered only five azimuth terms. The maximum error, in all three cases, occurs between azimuth angles of 120 degrees and 240 degrees. Though it is difficult to give precise reasons for such errors, part of these can perhaps be attributed to the bending and twisting of the blades (the authors in Reference 30 have indicated that the blades did experience some twisting and bending during the experiments). We would like to point out that the analysis accounted for only the first harmonic blade motions. Higher harmonic blade motions can significantly alter the total blade loading distribution in azimuth.

6.1 Discussion

We have, in this thesis, presented a technique to calculate the aerodynamic loading on the blades of a lifting rotor in steady translational flight. Outstanding advantages of this technique are that it neither requires the sectional airfoil data nor does it necessitate the knowledge of the rotor trailing wake. Since each of these two factors is very difficult to evaluate accurately (in fact, this has not yet been achieved), the advantages of our technique are obvious and far-reaching. We have successfully used this technique to calculate the blade loadings for a full scale NASA model rotor. The results thus obtained compare very well with those obtained experimentally by NASA in wind tunnel. The agreement, in fact, is excellent

for lower harmonics, say for first five azimuth terms (see Figure 6.4b). Our results, furthermore, show a better agreement with the experimental results than those obtained by using modified strip theory with refined wake models (Pizialli and others, Reference 17). Only for a few isolated azimuth harmonic terms do their results exhibit better agreement with the experimental results. The improved prediction of the blade loading in our analysis is particularly marked for lower harmonic terms, for example the zeroth and the first harmonics.

Our model, however, is only in the initial stages of development and will, undoubtedly, undergo improvements. It is therefore, we feel, potentially capable of yielding still better estimation of the blade loadings in forward flight. We made, it may be recalled, many simplifying assumptions during the various stages of development of the mathematical model and the numerical procedure. Many of these assumptions should and perhaps will be removed in future analysis. For example, the quasi-steady approach to the problem may be modified to exactly include the unsteady flow effects. An attempt, therefore, should be made to deduce a suitable governing integral equation from the unsteady flow equations. It would be desirable to obtain the integral equation in terms of the acceleration potential, rather than velocity potential which necessitates integration over the rotor wake. The quasi-static approach

may not, however, be a serious limitation of the present model since unsteady flow has little effect on the blade loadings below stall. The retreating and advancing blade stall are essentially associated with the boundary layer phenomenon over the rotating blades, and are thus difficult to include in any rotor analysis, including our proposed model. In modern high speed and heavily loaded helicopter rotors, the rotor blades invariably experience stall. It is, therefore, very desirable to somehow include the stall effects in our analysis. Even empirical corrections, accounting for only the first order effects, would greatly enlarge the scope of the proposed model. Compressibility, on the other hand, can be handled in our technique, though at a considerable expense of computer time. Approximate methods can, perhaps, be developed which will account for compressibility effects without unreasonably increasing the required computer time. In addition, efforts should be made to optimise the location of the pivot points, both along the blade span and in azimuth. We stated, in Section 5, that there were no guidelines available to suitably select the location of these pivot points. We, therefore, had to consider a large number of such points. Additional research in this field will, we hope, enable us to reduce the number of pivot points in the analysis and consequently will reduce the required computing time. Our model, as is now developed, cannot handle helicopter rotor loading problems

in hover and transitional flight, say at an advance ratio below 0.1. This is so because the equations for the fluid motion cannot be linearised for these flight conditions. Even though these flight regimes do not fall within the scope of the present work, it would nevertheless be useful to develop a similar procedure for these flight regimes. Non linearities of the flow would then have to be included in the analysis. Our model can be extended to solve the complete aeroelastic problem of the rotor blades. The equations of the blade motion, and those of the blade distortions are then to be integrated with the proposed analysis. This can be easily done.

We have in this thesis, only considered a single helicopter rotor in forward flight. Many other complex aerodynamic problems can also, in addition, be solved by using the proposed technique. One can, for example, analyse the case of many lifting rotors in forward flight. In fact, any problem involving a number of coplanar lifting surfaces in forward flight can be solved by using a procedure similar to the one we have advanced in this thesis. Some of these surfaces may even be allowed to have arbitrary motion in their own plane. Small out of plane motions, such as oscillations, can be handled in the analysis.

SECTION 7

SYMBOLS USED

FIGURES

REFERENCES

SYMBOLS USED

U	translational velocity of the rotor
u^*, v^*, w^*	perturbation velocities (section 3)
ω	induced velocity same as w
v_i	induced velocity (section 2)
v_o	induced velocity at the centre of the rotor
p^*	perturbation pressure
$oxyz$	non-rotating coordinate system (section 3)
$ox_by_bz_b$	rotating coordinate system fixed in the blade
c	blade chord
R	blade radius
r	distance of a point on the blade from the centre of the rotor
ℓ	aerodynamic loading per unit area
N_c	number of elementary loading distributions, chordwise
N_s	number of elementary loading distributions, spanwise
N_a	number of elementary loading distribution, azimuthwise
$a_{n_c n_s n_a}$	a loading coefficient
t	time
M	Mach number
C_L	coefficient of lift
α	geometric angle of attack
ρ	density
Ω	rotational velocity of the rotor

ψ azimuth angle, measured anti-clockwise from the downwind position

ϕ acceleration potential

μ advance ratio, $U\Omega/R$

ω_{NS} non-singular contribution in downwash

ω_S singular contribution in downwash

x_o dummy integration variable

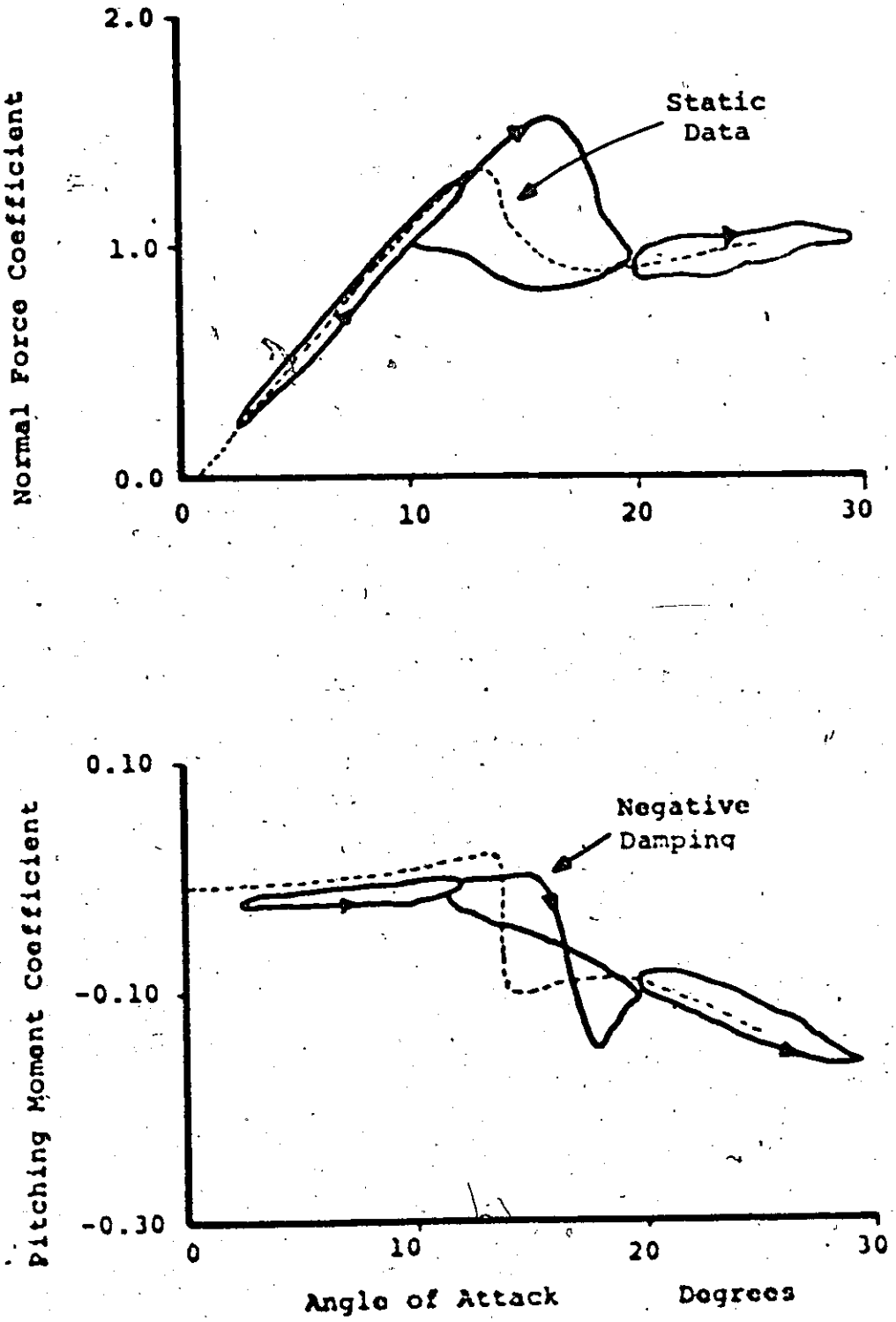

Figure 2 : Normal Force and Pitching Moment Characteristics for an Oscillating Airfoil. (Taken from Reference 9)

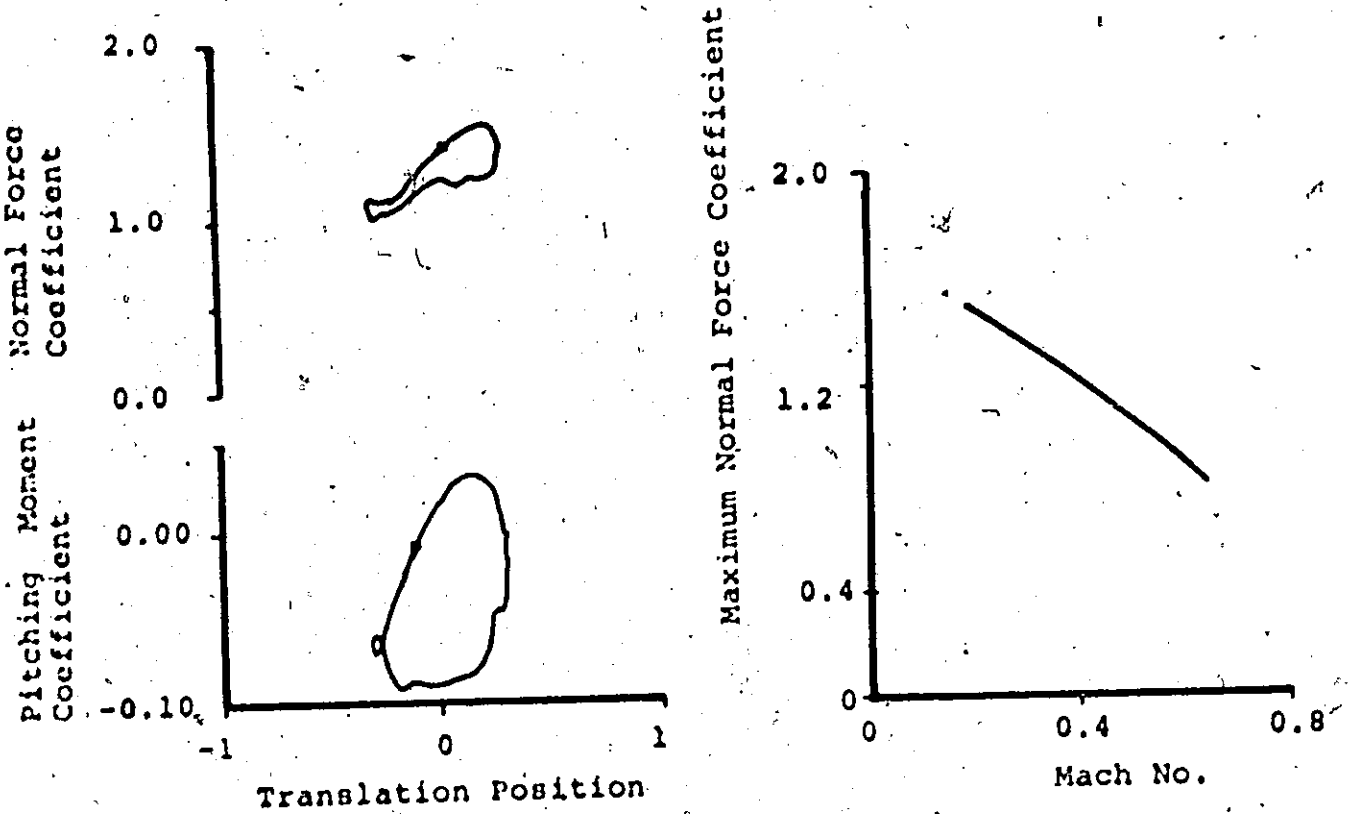

Figure 2.2: The Plunging Airfoil; Normal Force and Pitching Moment Characteristics (Taken from Reference 9)

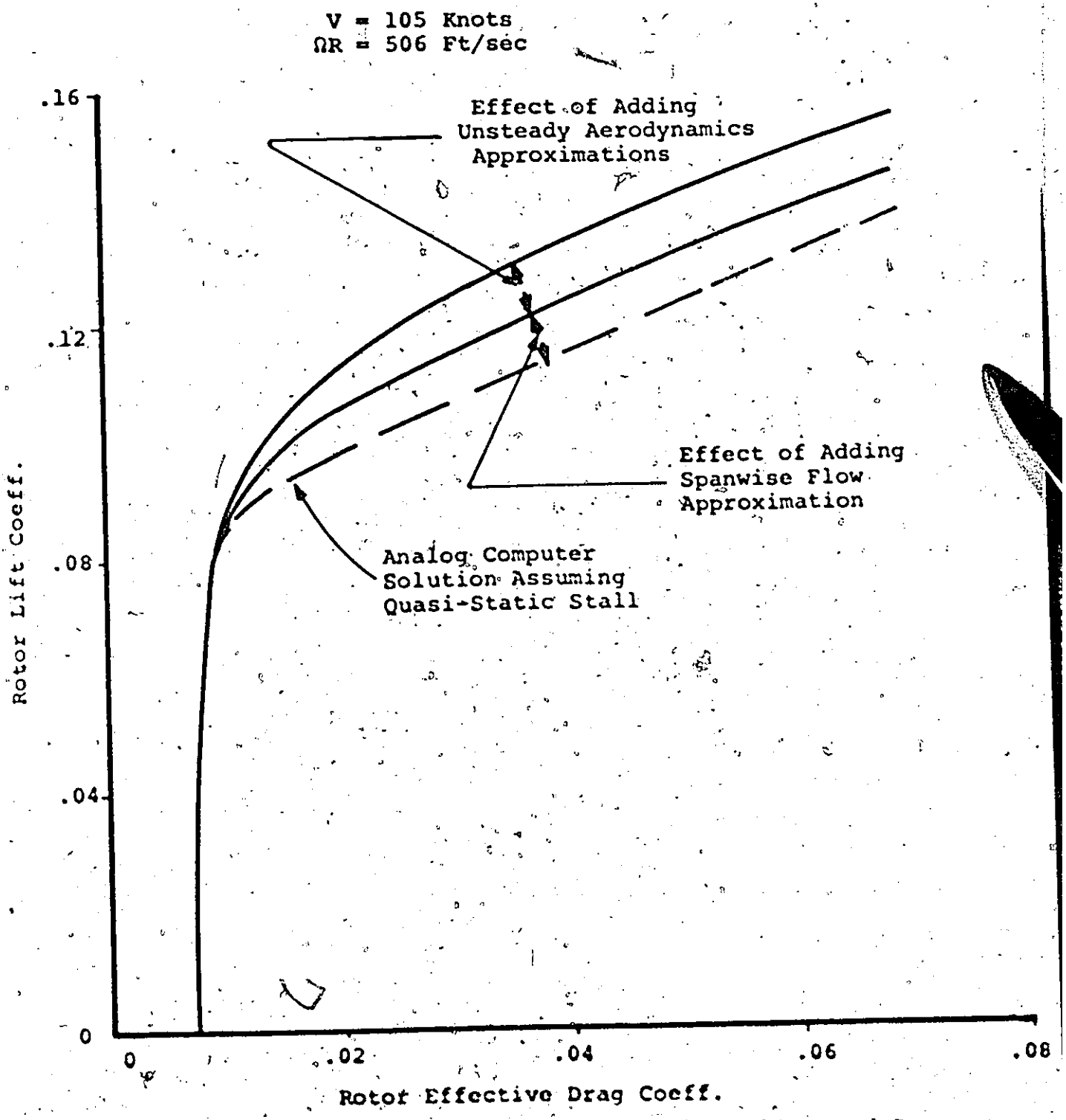

Figure 2.3: Performance Prediction for a High Speed Rotor (Taken from Reference 11)

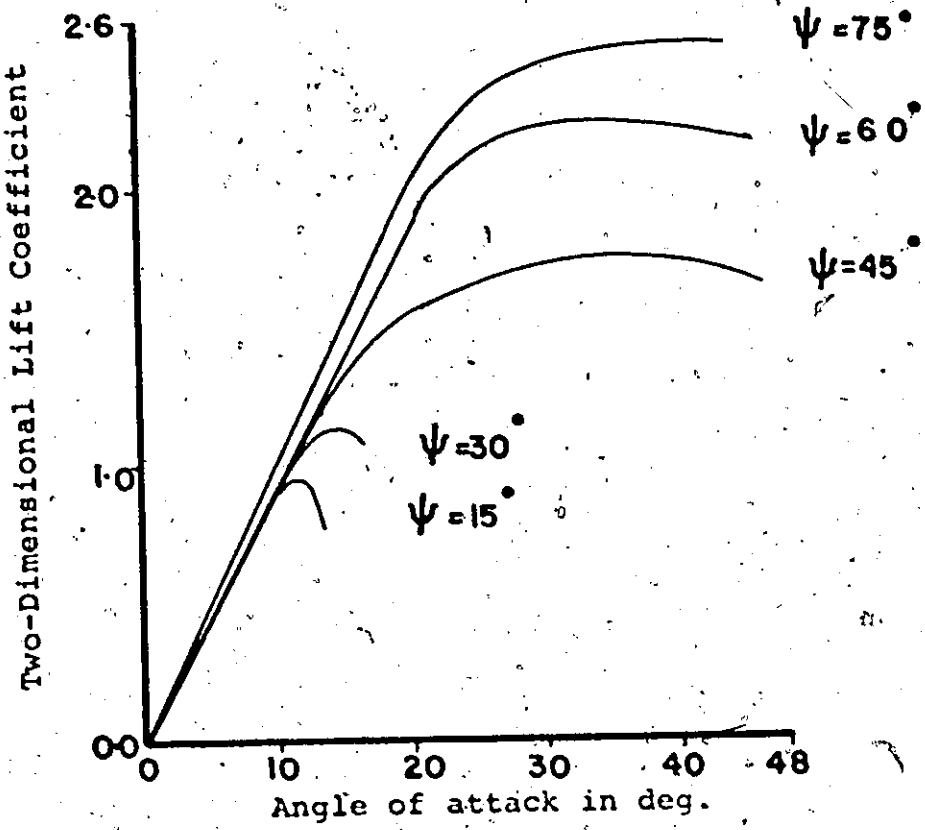

Figure 2.4: Lift Characteristics for a Yawed Wing (Reference 12).

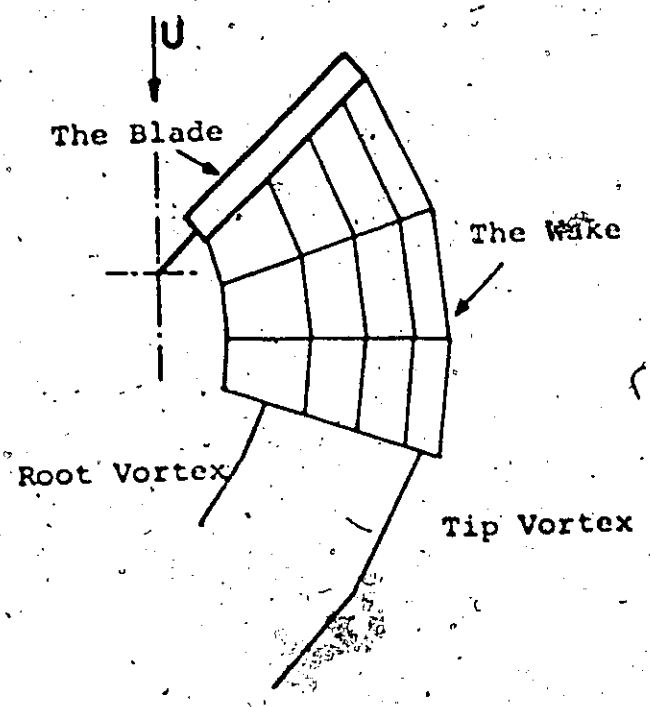

Figure 2.5: Idealised Blade-Wake Model (Reference 17).

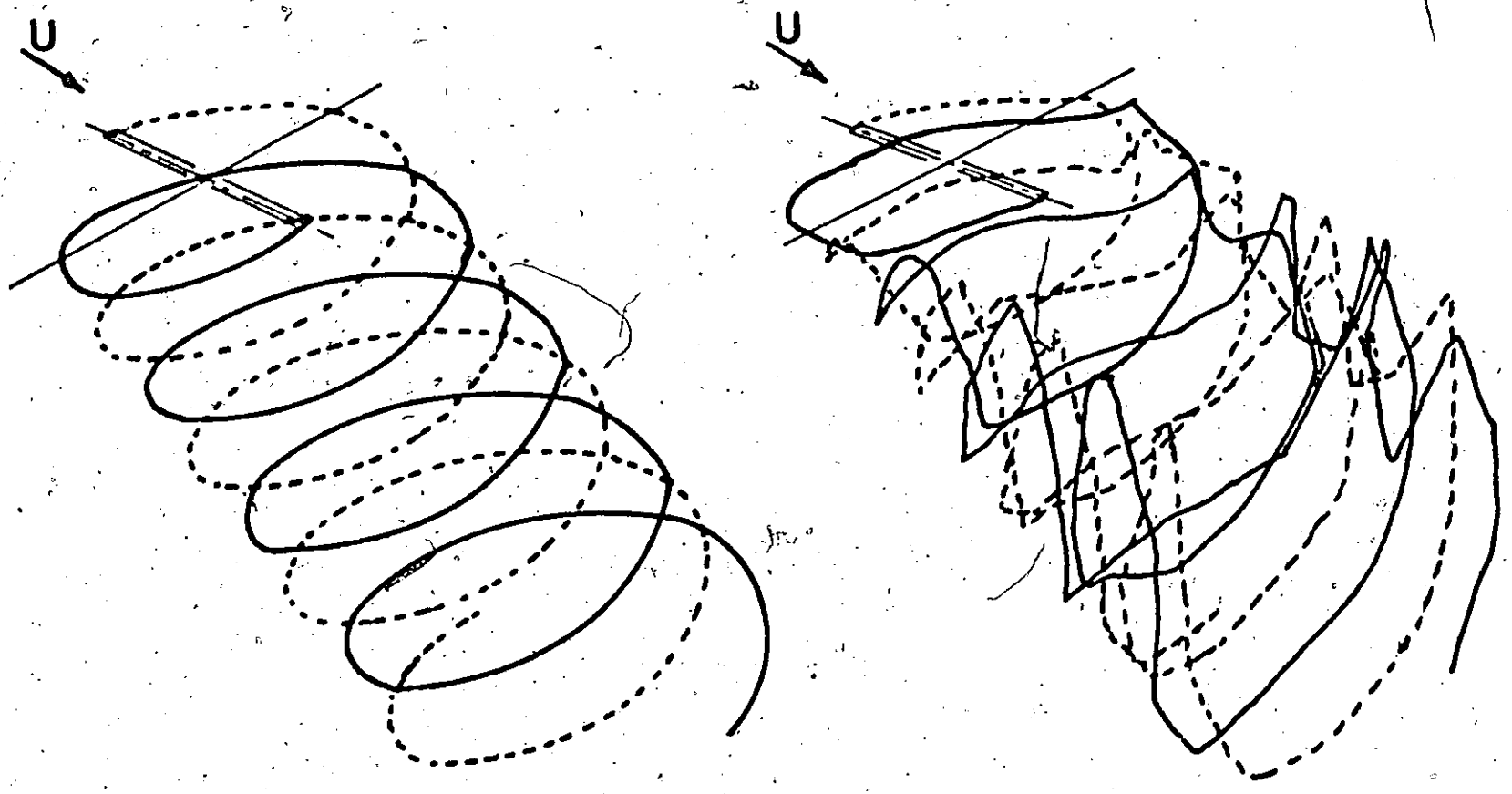

Skew-Helical Wake Configuration

Distorted Wake

Figure 2.6: The Idealised and the Computed Rotor Wake Structures (Taken from Reference 19)

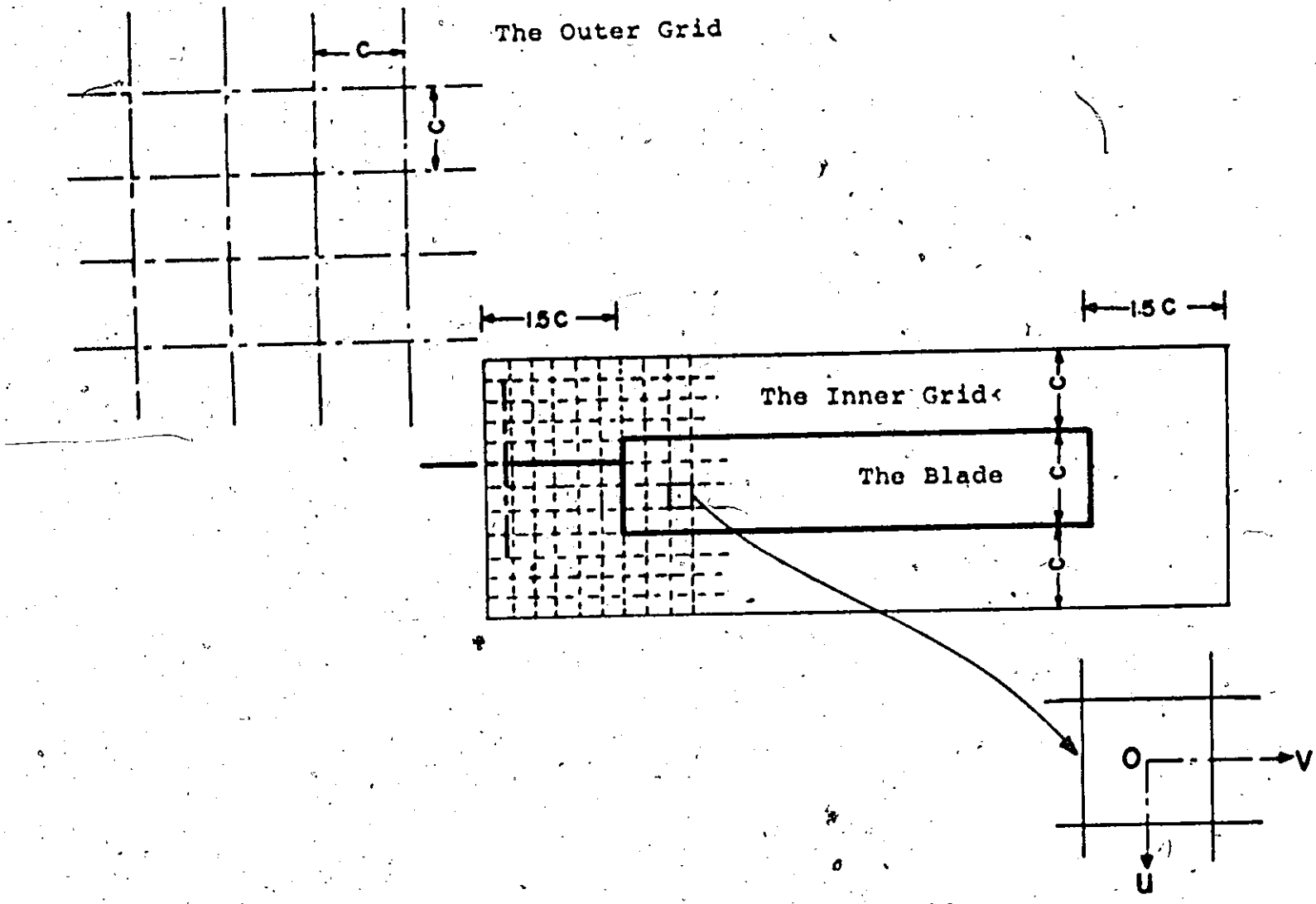

Figure 4.1: The Blade and the Grids

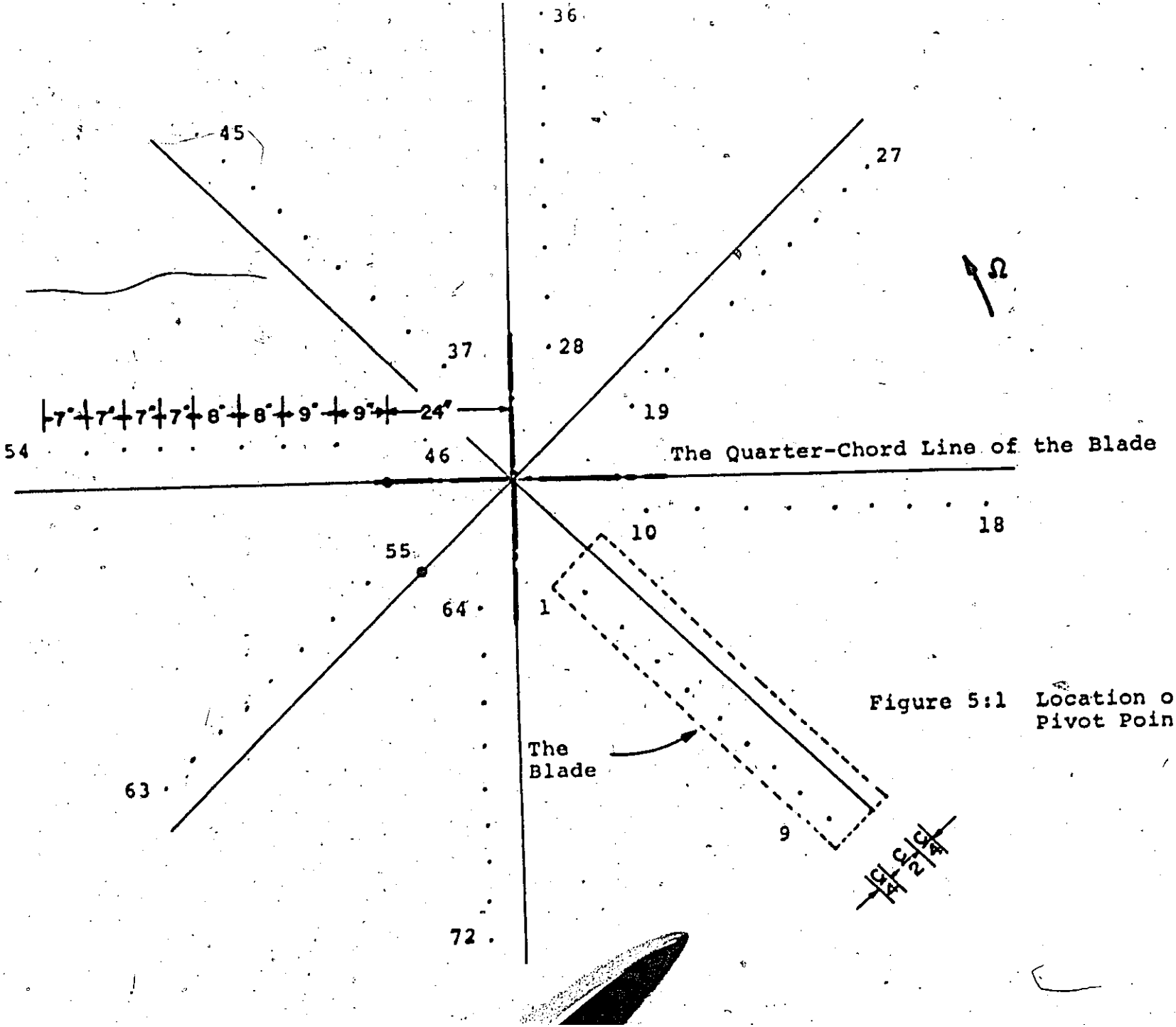

Figure 5:1 Location of Pivot Points

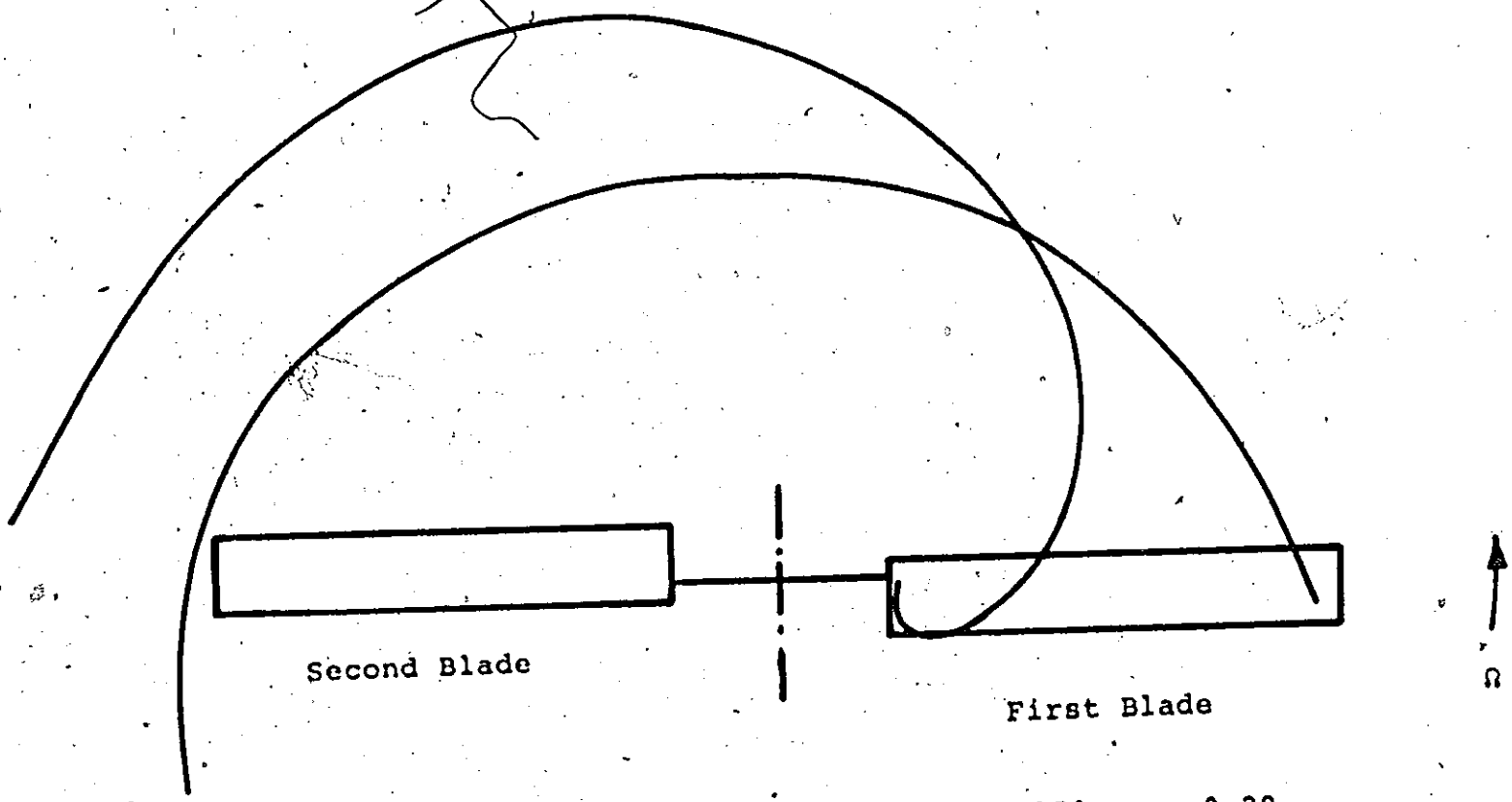

Figure 5.2a: The Trajectories for $\psi = 315°$, $\mu = 0.29$

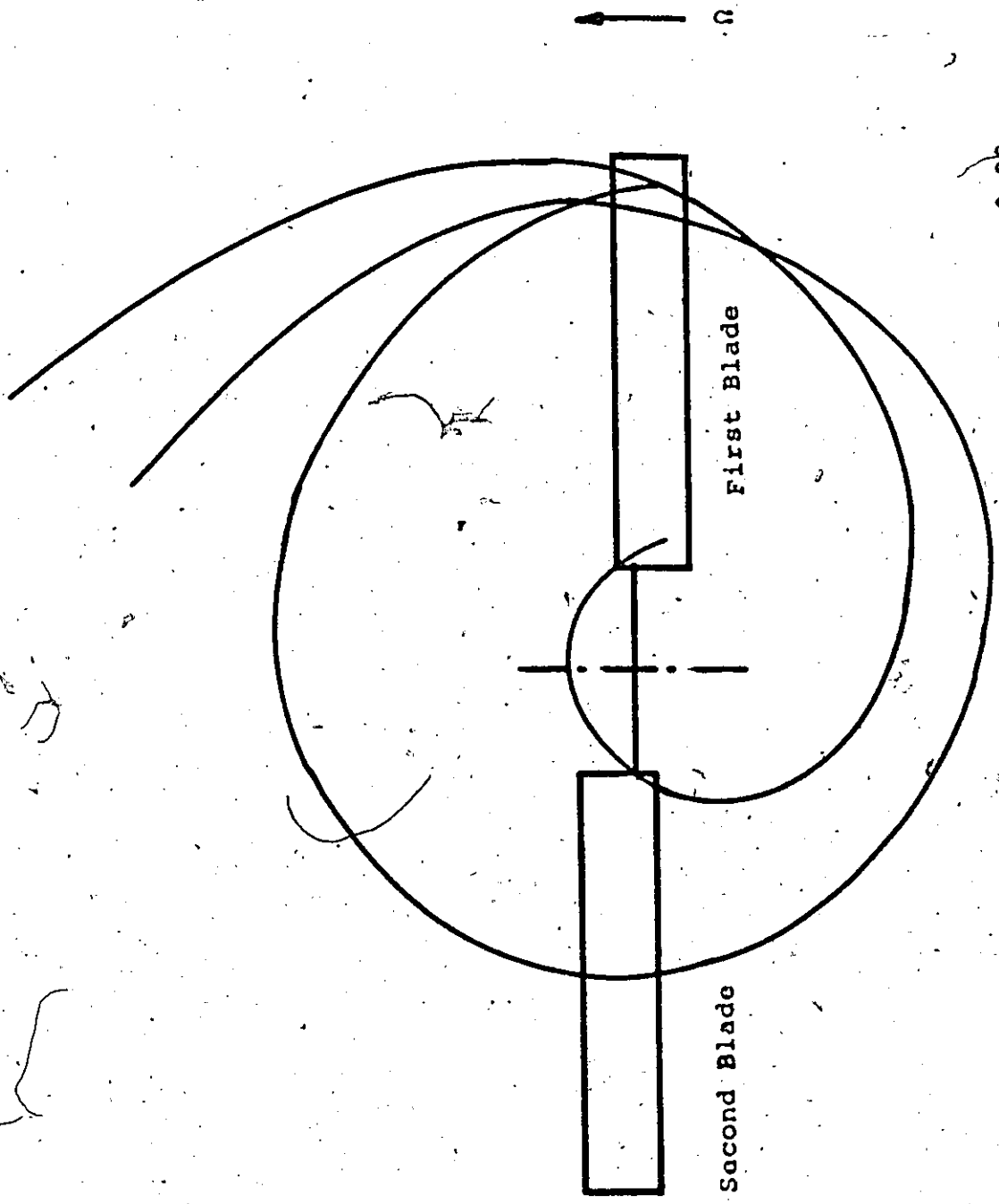

Figure 5.2b: The Trajectories for $\psi = 45°, \mu = 0.2$

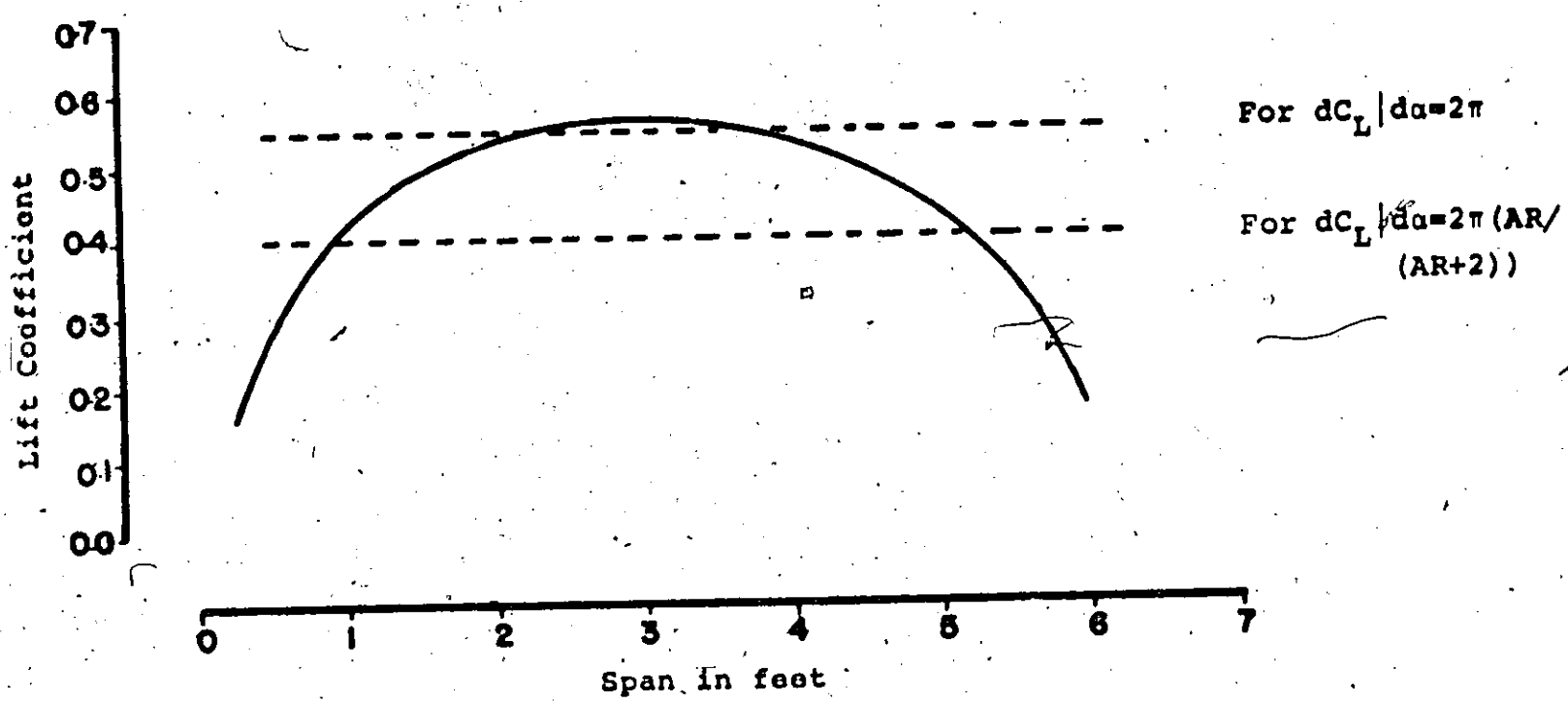

Figure 6:1 Distribution of the Lift Coefficient on an Unyawed Wing

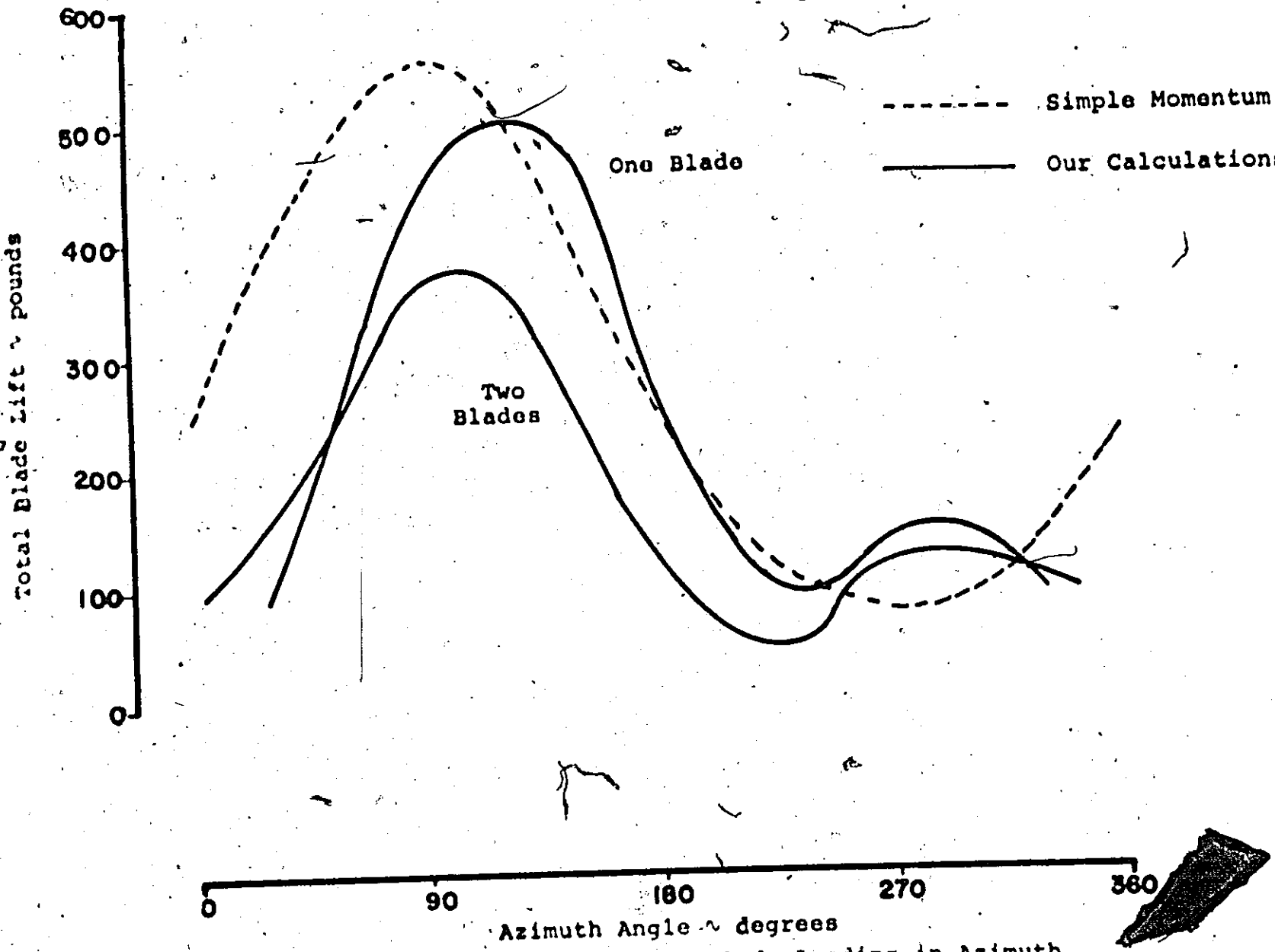

Figure 6.2: Variation of Total Blade Loading in Azimuth

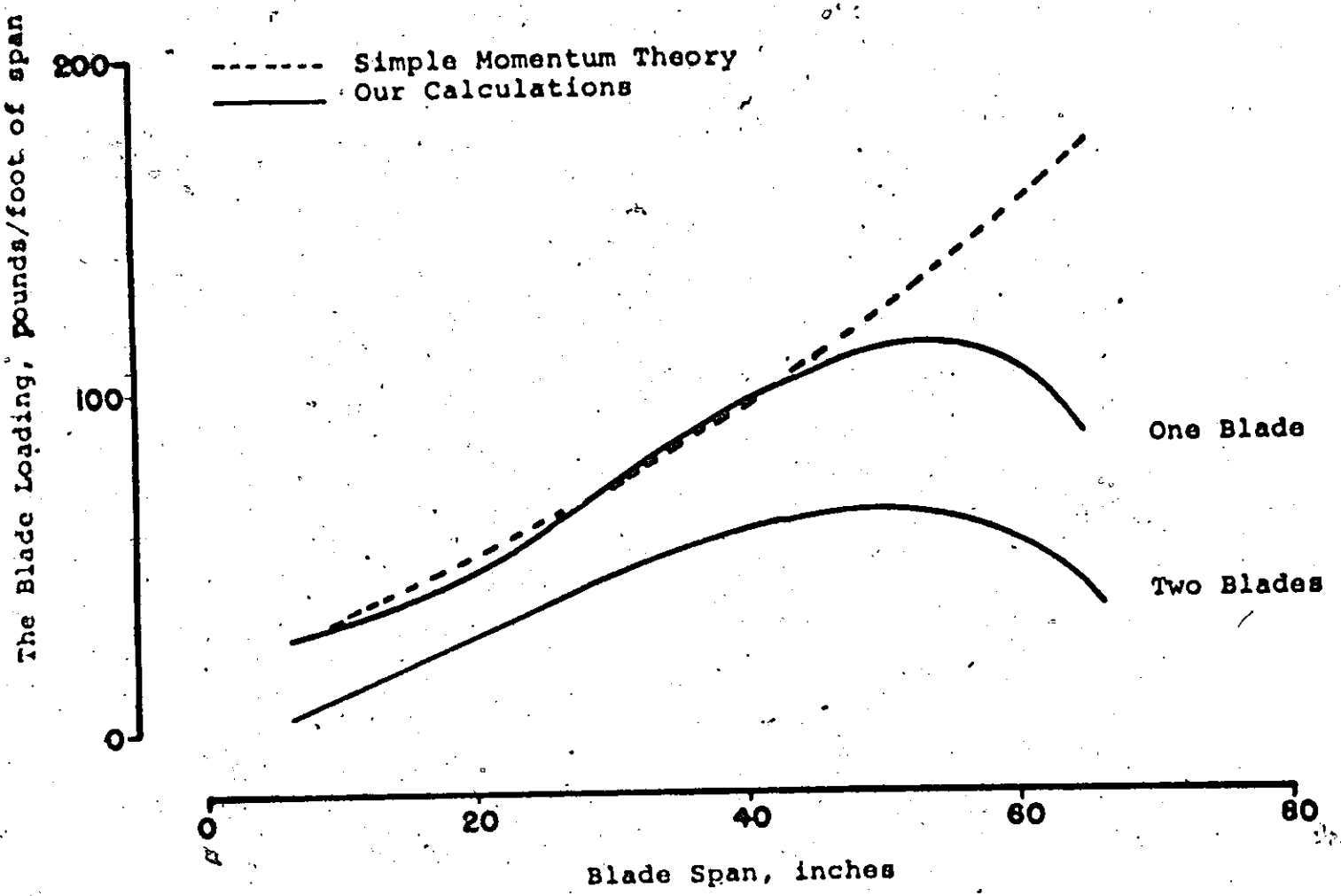

Figure 6.3a: Spanwise Variation of Blade Loading at ψ = 45 Degrees

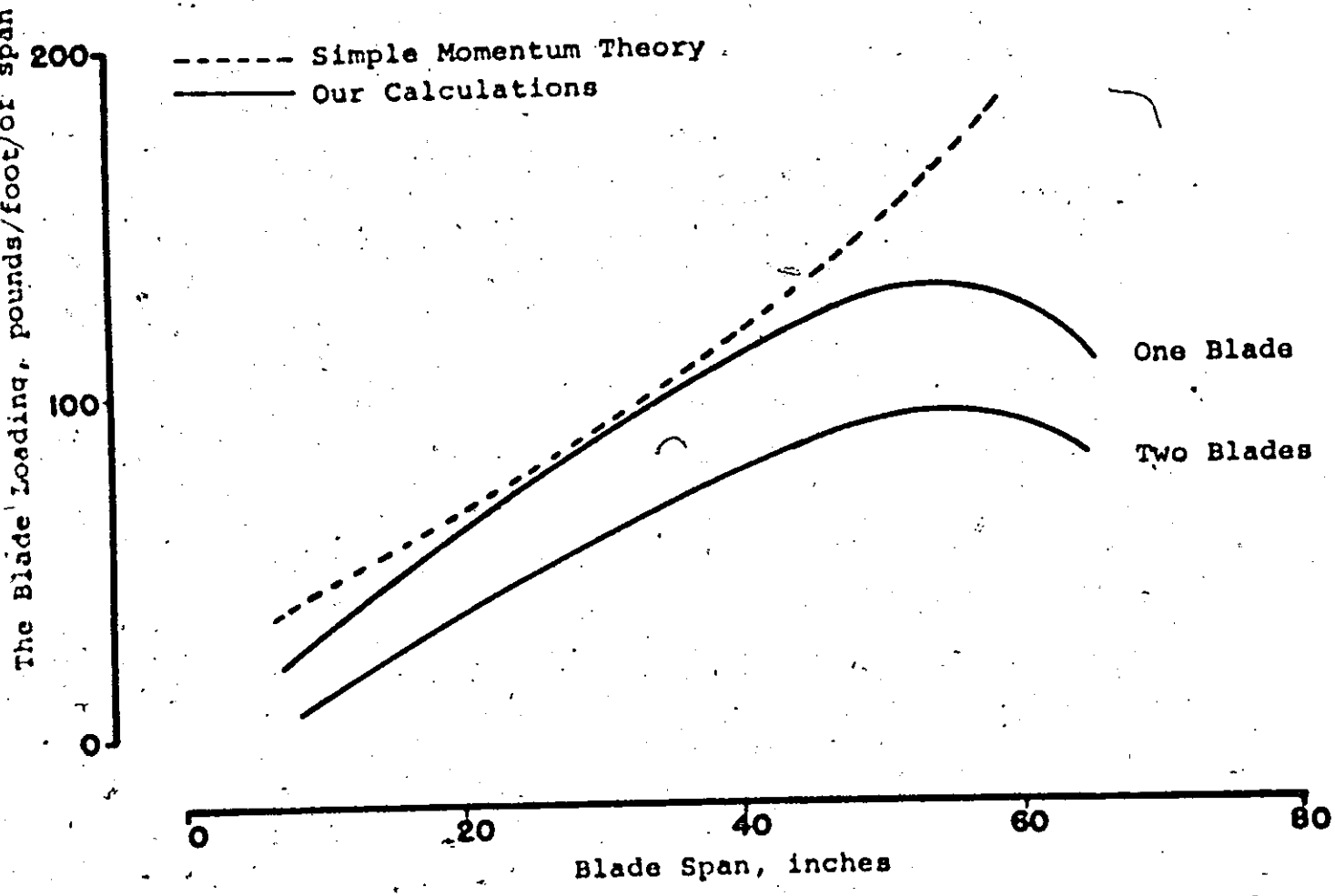

Figure 6:3b: Spanwise Variation of Blade Loading at $\psi = 90°$

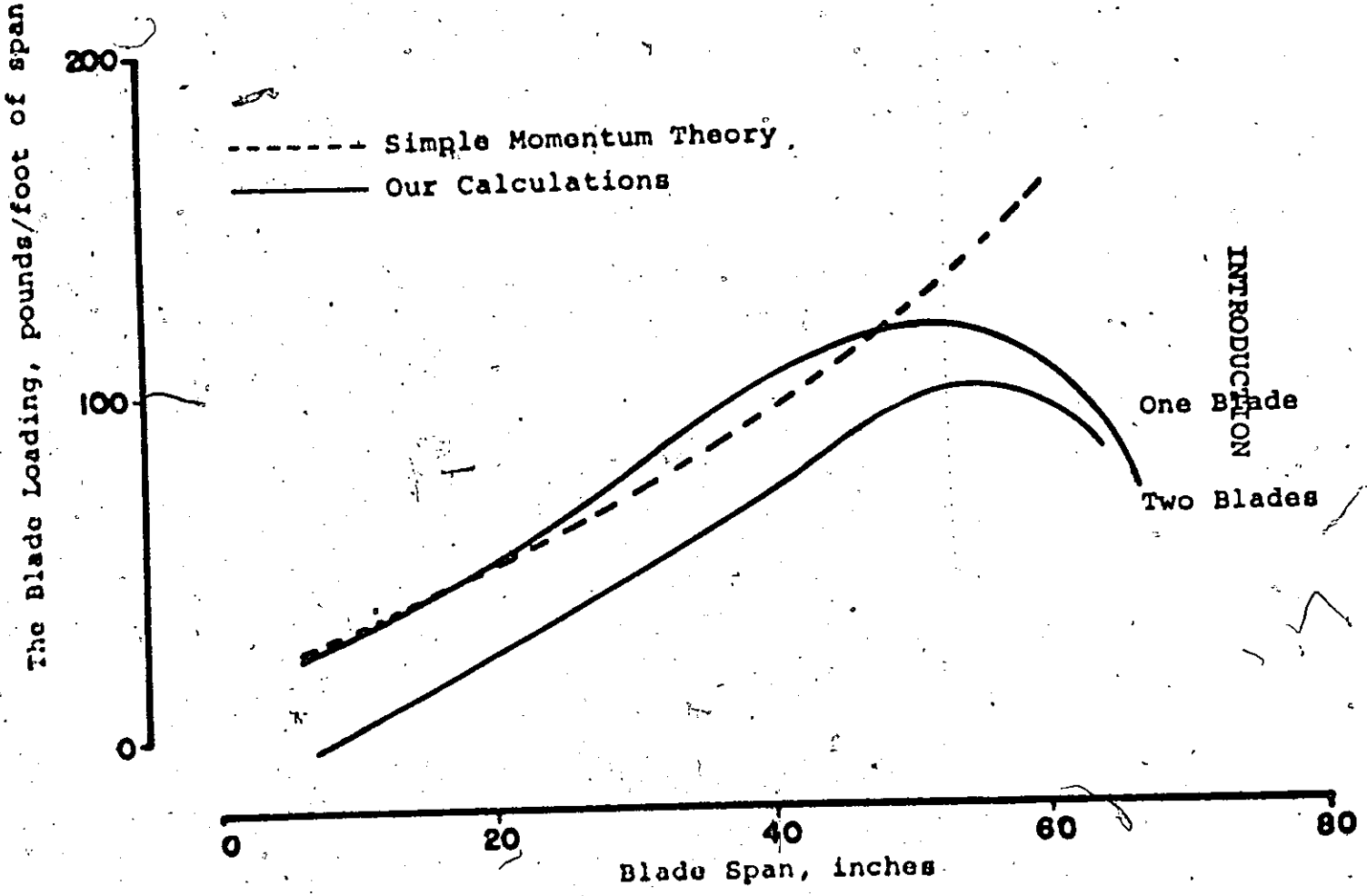

Figure 6.3c: Spanwise Variation of Blade Loading at $\psi = 135°$

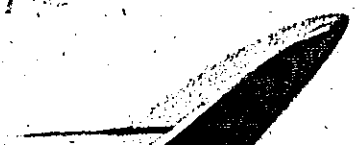

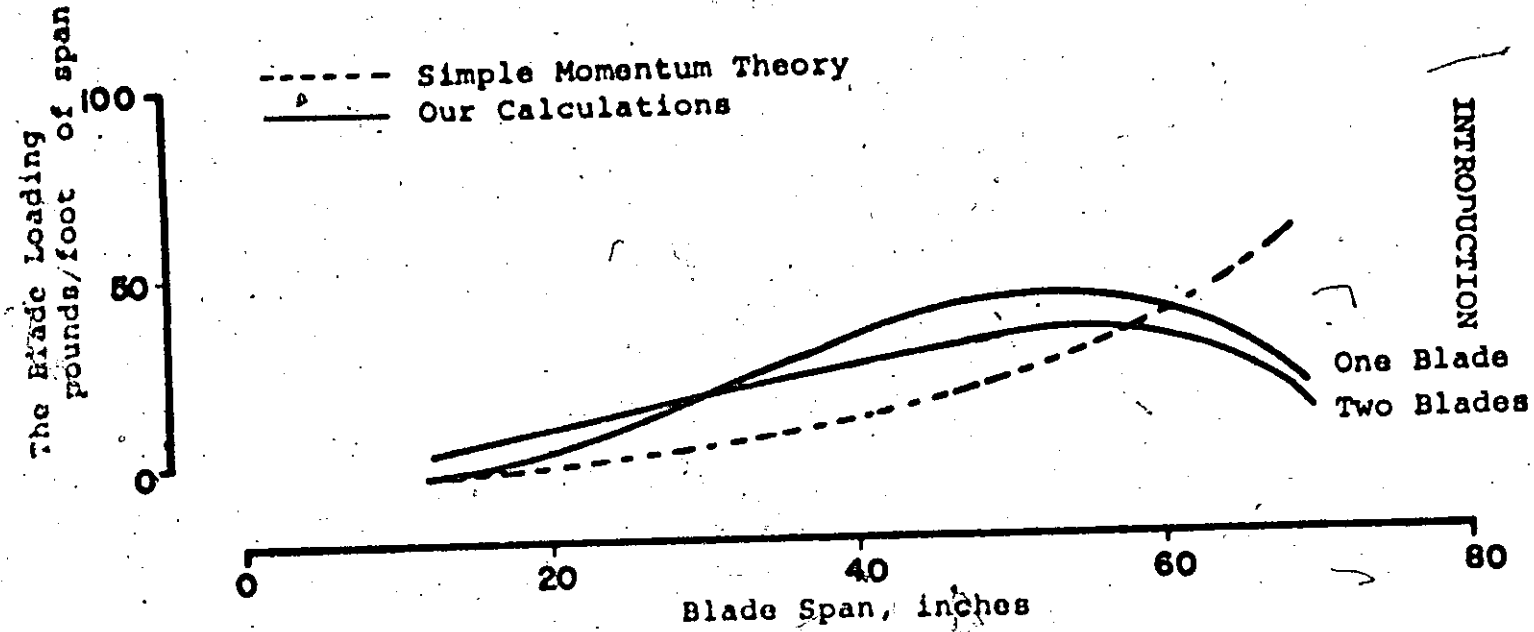

Figure 6.3d: Spanwise Variation of Blade Loading at $\psi = 270°$

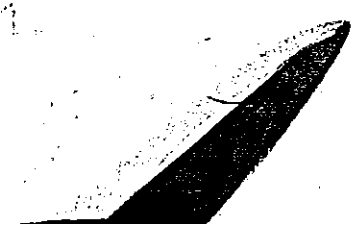

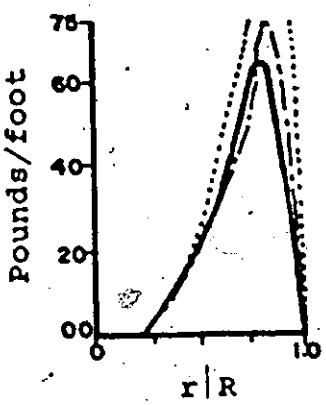

Zeroth Harmonic

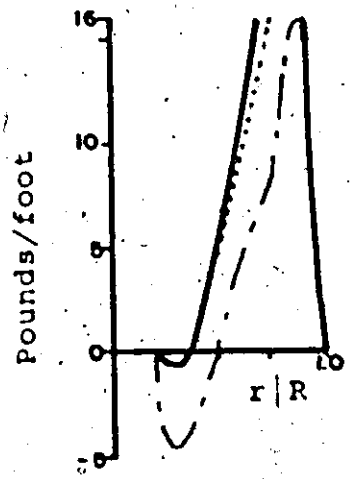

First Cosine Harmonic

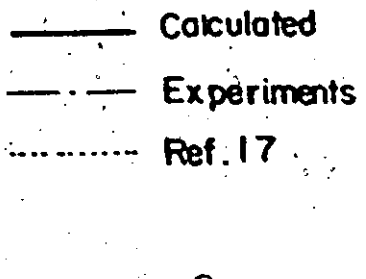

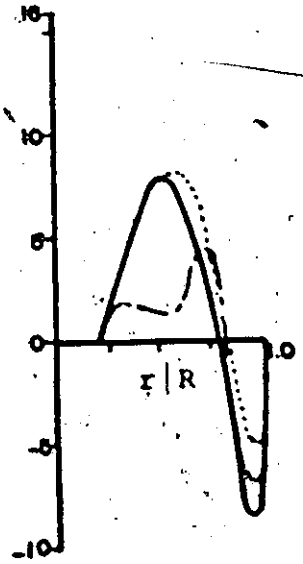

First Sine Harmonic

Figure 6.4a: Spanwise Distribution of Harmonics, with Three Azimuth Terms

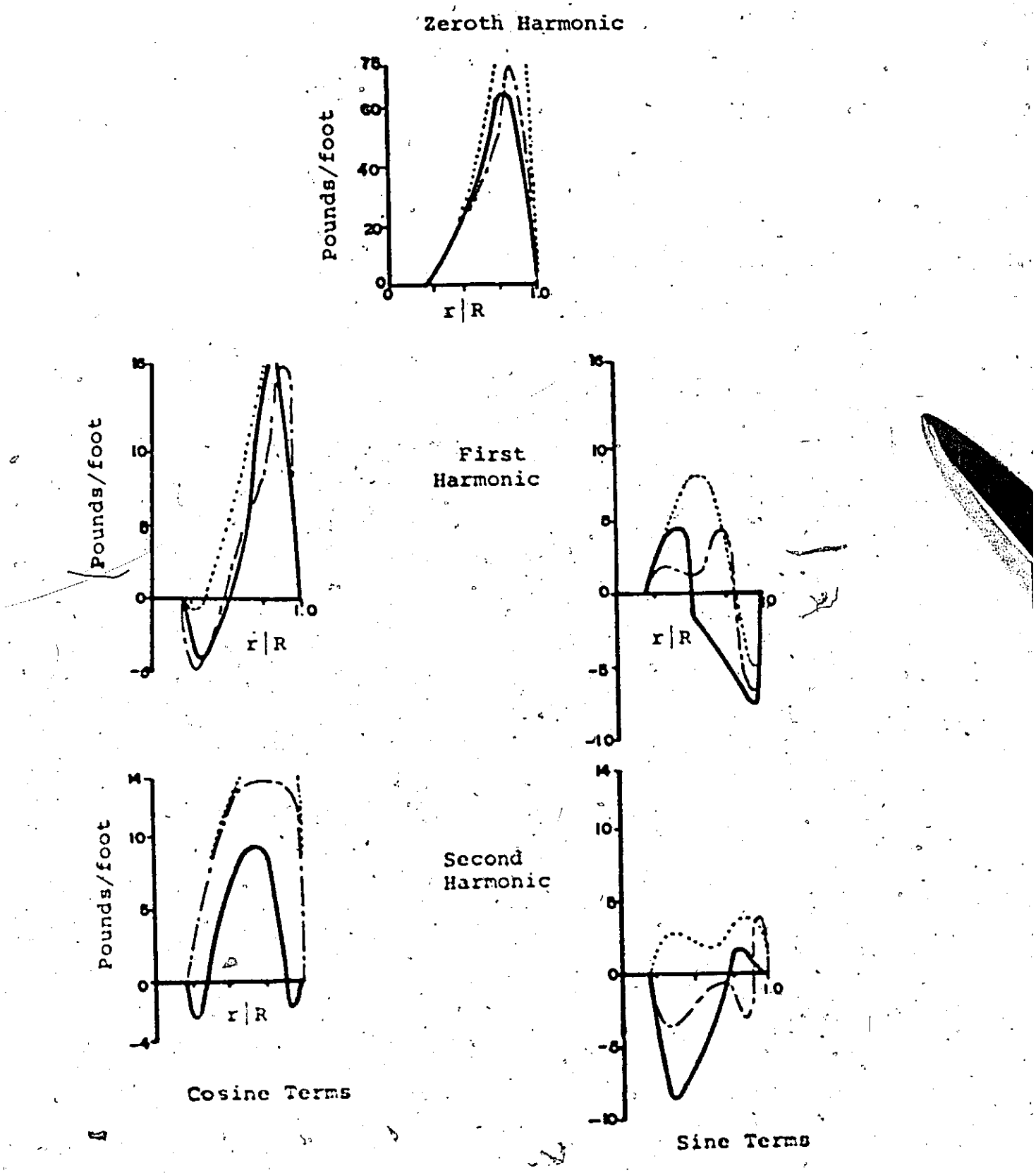

Figure 6.4b: Spanwise Distribution of Harmonics, with Five Azimuth Terms

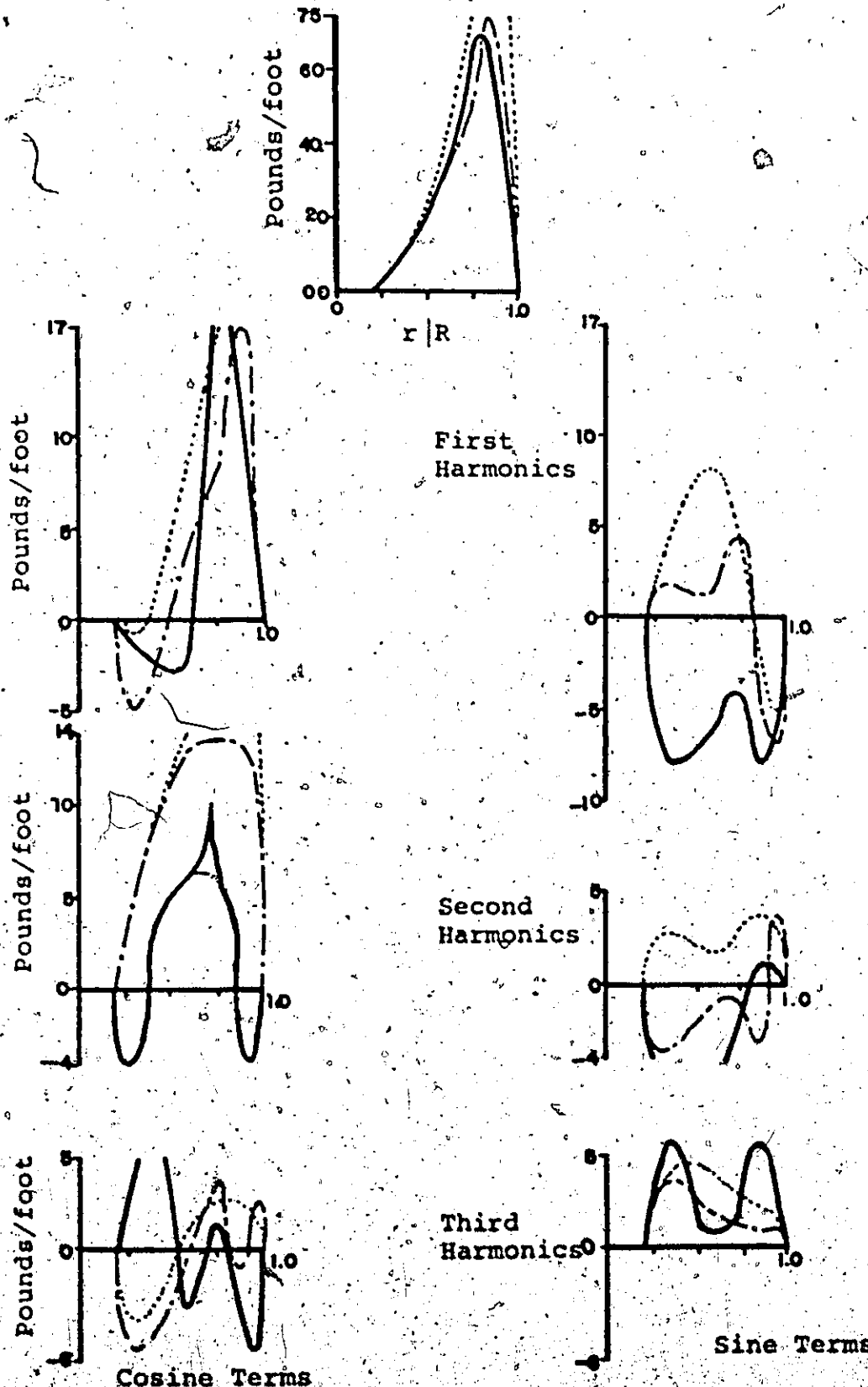

Figure 6.4c: Spanwise Distribution of Harmonics, with Seven Azimuth Terms

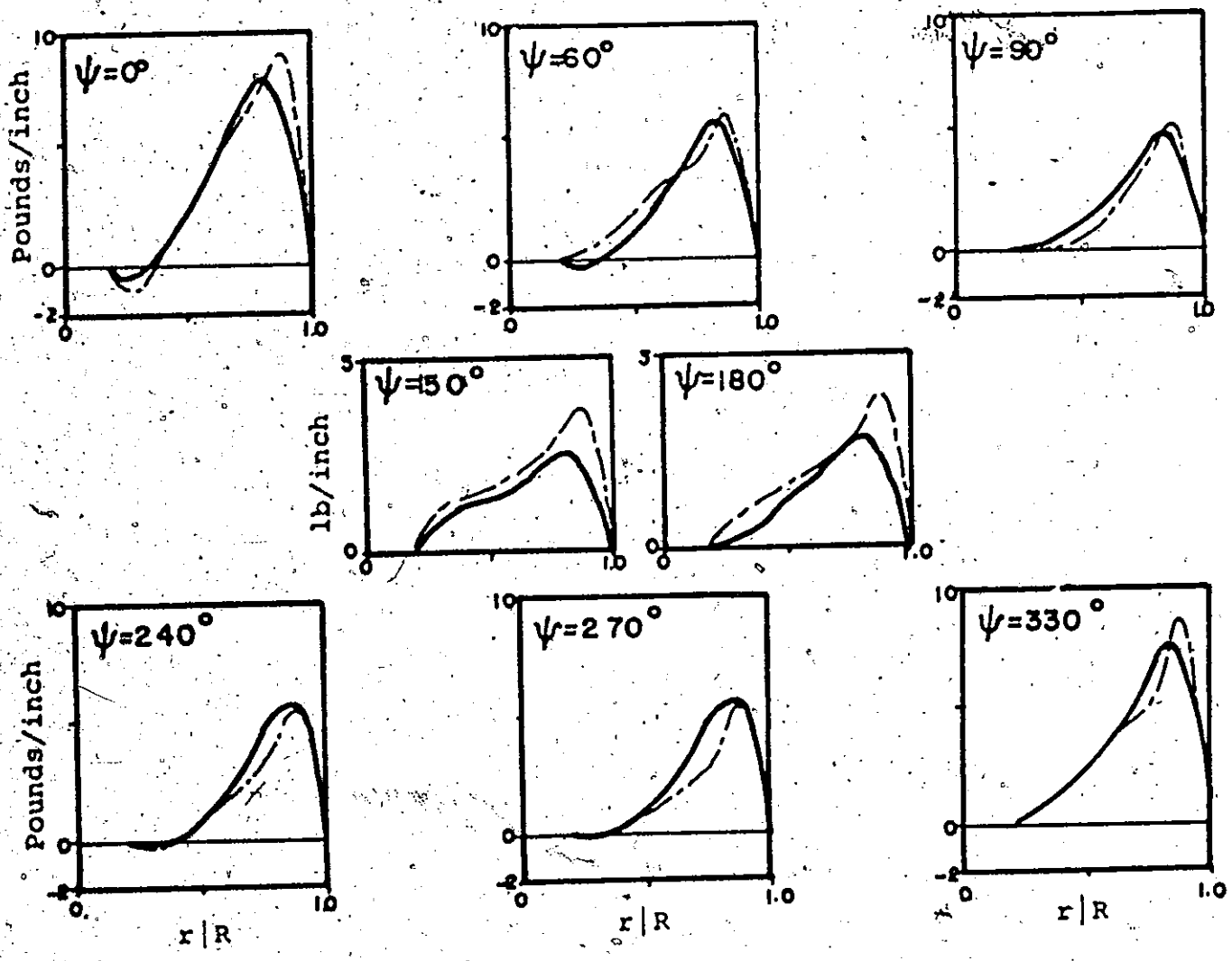

Figure 6.5: Spanwise Variation of Loading Over the Blade Span at Various Azimuth Positions.

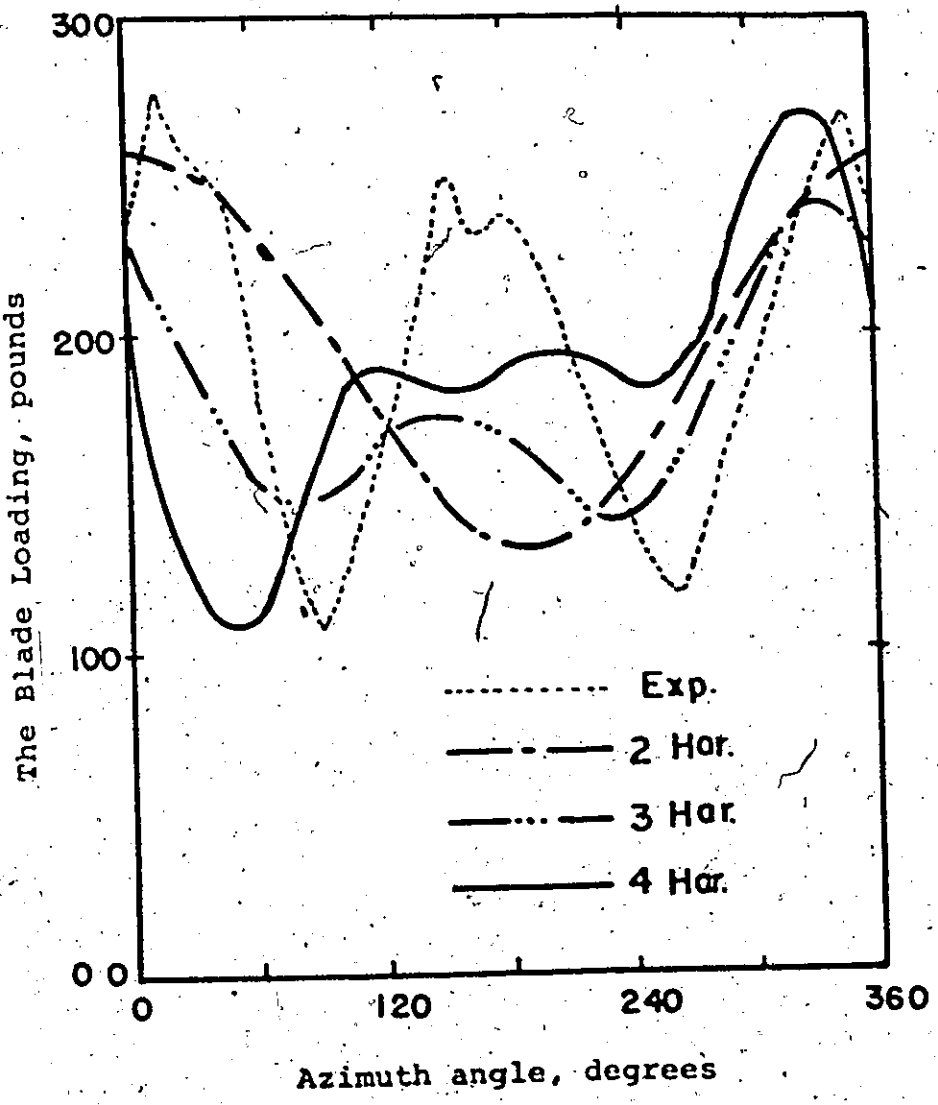

Figure 6.6: Total Blade Loading Around Azimuth

REFERENCES

1. Glauert, H.,"Airplane propellers", Vol. 4, Div. L. Aerodynamic Theory, ed. W. F. Durand, 1935.

2. Glauert, H. "A general theory of the autogyro" R & M No. 1111, 1926. Aeronautical Research Council, England.

3. Payne, P.R., "Helicopter dynamics and aerodynamics", Sir Isaac Pitman & Sons, 1956.

4. Coleman, R.P., Feingold, A.M., Steinpin, C. W., "Evaluation of induced velocity field of an idealized helicopter rotor", NACA ARR No L5E10, 1945.

5. Castles, W., DeLeew, H.J., "The normal component of induced velocity in the vicinity of a lifting rotor and some examples of its applications", NACA TN 21912, 1953.

6. Rainey, G.A., "Measurement of aerodynamic forces for various mean angles of attack on an airfoil oscillating in pitch and on two finite span wings oscillating in bending with emphasis on damping in the stall" NACA TN 3643 May, 1956.

7. Ham. N. D., Young, M.I., "Torsional oscillations of helicopter blades due to stall", J. of Aircraft, Vol. 3, No. 3, 1966.

8. Carta, F. O., Ham, N.D., "An analysis of stall flutter instability of helicopter rotor blades". AHS-forum No 130, May 1967.

9. Liiva, J., "Unsteady aerodynamic and stall effects on helicopter rotor blade airfoil sections", AIAA paper No 68-58 , January 1968.

10. Bislinghoff, R. L., et al., "Aeroelasticity". Addison Wesley Publication Co. Inc. Reading, Massachusetts, 1955.

11. Harris, F.D., "Rotor high speed performance - theory vs test", AHS Journal Vol. 15, No. 3, July 1970 .

12. Harris, F.D., "Preliminary studies of radial flow effects on rotor blades", AHS Journal, Vol. 11, No. 1 1966.

13. Purser, Paul E., Spearman, M., and Leroy, M. "Wind tunnel tests at low speed of swept and yawed wings having various planforms" NACA TN 2445 Dec. 1951.

14. Tanner, W.H. and Wohlfeld, R.M., "New experimental techniques in rotor-craft aerodynamics and their applications", AHS Journal, Vol. 15, No. 2, April 1970.

15. Child, Richard F., "An experimental investigation of an oscillatory airfoil in reverse flow", Paper presented at CAL/AVLABS 1969 Symposium on Aerodynamics of Rotary Wing and VTOL aircraft, June 18-20, 1969.

16. Willmer, M.A.P., "The loading of helicopter rotor blades in forward flight", R & M No. 3318, April 1959, & Aeronautical Research Council, England.

17. Pizialli, R. A., DuWalt, F.A., "A method for computing rotary wing airload distribution in forward flight", Cornell Aero. Lab Report 62-44, 1962.

18. Pizialli, R. A., "A method for predicting the aerodynamic loads and dynamic response of rotor blades", Cornell Aero. Lab. Report 65-74 Jan. 1966.

19. Crimi, P. "Theoretical prediction of the flow in the wake of a helicopter rotor. Part 1 - development of theory and results of computations. Part 2 - formulation and application of rotor-wake-flow computer program". Cornell Aero. Lab Report Nos BB-1994-S-1, BB-1994-S2. Sept. 1965.

20. Tararine, S. "Experimental and theoretical study of local induced velocity over a rotor disc". CAL/TRECOM Symposium proceedings, Vol. 1, June 1963.

21. Miller, R. H. "On the computation of airloads acting on rotor blades in forward flight" AHS Journal, Vol. 5, No. 2, April 1962.

22. Miller, R. H., "Unsteady airloads on helicopter rotor blades", Journal of the Royal Aeronautical Society, Vol. 61, No. 4, April 1964.

23. Miller, R. H., "Rotor blade harmonic air loading", Presented at the IAS 30th Annual Meeting, Paper No. 62-82, New York, 1962.

24. Jones, H. P., "Rotor Aerodynamics - Retrospect and Prospect" AGARD advisory Report 13, Sept. 1967.

25. Yaggy, P.F., "Pure and compound helicopters" AGARDograph No. 126, May 1968.

26. Stark, V.J.E., "Calculation of lifting forces on oscillating wings", Doctoral thesis, 1964, The Royal Institute of Technology, Stockholm.

27. Garner, H. C., "Theoretical calculation of the distribution of aerodynamic loading on a delta wing", R & M, No. 2819, 1949, Aeronautical Research Council, England.

28. Jordan, P.F., "Remarks on applied subsonic lifting surface theory", Technical Report 67-14, August 1967, Martin Marietta Corporation, Baltimore, U.S.A.

29. Multhopp, M. "Methods for calculating the lift distribution of wings (subsonic lifting surface theory)", R & M No. 2884, 1955, Aeronautical Research Council, England.

30. Rabbot, J.P., and Churchill, G.B., "Experimental investigation of the aerodynamic loading on a helicopter rotor blade in forward flight", NACA, RM L56107, 1956.

APPENDIX 1

SINGULAR INFLUENCE FUNCTION

Singular Influence Function $I_{\bar{n}\bar{n}}(o,o,o)$ (Equation 4-8)

1.1 $I^{1}_{\bar{n}\bar{n}}(o,o,o)$ (Equation 4-8a)

(a) Consider n = 1

$$I^{1}_{\bar{n}1}(o,o,o) = \int_{-1}^{+1} (P_{\bar{n}}(-u) + P_{\bar{n}}(u)) \frac{du}{(u^2+\beta^2)^{3/2}}$$

$$I^{1}_{11}(o,o,o) = 2 \left| \frac{u}{\beta^2 (u^2+\beta^2)^{1/2}} \right|_{-1}^{+1}$$

$$= \frac{4}{\beta^2\sqrt{1+\beta^2}}$$

$$= 2\sqrt{2} \text{ , for } \beta^2 = 1.0$$

$$I^{1}_{21}(0,0,0) = 0$$

$$I^{1}_{31}(o,o,o) = \int_{-1}^{+1} (3u^2 - 1) \frac{du}{(u^2+\beta^2)^{3/2}}$$

$$= 3 \int_{-1}^{+1} \frac{u^2 du}{(u^2+\beta^2)^{3/2}} - \frac{I^{1}_{11}}{2}$$

$$= 3 \left| \log_e (u + \sqrt{u^2+\beta^2}) - \frac{u}{(u^2+\beta^2)^{1/2}} \right|_{-1}^{+1} - \frac{2}{\beta^2\sqrt{1+\beta^2}}$$

$$= 3 \left(\log_e \left(\frac{1+\sqrt{1+\beta^2}}{-1+\sqrt{1+\beta^2}} \right) - \frac{2}{\sqrt{1+\beta^2}} \right) - \frac{2}{\beta^2\sqrt{1+\beta^2}}$$

$$= 3 \log_e (3 + 2\sqrt{2}) - 4\sqrt{2}, \text{ for } \beta^2 = 1.0$$

(b) Consider n = 2

$$I^1_{n2}(o,o,o) = \int_{-1}^{+1} \left(P_{\bar{n}}(-u) - P_{\bar{n}}(u)\right) \frac{du}{(u^2+\beta^2)^{3/2}}$$

Therefore

$$I^1_{12}(o,o,o) = 0.0$$

$$I^1_{22}(o,o,o) = -2 \int_{-1}^{+1} \frac{u}{(u^2+\beta^2)^{3/2}}\, du$$

$$= 2 \left| \frac{1}{(u^2+\beta^2)^{1/2}} \right|_{-1}^{+1}$$

$$= 0.0$$

$$I^1_{32}(o,o,o) = 0.0$$

(c) Consider n = 3

$$I^1_{n3}(o,o,o) = \int_{-1}^{+1} \{P_{\bar{n}}(u) + P_{\bar{n}}(-u)\} \frac{du}{(u^2+\beta^2)^{3/2}}$$

$$= I^1_{n1}(o,o,o)$$

1.2 $I^2_{nn}(o,o,o)$ (Equation 4.8b)

$$I^2_{nn}(o,o,o) = \int_{-1}^{+1} \{P_{\bar{n}}(1)P_n(v) + P_{\bar{n}}(-1)P_n(-u)\} \frac{dv}{(1+\beta^2 v^2)^{3/2}}$$

$$= \frac{1}{\beta^3} \int_{-1}^{+1} \{P_{\bar{n}}(1)P_n(v) + P_{\bar{n}}(-1)P_n(-v)\} \frac{dv}{\left(v^2+\frac{1}{\beta^2}\right)^{3/2}}$$

(a) Consider n = 1

$$I^2_{n1}(o,o,o) = \frac{1}{\beta^3}\int_{-1}^{+1} (P_n(1) + P_n(-1)\frac{dv}{(v^2+\frac{1}{\beta^2})^{3/2}}$$

$$= \frac{P_n(1)+P_n(-1)}{\beta^3}\int_{-1}^{+1}\frac{dv}{(v^2+\frac{1}{\beta^2})^{3/2}}$$

$$= \frac{P_n(1)+P_n(-1)}{\beta^3}\left|\frac{v}{\frac{1}{\beta^2}(v^2+\frac{1}{\beta^2})^{1/2}}\right|_{-1}^{+1}$$

$$= (P_n(1) + P_n(-1))\frac{2}{(1+\beta^2)^{1/2}}$$

Therefore

$$I^2_{11}(o,o,o) = \frac{4}{\sqrt{1+\beta^2}} = 2\sqrt{2}, \quad \text{for } \beta^2 = 1.0$$

$$I^2_{21}(o,o,o) = 0.0$$

$$I^2_{31}(o,o,o) = \frac{4}{\sqrt{1+\beta^2}} = 2\sqrt{2}\ , \text{ for } \beta^2 = 1.0.$$

(b) Consider n = 2

$$I^2_{n2}(o,o,o) = \frac{1}{\beta^3}\int_{-1}^{+1} v(P_n(1) + P_n(-1))\frac{dv}{(v^2+\frac{1}{\beta^2})^{3/2}}$$

Therefore

$$I^2_{12}(o,o,o) = 0.0$$

$$I^2_{22}(o,o,o) = 0.0$$

$$I^2_{32}(o,o,o) = 0.0$$

(c) Consider n = 3

$$I^2_{n3}(o,o,o) = \frac{1}{\beta^3}\int_{-1}^{+1} (P_n^-(1) + P_n^-(-1)) \frac{(3\frac{v^2-1}{2})}{(v^2+\frac{1}{\beta^2})^{3/2}}\, dv$$

$$= \frac{P_n^-(1)+P_n^-(1)}{2\beta^3}\Bigg| 3\left(\log_e \frac{\beta+\sqrt{1+\beta^2}}{-\beta+\sqrt{1+\beta^2}} - \frac{2\beta}{(1+\beta^2)^{1/2}}\right)$$

$$- \frac{2}{\frac{1}{\beta^3}(1+\beta^2)^{1/2}}\Bigg|$$

Therefore

$$I^2_{13}(o,o,o) = \frac{3}{\beta^3} \log_e \frac{\beta+\sqrt{1+\beta^2}}{-\beta+\sqrt{1+\beta^2}} - \frac{6}{\beta^2\sqrt{1+\beta^2}} - \frac{2}{\sqrt{1+\beta^2}}$$

$$= 3 \log_e(3+2\sqrt{2}) - 4\sqrt{2}, \text{ for } \beta = 1.0$$

and

$$I^2_{23}(o,o,o) = 0.0$$

$$I^2_{33}(o,o,o) = I^2_{13}(o,o,o)$$

$$= 3 \log_e(3+2\sqrt{2}) - 4\sqrt{2}, \text{ for } \beta = 1.0$$

1.3 $I^3_{\bar{n}n}(o,o,o)$ (Equation 4.8c)

$$I^3_{\bar{n}n}(o,o,o) = \int_{-1}^{+1}\int_{-1}^{+1} \left(uP_n(v)\ \frac{\partial}{\partial u}\ P_{\bar{n}}(u) + vP_{\bar{n}}(u)\ \frac{\partial}{\partial v}\ P_n(v)\right)\ \frac{dudv}{r^3}$$

(a) Consider n = 1

$$I^3_{\bar{n}1}(o,o,o) = \int_{-1}^{+1}\int_{-1}^{+1} u\ \frac{\partial}{\partial u}\ P_{\bar{n}}(u)\ \frac{dudv}{r^3}$$

Therefore

$$I^3_{11}(o,o,o) = 0.0$$

$$I^3_{21}(o,o,o) = \int_{-1}^{+1}\int_{-1}^{+1} \frac{u\ dudv}{(u^2+\beta^2v^2)^{3/2}}$$

$$= 0.0$$

$$I^3_{31}(o,o,o) = \int_{-1}^{+1}\int_{-1}^{+1} \frac{3u^2\ dudv}{(u^2+v^2\beta^2)^{3/2}}$$

$$= 3\left|\left|\ v\ \log_e\left(u + \sqrt{u^2+\beta^2v^2}\right)\right|_{-1}^{+1}\right|_{-1}^{+1}$$

$$= 6\ \log_e \frac{1+\sqrt{1+\beta^2}}{-1+\sqrt{1+\beta^2}}$$

$$= 6\ \log_e(3+2\sqrt{2}), \quad \text{for } \beta^2 = 1.0$$

(b) Consider n = 2

$$I^3_{\bar{n}2}(o,o,o) = \int_{-1}^{+1}\int_{-1}^{+1} \left(uv\ \frac{\partial}{\partial u}\ P_{\bar{n}}(u) + vP_{\bar{n}}(u)\right)\frac{dudv}{r^3}$$

$$\equiv 0.0$$

(c) Consider n = 3

$$I^3_{n3}(o,o,o) = \int_{-1}^{+1}\int_{-1}^{+1} \left(u\left(\frac{3v^2-1}{2}\right) \frac{\partial}{\partial u} P_n^-(u) + vP_n^-(u)\,(3v)\right) \frac{dudv}{r^3}$$

$$= \int_{-1}^{+1}\int_{-1}^{+1} \left(\frac{3}{2}uv^2 - \frac{u}{2}\right) \frac{\partial}{\partial u} P_n^-(u) + 3v^2 P_n^-(u) \frac{dudv}{r^3}$$

$$= \int_{-1}^{+1}\int_{-1}^{+1} \left[-\frac{u}{2}\frac{\partial}{\partial u} P_n^-(u) + 3v^2 P_n^-(u)\right] \frac{dudv}{r^3} + \frac{3}{2}uv^2 \frac{\partial}{\partial u} P_n^-(u) \frac{dudv}{r^3}$$

Therefore,

$$I^3_{13}(o,o,o) = \int_{-1}^{+1}\int_{-1}^{+1} \frac{3v^2 dudv}{r^3}$$

$$= 3\left|\left|\frac{u}{\beta^3} \log_e \left(\sqrt{u^2+\beta^2v^2} + \beta v\right)\right|_{-1}^{+1}\right|_{-1}^{+1}$$

$$= \frac{6}{\beta^3} \log_e \frac{\beta+\sqrt{1+\beta^2}}{-\beta+\sqrt{1+\beta^2}}$$

$$= 6 \log_e (3+2\sqrt{2}), \quad \text{for} \quad \beta^2 = 1$$

$$I_{23}^{3}(o,o,o) = 0.0$$

$$I_{33}^{3}(o,o,o) = \int_{-1}^{+1}\int_{-1}^{+1} \left[-\frac{3}{2}u^2 + 3v^2\left(\frac{3u^2-1}{2}\right) + \frac{3}{2}uv^2(3u)\right]\frac{dudv}{r^3}$$

$$= -\frac{3}{2}\int_{-1}^{+1}\int_{-1}^{+1}\frac{u^2dudv}{r^3} + 9\int_{-1}^{+1}\int_{-1}^{+1}\frac{u^2v^2dudv}{r^3}$$

$$-\frac{3}{2}\int_{-1}^{+1}\int_{-1}^{+1}\frac{v^2dudv}{r^3}$$

$$= -3\log_e\frac{1+\sqrt{1+\beta^2}}{-1+\sqrt{1+\beta^2}} - \frac{3}{\beta^2}\log_e\frac{\beta+\sqrt{1+\beta^2}}{-\beta+\sqrt{1+\beta^2}}$$

$$+ 9\,\frac{2}{3}\left(\frac{1}{\beta^2}\log_e\frac{\beta+\sqrt{1+\beta^2}}{-\beta+\sqrt{1+\beta^2}} + \log_e\frac{1+\sqrt{1\beta^2}}{-1+\sqrt{1+\beta^2}}\right.$$

$$\left.-\frac{2}{\beta^2}\sqrt{1+\beta^2}\right)$$

$$= 3\left[\frac{1}{\beta^2}\log_e\frac{\beta+\sqrt{1+\beta^2}}{-\beta+\sqrt{1+\beta^2}} + \log_e\frac{1+\sqrt{1+\beta^2}}{-1+\sqrt{1+\beta^2}}\right.$$

$$\left.-\frac{2}{\beta^2}\sqrt{1+\beta^2}\right]$$

$$= 6\log_e(3+2\sqrt{2}) - 2\sqrt{2}\,, \quad \text{for} \quad \beta^2 = 1.0$$

APPENDIX 2

THE COMPUTER PROGRAMS

Various computer programs used in this thesis are reproduced in the following pages. Below is the list of these programs.

(1) Calculate non-singular influence function

Typical Running Time: 30 seconds, $n = \bar{n} = 1,2,3$.

(2) Calculate generalised Fourier coefficients

Typical Running Time: 40 seconds, $n = \bar{n} = 1,2,3$.

(3) Obtain $(\omega_x)_{NS}$ for inner grid

Typical Running Time: 30 seconds, $n = \bar{n} = 1$.

(4) Obtain $(\omega_x)_{NS}$ for outer grid

Typical Running Time: 30 seconds, $n = \bar{n} = 1$.

(5) Integrate along Trajectories to obtain ω_{NS}.

Typical Running Time: (for one pivot point):

9 seconds for one blade, 3 seconds for additional blade.

(6) Integrate along the trajectories to obtain ω_S

Typical Running Time (for one pivot point) : 6 seconds for two blades.

(7) Obtain boundary conditions

Typical Running Time: 15 seconds.

(8) Solve the integral set of linear algebraic equations and obtain blade loadings

Typical Running Time: 400 seconds for 35 loading coefficients.

(9) Obtain the blade loadings using the strip theory with uniform downwash

Typical Running Time: 15 seconds.

COMPUTER PROGRAM LISTING NO. 1

```
      DIMENSION ZINF1(9),PI(3,9),ZKER(9,9),ZINF2(16,33,9),ZINF(3,3)
      FLAGK=0.0
      FLAGIF=1.0
      FLAGIF=0.0
      FLAGPI=0.0
      DATA
      WING DIMENSION
      SPAN=73.5/12.0
      CHORD=14.0/12.0
      CEXT=1.5*CHORD
      SEXT=1.5*CHORD
      BOX SIZE
      DELTA=3.5/2.0/12.0
      NCEXT=IFIX(CEXT/(2.0*DELTA))
      NSEXT=IFIX(SEXT/(2.0*DELTA))
      ZMACH=0.0
      ZMACH=0.6
      BETA=SQRT(1.0-ZMACH*ZMACH)
      NNBP=3
      NNP=3
      NPT=NNP*NNBP
      GRID SIZE IN BOX----FOR  INFLUENCE FUNCTIONS
      NINF=5
      NINF=9

      TOTAL NUMBER OF SPANWISE STATIONS
      NMUS=IFIX((SPAN+2.0*SEXT)/(2.0*DELTA))
      TOTAL NUMBER OF CHORDWISE STATIONS
      NMUC=IFIX((CHORD+2.0*CEXT)/(2.0*DELTA))
      TATAL NUMBER OF SPANWISE STATIONS ON THE WING
      NNUS=IFIX(SPAN/(2.0*DELTA))
      TOTAL NUMBER OF CHORDWISE STATIONS ON THE WING
      NNUC=IFIX(CHORD/(2.0*DELTA))

      DO 83 K=1,NMUC
      DO 83 J=1,NMUS
      DO 82 KK=1,NPT
   82 ZINF2(K,J,KK)=0.0
   83 CONTINUE

      CONTRIBUTION TO WX FROM EACH SQUARE BOX
      DO 1 INU=1,NNUC
      XW=DELTA*(INU-1)*2.0*DELTA
      IF((FLAGIF.EQ.0.0).AND.(INU.GT.1)) GO TO 1
      MUCR=NCEXT+INU
      DO 2 JNU=1,NNUS
      IF((FLAGIF.EQ.0.0).AND.(JNU.NE.NNUS)) GO TO 2
      YW=-SPAN/2.0+DELTA*(JNU-1)*2.0*DELTA
```

```
      MUSR=NSEXT+JNU
      WRITE(6,100) XW,YW
      WRITE(6,999)
      WRITE(6,999)


C     CHOOSE THE POINT WHERE WX IS TO EVALUATED
      DO 91 I=1,NNP
      DO 91 J=1,NNBP
      ZINF(I,J)=0.0
      DO 21 MUC=1,NMUC
      IF((FLAGIF.EQ.0.0).AND.(MUC.LT.(NCEXT+1))) GO TO 21
      XMU=-CEXT+DELTA+(MUC-1)*2.0*DELTA
      SIGNX=1.0
      IF(MUC.LT.MUCB) SIGNX=-1.0
      DO 20 MUS=1,NMUS
      IF(MUS.GT.MUSB) GO TO 20
      YMU=-SPAN/2.0-SEXT +DELTA+(MUS-1)*2.0*DELTA
      SIGNY=1.0
      IF(MUS.LT.MUSB) SIGNY=-1.0

      IX=IABS(MUC-INU-NCEXT)
      IY=IABS(MUS-JNU-NSEXT)
      IF((IX.EQ.0).AND.(IY.EQ.0)) GO TO 20
      IX1=IX+1
      IY1=IY+1


C     CALCULATE THE KERNAL AT THE GRID POINTS
      DO 36 I=1,NINF
      YWV=YW-DELTA+(I-0.5)*2.0*DELTA/NINF
      DO 35 J=1,NINF
      XWV=XW-DELTA+(J-.5)*2.0*DELTA/NINF
      ZKER(J,I)=1./((((XMU-XWV)*(XMU-XWV)+BETA*BETA*(YMU-YWV)*(YMU-YWV))
     )**1.5)
C     THE CORRESSPONDING POLYNOMIALS
      IF(FLAGPI.NE.0.0) GO TO 37
      U=-1.0+(2.0*J-1)/NINF
      PI(1,J)=1.0
      PI(2,J)=U
      PI(3,J)=(3.0*U*U-1.0)/2.0
      WRITE(6,105) (PI(IP,J),IP=1,3)
   37 CONTINUE
   36 CONTINUE
      FLAGPI=2.0
   35 CONTINUE
      IF(FLAGK.EQ.0.0) WRITE(6,104) ZKER
      FLAGK=1.0
   20 CONTINUE


C     SUMMATION OVER VARIOUS DEGREES OF THE POLYNOMIAL
      DO 26 NP=1,NNP
```

```
      DO 25 NBP=1,NNBP
      NPP=NBP+(NP-1)*3

      INFLUENCE COEFFICIENT
      DO 92 I=1,NINF
   92 ZINF1(I)=0.0
      DO 41 I=1,NINF
      DO 40 J=1,NINF
      ZINF1(I)=ZINF1(I)+ZKER(I,J)*PI(NP ,J)
   40 CONTINUE
   41 CONTINUE
      ZINF(NP,NBP)=0.0
      DO 42 I=1,NINF
      ZINF(NP,NBP)=ZINF(NP,NBP)+ZINF1(I)*PI(NBP,I)
   42 CONTINUE
      ZINF(NP,NBP)=ZINF(NP,NBP)*4.0/(NINF*NINF)
      ZINF2(IX1,IY1,NPP)=ZINF(NP,NBP)
      IF(FLAGIF.EQ.0.0) WRITE(6,109) IX1,IY1,ZINF(NP,NBP),NPP
      IF(NBP.EQ.2)   ZINF2(IX1,IY1,NPP)=ZINF2(IX1,IY1,NPP)*SIGNX
      IF(NP .EQ.2)   ZINF2(IX1,IY1,NPP)=ZINF2(IX1,IY1,NPP)*SIGNY
   25 CONTINUE
   26 CONTINUE
      IF(FLAGIF.EQ.0.0) WRITE(7,202) IX1,IY1,ZINF2(IX1,IY1,1)
      IF(FLAGIF.EQ.0.0) WRITE(7,203)(ZINF2(IX1,IY1,N),N=2,9)
   30 CONTINUE
   31 CONTINUE
    2 CONTINUE
    3 CONTINUE
  100 FORMAT(1H1,10X,3HXW=,F10.4,10X,3HYW=,F10.4)
  104 FORMAT(10X,4HZKER,   5F15.9)
  105 FORMAT(10X,2HPI,5X,3F10.4)
  109 FORMAT(10X,*IX*,5X,I3,10X,*IY*,5X,I3,10X,*ZINF*,5X,F10.4,10X,I3)
  201 FORMAT(I3,5X,I3,5X,F15.8)
  203 FORMAT(4F15.8)
  300 FORMAT(10X,2H   )
      STOP
      END
```

CD TOT 0144

COMPUTER PROGRAM LISTING NO. 2

```
      DIMENSION COEC(5),COES(5),COE(19,19,5 ),PA(3,19),COEX(21,5 ),
     1ALPHA(3,3,5)

C     THIS PROGRAM CALCULATES ALPHA

      PIE=4.0*ATAN(1.0)
      LOOUT=0

      DATA
      WING DIMENSION
      SPAN=73.5/12.0
      CHORD=14.0/12.0
      CEXT=1.5*CHORD
      SEXT=1.5*CHORD
      BOX SIZE
      DELTA=3.5/2.0/12.0
      NCEXT=CEXT/(2.0*DELTA)
      NSEXT=SEXT/(2.0*DELTA)
      NBOD=3
      NWD=3

C     LOADING COEFFICIENTS
      CHORDWISE
      NLC=2
      NLC=1
      SPANWISE
      NLS=1
      NLS=5
      NL=NLC*NLS


C     TOTAL NUMBER OF SPANWISE STATIONS
      NNUS=IFIX((SPAN+2.0*SEXT)/(2.0*DELTA))
C     TOTAL NUMBER OF CHORDWISE STATIONS
      NNUC=IFIX((CHORD+2.0*CEXT)/(2.0*DELTA))
      TATAL NUMBER OF SPANWISE STATIONS ON THE WING
      NNUS=IFIX(SPAN/(2.0*DELTA))
      TOTAL NUMBER OF CHORDWISE STATIONS ON THE WING
      NNUC=IFIX(CHORD/(2.0*DELTA))
      NDT=NWD*NWD


C     CONTRIBUTION TO WX FROM EACH SQUARE BOX
      DO 1 INU=1,NNUC
```

```
NALP=7
IF(INU.EQ.1) GO TO 1
IF(INU.EQ.1) NALP=19
XW=DELTA+(INU-1)*2.0*DELTA
DO 2 JNU=1,NNUS
YW=-SPAN/2.0+DELTA+(JNU-1)*2.0*DELTA
WRITE(6,100) XW,YW
WRITE(6,999)
WRITE(6,999)
```

```
THE LOAD MATRIX IS CALCULATED
NR=1
RN=NR
DELTAE=DELTA/RN
FLAGPA=0.0

XWW=XW
YWW=YW
NALP=NALP
DELALP=DELTAE/NALP
CORRESPONDING LOAD MATRIX
XWBOX=XWW-DELTAE-DELALP
DO 11 I=1,NALP
XWBOX=XWBOX+2.0*DELALP
PHI=ACOS((-2.0*XWBOX+CHORD)/CHORD)
CHORDWISE LOADING FUNCTIONS
COEC(1)=COS(PHI/2.0)/SIN(PHI/2.0)
IF(NLC.EQ.1) GO TO 4
DO 5 ILC=2,NLC
ZILC=ILC
COEC(ILC)=-SIN(PHI*(ZILC-1.0))
CONTINUE
CONTINUE
YWBOX=YWW-DELTAE-DELALP
DO 10 J=1,NALP
YWBOX=YWBOX+2.0*DELALP
THETA=PIE*(0.5+YWBOX/SPAN)
DO 4 ILS=1,NLS
ZILS=ILS
COES(ILS)=SIN(ZILS*THETA)
CONTINUE
DO 8 K=1,NL
KK=1+(K-1)/NLS
KKK=K-(KK-1)*NLS
COE(1,J,K)=COEC(KK)*COES(KKK)
CONTINUE

THE POLYNOMIAL MATRIX FOR FOURIER COEFFICIENTS
IF(FLAGPA.NE.0.0) GO TO 9
U=-1.0+(2.0*J-1)/NALP
PA(1,J)=1.0
PA(2,J)=U
PA(3,J)=(3.0*U*U-1.0)/2.0
```

```
      CONTINUE
      CONTINUE
      FLAGPA=1.0
   11 CONTINUE
      IF(LDOUT.NE.0) GO TO 66
      WRITE(6,114)
      WRITE(6,999)
      WRITE(6,101) (((COF(I,J,K),K=1,NL),J=1,MALP),I=1,MALP)
      WRITE(6,102) PA
      WRITE(6,999)
      LDOUT=1
   61 CONTINUE
   66 CONTINUE

C     SUMMATION OVER VARIOUS DEGREES OF THE POLYNOMIAL
      DO 26 NP=1,NNP
      DO 25 NRP=1,NNRP
      NRP=NRP+(NP-1)*3

C     OBTAIN THE FOURIER COEFFICIENT
      DO 46 I=1,MALP
      DO 93 KK=1,NL
   93 COFX(I,KK)=0.0
      DO 45 J=1,MALP
      DO 47 K=1,NL
      COFX(I,K)=COFX(I,K)+COF(I,J,K)*PA(NP,J)
   47 CONTINUE
   45 CONTINUE
   46 CONTINUE
      DO 94 KK=1,NL
      ALPHA(NP,NRP,KK)=0.0
   94 CONTINUE
      DO 51 I=1,MALP
      DO 50 K=1,NL
      COFX(I,K)=COFX(I,K)*PA(NRP,I)
      ALPHA(NP,NRP,K)=ALPHA(NP,NRP,K)+COFX(I,K)
   50 CONTINUE
   51 CONTINUE
      DO 53 K=1,NL
      ALPHA(NP,NRP,K)=ALPHA(NP,NRP,K)*(NRP-0.5)*(NP-0.5)*4.0/(MALP*MALP)
   53 CONTINUE
   25 CONTINUE
   26 CONTINUE
      WRITE(6,112) (((ALPHA(I,J,K),K=1,NL),J=1,NRP),I=1,NP)
      WRITE(7,200) (((ALPHA(I,J,K),K=1,NL),J=1,NRP),I=1,NP)
      CONTINUE
      CONTINUE
      FORMAT(1H1,10X,3HXX=,F10.4,10X,3HYY=,F10.4)
      FORMAT(10X,10HLOAD MATRIX,5X,5E20.4)
      FORMAT(10X,3HPA,5X,7E10.6)
  101 FORMAT(10X,5HALPHA,/,5E15.4///)
  114 FORMAT(///20X,15HTHE LOAD MATRIX)
  200 FORMAT(5E14.8)
  999 FORMAT(10X,2H  )
```

```
STOP
END
```

CD TOT 0167

COMPUTER PROGRAM LISTING NO. 3

```
 DIMENSION
1ALPHA(3,3,5)
2,WX(16,33,5),ZINF2(16,33,9)
4,ZINF(3,3)

 THIS PROGRAM CALCULATES WN
 IT READS ALPHA AND ZINF2

 PIE=4.0*ATAN(1.0)
 FLAG6=0.0
 FLAGWX=1.0
 FLAGWX=0.0
 FLAGIR=1.0
 FLAGIR=0.0
 FLAGAR=1.0
 FLAGAR=0.0
 INPP=5
 INPP2=15

 DATA
 WING DIMENSION
 SPAN=33.5/12.0
 CHORD=14.0/12.0
 CEXT=1.5*CHORD
 SEXT=1.5*CHORD
 BOX SIZE
 DELTA=3.5/2.0/12.0
 DELTA3=(2.0*DELTA)**3.0
 NCEXT=IFIX(CEXT/(2.0*DELTA))
 NSEXT=IFIX(SEXT/(2.0*DELTA))
 NRRP=2
 NNP=2
 NNRP=3
 NRP=3

 NNP=1
 NNRP=1

 LOADING COEFFICIENTS
 CHORDWISE
 NLC=2
 NLC=1
 SPANWISE
 NLS=1
 NLS=5
 NL=NLC*NLS
```

```
      TOTAL NUMBER OF SPANWISE STATIONS
      NMUS=IFIX((SPAN+2.0*SEXT)/(2.0*DELTA))
      TOTAL NUMBER OF CHORDWISE STATIONS
      NMUC=IFIX((CHORD+2.0*CEXT)/(2.0*DELTA))
      TATAL NUMBER OF SPANWISE STATIONS ON THE WING
      NNUS=IFIX(SPAN/(2.0*DELTA))
      TOTAL NUMBER OF CHORDWISE STATIONS ON THE WING
      NNUC=IFIX(CHORD/(2.0*DELTA))
      NPT=NNP*NNBP

      DO 83 K=1,NMUC
      DO 83 J=1,NMUS
      DO 82 KK=1,NPT
   82 ZINF2(K,J,KK)=0.0
      DO 83 I=1,NL
      WX(K,J,I)=0.0
   83 CONTINUE
      NMUC1=NMUC-NCEXT
      NMUS1=NMUS-NSEXT
      DO 150 K=1,NMUC1
      DO 150 KK=1,NMUS1
      J=1-KK+NMUS1
      IF(FLAGIP.EQ.0.0) READ(5,202)IX,IY,ZINF2(K,J,1)
      IF(FLAGIP.EQ.0.0) READ(5,203)(ZINF2(K,J,KL), KL=2,9)
  150 CONTINUE


      CONTRIBUTION TO WX FROM EACH SQUARE BOX
      DO 1 INU=1,NNUC
      MUCB=NCEXT+INU
      DO 2 JNU=1,NNUS
      MUSB=NSEXT+JNU
      WRITE(6,999)
      WRITE(6,998)
      WRITE(6,110) INU,JNU

      IF(FLAGAR.EQ.0.0) READ(5,200) (((ALPHA(I,J,K),K=1,NL),J=1,3),
     1I=1,3)

      CHOOSE THE POINT WHERE WX IS TO EVALUATED
      DO 21 MUC=1,NMUC
      SIGNX=1.0
      IF(MUC.LT.MUCB) SIGNX=-1.0
      DO 20 MUS=1,NMUS
      SIGNY=1.0
      IF(MUS.LT.MUSB) SIGNY=-1.0

      IX=IABS(MUC-INU-NCEXT)
      IY=IABS(MUS-JNU-NSEXT)
      IF(IY.EQ.0) GO TO 20
      IX1=IX+1
      IY1=IY+1
```

```
      SUMMATION OVER VARIOUS DEGREES OF THE POLYNOMIAL
      FLAG6=1.0
      FLAG6=0.0
      IF((IX.LT.INPP).AND.(IY.LT.INPP))  FLAG6=1.0
      DO 26 NP=1,NNP
      DO 25 NBP=1,ANBP
      NPP=NBP+(NP-1)*3
      IF(FLAG6.NE.0.0) GO TO 63
      IF(((IX.GT.INPP2).OR.(IY.GT.INPP2)).AND.(NBP.GT.1)) GO TO 27
   63 CONTINUE


      INFLUENCE COEFFICIENT
      ZINF(NP,NBP)=ZINF2(IX1,IY1,NPP)
      IF(NBP.EQ.2) ZINF(NP,NBP)=ZINF(NP,NBP)*SIGNX
      IF(NP .EQ.2) ZINF(NP,NBP)=ZINF(NP,NBP)*SIGNY



      DO 60 K=1,NL
      WX(NUC,NUS,K)=WX(NUC,NUS,K)+ALPHA(NP,NBP,K)*ZINF(NP,NBP)
   60 CONTINUE
   25 CONTINUE
   26 CONTINUE
   27 CONTINUE
      CONTINUE
   21 CONTINUE
      IF(FLAGWX.EQ.0.0) GO TO 65
      DO 64 I=1,NNUC
      DO 64 J=1,NNUS
      DO 64 K=1,NL
      WX(I,J,K)=0.0
   64 CONTINUE
   65 CONTINUE
      CONTINUE
      CONTINUE
      WRITE(6,112)
      DO 10 I=1,NNUC
      DO 10 J=1,NNUS
      WRITE(6,111) I,J,(WX(I,J,K),K=1,NL)
   10 CONTINUE
      IF(FLAGWX.EQ.0.0) WRITE(7,200) (((WX(I,J,K),K=1,NL),J=1,NNUS),
     1I=1,NNUC)
  200 FORMAT(10X,'INU=',2X,I3,5X,'JNU=',2X,I3)
  111 FORMAT(10X,I3,5X,I3,10X,5E10.2)
  112 FORMAT(10X,'NUC',5X,'NUS',20X,'WX(I)',I=1,NL)
      FORMAT(5E14.8)
  113 FORMAT(I3,5X,I3,5X,E15.8)
      FORMAT(4E15.8)
      +-
      STOP
      END
```

COMPUTER PROGRAM LISTING NO. 4

```
      DIMENSION
     1ALPHA(3,3,5)
     2,WX(20,20,5)
     3,ZINF(3,3)

      WN FOR REGION A

      PIE=4.0*ATAN(1.0)
      FLAGK=0.0
      FLAGWX=1.0
      FLAGWX=0.0
      FLAGAR=0.0

      DATA
      WING DIMENSION
      SPAN=73.5/12.0
      CHORD=14.0/12.0
      CEXT=1.5*CHORD
      SEXT=1.5*CHORD
      BOX SIZE
      DELTA=3.5/2.0/12.0
      NCEXT=CEXT/(2.0*DELTA)
      NSEXT=SEXT/(2.0*DELTA)
      NNP=1
      NMRP=1
      ZMACH=0.0
      BETA2=1.0-ZMACH*ZMACH

      LOADING COEFFICIENTS
      CHORDWISE
      NLC=2
      NLC=1
      SPANWISE
      NLS=1
      NLS=5
      NL=NLC*NLS

      TOTAL NUMBER OF SPANWISE STATIONS
      NMUS=20
      TOTAL NUMBER OF CHORDWISE STATIONS
      NMUC=20
      TATAL NUMBER OF SPANWISE STATIONS ON THE WING
      NNUS=IFIX(SPAN/(2.0*DELTA))
      TOTAL NUMBER OF CHORDWISE STATIONS ON THE WING
      NNUC=IFIX(CHORD/(2.0*DELTA))
```

```
      NPT=NNP*NNBP

      DO 83 K=1,NMUC
      DO 83 J=1,NMUS
      DO 83 I=1,NL
      WX(K,J,I)=0.0
   83 CONTINUE


C     CONTRIBUTION TO WX FROM EACH SQUARE BOX
      DO 1 INU=1,NNUC
      XW=DELTA+(INU-1)*2.0*DELTA
      DO 2 JNU=1,NNUS
      YW=-SPAN/2.0+DELTA+(JNU-1)*2.0*DELTA
      WRITE(6,110) INU,JNU
      WRITE(6,999)

      IF(FLAG2.EQ.0.0) READ(5,200)(((ALPHA(I,J,K),K=1,NL),J=1,3),
     1I=1,3)

C     CHOOSE THE POINT WHERE WX IS TO EVALUATED
      XMU=-147.0/12.0
      DO 21 MUC=1,NMUC
      XMU=XMU+14.0/12.0
      YMU=-21.75/12.0
      DO 20 MUS=1,NMUS
      YMU=YMU+14.3/12.0
      IF((MUC.EQ.11).AND.((MUS.GT.11).AND.(MUS.LT.23))) GO TO 20


C     SUMMATION OVER VARIOUS DEGREES OF THE POLYNOMIAL
      DO 26 NP=1,NNP
      DO 25 NBP=1,NNBP
      NBP=NBP+(NP-1)*3


C     INFLUENCE COEFFICIENT
      ZINF(NP,NBP)=4./((XW-XMU)*(XW-XMU)+DELTA2)*(YW-YMU)*(YW-YMU))**1.5


      DO 60 K=1,NL
      WX(MUC,MUS,K)=WX(MUC,MUS,K)+ALPHA(NP,NBP,K)*ZINF(NP,NBP)
   60 CONTINUE

   25 CONTINUE
   26 CONTINUE
   20 CONTINUE
   21 CONTINUE
      IF(FLAGXX.EQ.0.0) GO TO 65
```

```
      DO 64 I=1,NMUC
      DO 64 J=1,NMUS
      DO 64 K=1,NL
      WX(I,J,K)=0.0
   64 CONTINUE
   65 CONTINUE
      CONTINUE
      CONTINUE
      WRITE(6,112)
      DO 10 I=1,NMUC
      DO 10 J=1,NMUS
      WRITE(6,111) I,J,(WX(I,J,K),K=1,NL)
   10 CONTINUE
      IF(FLAGWX.EQ.0.0) WRITE(7,200) (((WX(I,J,K),K=1,NL),J=1,NMUS),
     1I=1,NMUC)
  110 FORMAT(10X,*IMU*,2X,I3,5X,*JMU*,2X,I3)
  111 FORMAT(10X,I3,5X,I3,10X,5E10.2)
  112 FORMAT(1H1,10X,*MUC*,5X,*MUS*,25X,*WX(I),I=1,NL*//)
      FORMAT(5E14.8)
  200 FORMAT(10X,2H    )
      STOP
      END
        6400 END OF RECORD
```

CO TOT 0131

COMPUTER PROGRAM LISTING NO. 5

```
      DIMENSION BCX(78),BCY(78)
      COMMON/JHA/ W(78,35), BC(78)
      COMMON/BOUND/BCSIE(8),BCRAD(78),BCCHOD(2),AC(3),AF(3)
      COMMONXNVARS/NBC,NLT
      COMMON/SK/PIF,RAD,CHORD,NLS,NLC,RO,NL,INB
      COMMON/SK1/WX(16,33,5),WXA(20,20,5),WXT(2,2)
      COMMON/SK2/ZIBC,ZNB,ZL1,ZL2,FLAGA,CEXT, SEXT, DELTA
     1,U,ROT,C1,X1,BCX0(78),BCY0(78),BSIE(8)
     2,NLSIE,FACTOR(7)
     3,ISIE,DSIE,FLAGOG
      EXTERNAL WNEG


      CALCULATE WN OR/AND BC.


      ROTOR DATA
      PIF=ATAN(1.0)*4.0
      RADIAN=180.0/PIF
      FLAGBC=0.0
      FLAGBC=1.0
      FLAGW=0.0
      FLAGW=1.0
      RAD=73.5/12.0
      X1=18.0/12.0
      CHORD=14.0/12.0
      C1=CHORD/4.0
      VTIP=483.0
      VMU=0.29
      ROT=VTIP/(RAD+X1)
      RPM=ROT*60.0/2.0/PIF
      U=VTIP*VMU
      NBLADE=1
      NBLADE=2
      DSIE=2.0*PIF/FLOAT(NBLADE)
      RO=0.00238

      B.C. DATA
      NBCSIE=6
      NBCSIE=8
      NBCSIE=1
      NBCRAD=4
      NBCRAD=9
      NBCRAD=1
      NBCRAD=5
      NBCCHD=2
      NBCCHD=1
      NBC=NBCSIE*NBCRAD*NBCCHD
      THE POINTS IN THE ROTOR DISC WHERE BC ARE SATISFIED
```

```
DO 1 I=1,NBCSIE
READ(5,100) BCSIE(I)
BCSIE(I)=BCSIE(I)/RADIAN
CONTINUE
READ(5,102) (BCCHOD(I),I=1,NBCCHD)
BCCHOD(1)=BCCHOD(1)/12.0
READ(5,101) (BCRAD(I),I=1,NBCRAD)
DO 6 I=1,NBCRAD
BCRAD(I)=BCRAD(I)/12.0
CONTINUE

LOADING DATA
NMUC=16
NMUS=33
NLC=2
NLC=1
NLS=1
NLS=5
NLSIE=1
NLSIE=5
NLSIE=7
NL=NLC*NLS
NLT=NL*NLSIE
NNLT=NLT+2
KG=NLT*(NLT+7)/2
ARC1=-19.25/12.0
ARC2= 33.25/12.0
ARC3=-56.0/12.0
ARC4= 56.00/12.0

DO 4 I=1,NBC
DO 4 J=1,NLT
W(I,J)=0.0
CONTINUE


THE INITIAL POSITION OF EACH BC POIN IN ROTOR DISC AXIS
DO 2 ISIE=1,NBCSIE
DO 2 ICHOD=1,NBCCHD
DO 2 IRAD=1,NBCRAD
KBC=IRAD+(ICHOD-1)*NBCRAD+(ISIE-1)*(NBCRAD*NBCCHD)
BCX(KBC)=(X1+BCRAD(IRAD))*COS(BCSIE(ISIE))+(BCCHOD(ICHOD)-C1)*
1SIN(BCSIE(ISIE))
BCY(KBC)=-(X1+BCRAD(IRAD))*SIN(BCSIE(ISIE))+(BCCHOD(ICHOD)-C1)*
1COS(BCSIE(ISIE))
BCY(KBC)=-BCY(KBC)
BCX0(KBC)=BCX(KBC)
BCY0(KBC)=BCY(KBC)
CONTINUE
WRITE(6,111) (BCX(I),I=1,NBC)
WRITE(6,112) (BCY(I),I=1,NBC)
WRITE(6,999)
WRITE(6,999)
WRITE(6,999)
```

```
      IF(FLAGW.EQ.0.0) GO TO 472

      READ THE WX DATA
      DO 3 I=1,NMUC
      DO 3 J=1,NMUS
      READ(5,200) (WX(I,J,K),K=1,NL)
    3 CONTINUE
      DO 51 I=1,20
      DO 51 J=1,20
      READ(5,200) (WXA(I,J,K),K=1,NL)
   51 CONTINUE


      TAKE ONE BC POINT
      DO 20 IBC=1,NBC
      ZIBC=IBC
      SUMMATION OVER BLADES
      DO 15 NB=1,NBLADE
      ZNB=NB
      MUC1=16

      TIM1=0.0
      ISIE=1+(IBC-1)/(NBCRAD*NBCCHD)
      BSIE(NB)=BCSIE(ISIE)-(ZNB-1.0)*DSIE
      FLAGA=1.0
   15 CONTINUE
      DELTIM=2.5/RADIAN/ROT
      DELTIM=2.0/RADIAN/ROT
      DELTIM=5.0/RADIAN/ROT
      IF(FLAGA.EQ.0.0) DELTIM=15.0/RADIAN/ROT
      IF(FLAGA.EQ.0.0) DELTIM=25.0/RADIAN/ROT
      TIM2=TIM1+DELTIM
      TIMA=(TIM1+TIM2)/2.0
      BCX(IBC)=BCX0(IBC)-TIM2*U
      SIE=BSIE(NB)-TIM2*ROT
      SIEDEG=SIE*RADIAN

      THE LOAD ON THE BLADE
      FACTOR(1)=1.0
      FACTOR(2)=SIN(SIE)
      FACTOR(3)=COS(SIE)
      FACTOR(4)=SIN(2.0*SIE)
      FACTOR(5)=COS(2.0*SIE)
      FACTOR(6)=SIN(3.0*SIE)
      FACTOR(7)=COS(3.0*SIE)


      LOCATE THE BC POINT IN THE BLADE MASH
      BCXD=BCX(IBC)*COS(SIE)+BCY(IBC)*SIN(SIE)
      BCYD=-BCX(IBC)*SIN(SIE)+BCY(IBC)*COS(SIE)
```

```
      BCXB=-BCYD+C1
      BCYB=BCXD-RAD/2.0-X1
      FLAGA=1.0
      IF((BCXB.LT.ABC1).OR.(BCXB.GT.ABC2).OR.(BCYB.LT.ABC3).OR.
     1(BCYB.GT.ABC4))  FLAGA=0.0
      IF(FLAGA.EQ.0.0) GO TO 44
      DELTA=3.5/2.0/12.0
      CEXT=21.0/12.0
      SEXT=CEXT
      NMUC=16
      NMUS=32
      GO TO 45
   44 CONTINUE
      DELTA=7.0/12.0
      CEXT=140.0/12.0
      SEXT=CEXT
      NMUS=20
      NMUC=20
   45 CONTINUE
      MUC=1+(BCXB+CEXT-DELTA)/(2.0*DELTA)
      MUS=1+(BCYB+SEXT+RAD/2.0-DELTA)/(2.0*DELTA)
      ZMUC=MUC
      ZMUS=MUS
      WRITE(6,113) NB,SIEDEG,IBC,BCXB,BCYB,ZMUC,ZMUS
      IF((MUC.LT.1).OR.(MUC.GE.NMUC)) GO TO 19
      IF((MUS.LT.1).OR.(MUS.GE.NMUS)) GO TO 19
      FLAGOG=2.0
      IF((FLAGA.EQ.0.0).OR.(MUC.GE.12)) FLAGOG=0.0
      IF((MUC).GT.7).AND.(MUC.GE.7)) FLAGOG=1.0
      IF((MUC).LE.7).AND.(MUC.LT.7)) FLAGOG=2.0


      DO 26 L1=1,NL
      DO 25 L2=1,NLSIE
      ZL1=L1
      ZL2=L2
      KK=L2+(L1-1)*NLSIE
      IF(FLAGOG.NE.0.0) CALL OG10(TIM1,TIM2,WNEG,D)
      IF(FLAGOG.EQ.0.0)   D=DELTIM*WNEG(TIMA)
      W(IBC,KK)=W(IBC,KK)+D
   25 CONTINUE
   26 CONTINUE

      TIM1=TIM2
      MUC1=MUC
      GO TO 10
   19 CONTINUE
      WRITE(6,114)
   18 CONTINUE
      DO 60 JJ=1,NL
      IF(NB.EQ.NBLADE)
     1WRITE(7,200) (W(IBC,J),J=JJ,NLT,NLSIE)
      IF(NB.EQ.NBLADE)
     1WRITE(6,110) (W(IBC,J),J=JJ,NLT,NLSIE)
   60 CONTINUE
      WRITE(6,999)
      WRITE(6,999)
```

```
15    CONTINUE
20    CONTINUE


472 CONTINUE
    WRITE(6,998)
    DO 62 IBC=1,NBC
    DO 62 JJ=I,NL
    WRITE(6,110) (W(IBC,J),J=JJ,NLT,NLSIE)
62  CONTINUE
    WRITE(6,999)
    WRITE(6,999)
    WRITE(6,999)


    THE GIVEN BC
    IF(FLAGBC.EQ.0.0) GO TO 474
    CALL BCS(U,ROT,C1,X1,NBCSIE,NBCRAD,NBCCHD)
474 CONTINUE
    WRITE(6,998)
    WRITE(6,116) (BC(I),I=1,NBC)
    WRITE(6,998)



100 FORMAT(F10.4)
101 FORMAT(5F10.4)
102 FORMAT(2F10.4)
110 FORMAT(5X,1HW,4X,10(E9.5,2X))
111 FORMAT(10X,3HBCX,7X,10E8.3)
112 FORMAT(10X,3HBCY,7X,10E8.3)
113 FORMAT(5X,I1,5X,E8.2,5X,I3,5X,F6.2,5X,F6.2,5X,F6.3,5X,F6.3)
114 FORMAT(10X,22HTOO FAR FROM THE BLADE)
116 FORMAT(10X,4HBC,C,  5X,5E20.8)
500 FORMAT(5E14.8)
998 FORMAT(1H1)
999 FORMAT(10X,1H )
    END


    FUNCTION WNEG(TIM)
    DIMENSION XINT(10),YINT(10)
    COMMON/SK/PIE,RAD,CHORD,NLS,NLC,RO,NL,INB
    COMMON/SK1/WX(16,33,5),WXA(20,20,5),WXT(2,2)
    COMMON/SK2/ZIBC,ZNB,ZL1,ZL2,FLAGA,CEXT, SEXT, DELTA
   1,U,ROT,C1,X1,BCX0(78),BCY0(78),BSIE(8)
   2,NLSIE,FACTOR(7)
   3,ISIE,DSIE,FLAGOG


    IBC=ZIBC
    NB=ZNB
    L1=ZL1
    L2=ZL2
    K=L1
    LFACT=L2

    BCY=BCY0(IBC)
    BCX=BCX0(IBC)-TIM*U
```

```
      SIE=BSIF(NB)-ROT*TIM
      BCXB=C1+BCX*SIN(SIE)-BCY*COS(SIE)
      BCYB=BCX*COS(SIE)+BCY*SIN(SIE)-RAD/2.0-X1

      MUC=1+(BCXB+CEXT-DELTA)/(2.0*DELTA)
      MUS=1+(BCYB+SEXT+RAD/2.0-DELTA)/(2.0*DELTA)
      ZMUC=MUC
      ZMUS=MUS
      DELX=ABS(BCXB+CEXT-2.0*DELTA*(ZMUC-0.5))
      DELY=ABS(BCYB+SEXT+RAD/2.0-2.0*DELTA*(ZMUS-0.5))
      FACTX=DELX/(2.0*DELTA)
      FACTY=DELY/(2.0*DELTA)

      FIND THE CORRESSPONDING WX
      IF(FLAGOG.NE.0.0) GO TO 47
      DO 27 IMUC=1,2
      M1C=MUC+(IMUC-1)
      DO 28 IMUS=1,2
      M1S=MUS+(IMUS-1)
      IF(FLAGA.EQ.0.0) WXT(IMUC,IMUS)=WXA(M1C,M1S,K)*FACTOR(LFACT)
      IF(FLAGA.NE.0.0) WXT(IMUC,IMUS)= WX(M1C,M1S,K)*FACTOR(LFACT)
   28 CONTINUE
   27 CONTINUE

      INTERPOLATE
      KK=1
      WNEG      =WXT(1,1)*(1.0-FACTX-FACTY+FACTX*FACTY)+
     1+WXT(1,2)*(FACTY-FACTX*FACTY)+WXT(2,1)*(FACTX-FACTX*FACTY)
     2+WXT(2,2)*FACTX*FACTY
      RETURN



   47 CONTINUE
      MUS1=MUS+1
      IF(FLAGOG.NE.1.0) GO TO 1
      NCEXT=7
      DO 49 INT1=1,NCEXT
      INTP=6+INT1
      ZINTP=FLOAT(INTP)
      YINT(INT1)=WX(INTP,MUS,K)*FACTOR(LFACT)+FACTY*(WX(INTP,MUS1,K)
     1*FACTOR(LFACT)-WX(INTP,MUS,K)*FACTOR(LFACT))
      XINT(INT1)=(ZINTP-1.0)*2.0*DELTA
   49 CONTINUE
      XINTP=BCXB
      CALL AL1(XINTP,XINT,YINT,WNEG,NCEXT,0.1,IER)
      RETURN

      CONTINUE
      IF(FLAGOG.NE.2.0) GO TO 2
      NCEXT=4
      DO 50 INT2=1,NCEXT
      INTP=5+INT2
      ZINTP=FLOAT(INTP)
      YINT(INT2)=WX(INTP,MUS,K)*FACTOR(LFACT)+FACTY*(WX(INTP,MUS1,K)
     1*FACTOR(LFACT)-WX(INTP,MUS,K)*FACTOR(LFACT))
```

```
      XINT(INT2)=(ZINTP-1.0)*2.0*DELTA
50    CONTINUE
      XINTP=BCXB+DELTA
      CALL ALI(XINTP,XINT,YINT,WNEG,NCEXT,0.1,IER)
      RETURN

7     CONTINUE
      NCEXT=7
      DO 53 INT3=1,NCEXT
      INTP=INT3
      ZINTP=FLOAT(INTP)
      YINT(INT3)=WX(INTP,MUS,K)*FACTOR(LFACT)+FACTY*(WX(INTP,MUS1,K)
     1*FACTOR(LFACT)-WX(INTP,MUS,K)*FACTOR(LFACT))
      XINT(INT3)=(ZINTP-1.0)*2.0*DELTA
53    CONTINUE
      XINTP=BCXB+11.0*DELTA
      CALL ALI(XINTP,XINT,YINT,WNEG,NCEXT,0.1,IER)
      RETURN
      END
```

CD TOT 0135

COMPUTER PROGRAM LISTING NO. 6

```
      DIMENSION FACTOR(7),BCX(72),BCY(72),BSIE(8)
     1,BCRAD(13),BCCHOD(2)
     2,WP(72,7,5),WXTRC(35)
      COMMON U,ROT,DSIE,SIED,RAD,CHORD,X1,C1
     1,IBC,ZNB,ZINC,ZINS,ZL2,ZNBL,BCSIE(8),FLAGCO
     2,BCX0(72),BCY0(72)
      EXTERNAL WPOS

      TOTAL SINGULARITY CONTRIBUTION


      ROTOR DATA
      PIE=ATAN(1.0)*4.0
      RADIAN=180.0/PIE
      RAD=73.5/12.0
      X1=18.0/12.0
      CHORD=14.0/12.0
      C1=CHORD/4.0
      VTIP=0.0
      VTIP=483.0
      VMU=0.29
      U=150.0
      U=VTIP*VMU
      NBLADE=1
      NBLADE=2
      DSIE=2.0*PIE/FLOAT(NBLADE)
      ROT=VTIP/(RAD+X1)
      RPM=ROT*60.0/2.0/PIE
      RO=0.00238
      TOLL=1.0E-04
      TOLU=1.0E-8
      ITER=20

      B.C. DATA
      NBCSIE=8
      NBCSIE=2
      NBCSIE=1
      NBCRAD=1
      NBCRAD=9
      NBCCHD=2
      NBCCHD=1
      NBC1=NBCRAD*NBCCHD
      NBC=NBCSIE*NBCRAD*NBCCHD
      THE POINTS IN THE ROTOR DISC WHERE BC ARE SATISFIED
      DO 1 I=1,NBCSIE
      READ(5,100) BCSIE(I)
      BCSIE(I)=BCSIE(I)/RADIAN
    1 CONTINUE
```

```
      READ(5,102) (BCCHOD(I),I=1,NBCCHD)
      BCCHOD(-1)=BCCHOD(1)/12.0
      READ(5,101) (BCRAD(I),I=1,NBCRAD)
      DO 6 I=1,NBCRAD
      BCRAD(I)=BCRAD(I)/12.0
    6 CONTINUE

      LOADING DATA
      NLC=2
      NLC=1
      NLS=1
      NLS=5
      NLSIE=1
      NLSIE=7
      NL=NLC*NLS
      NLT=NL*NLSIE
      DELTA=3.5/2.0/12.0
      ZMACH=0.6
      BETA2=1.0-ZMACH*ZMACH
      ZINN1=0.0/BETA2/SQRT(1.0+BETA2)/(DELTA**3.0)
      ZINN1=ZINN1*BETA2

      DO 50 I=1,NBC
      DO 50 J=1,NLSIE
      DO 50 K=1,NL
   50 WB(I,J,K)=0.0



      THE INITIAL POSITION OF EACH BC POIN IN ROTOR DISC AXIS
      DO 2 ISIE=1,NBCSIE
      DO 2 ICHOD=1,NBCCHD
      DO 2 IRAD=1,NBCRAD
      KBC=IRAD+(ICHOD-1)*NBCRAD+(ISIE-1)*(NBCRAD*NBCCHD)
      BCX(KBC)=(X)+BCRAD(IRAD))*COS(BCSIE(ISIE))+(BCCHOD(ICHOD)-C1)*
     1SIN(BCSIE(ISIE))
      BCY(KBC)=-(X)+BCRAD(IRAD))*SIN(BCSIE(ISIE))+(BCCHOD(ICHOD)-C1)*
     1COS(BCSIE(ISIE))
      BCY(KBC)=-BCY(KBC)
      BCX0(KBC)=BCX(KBC)
      BCY0(KBC)=BCY(KBC)
    2 CONTINUE
      WRITE(6,111) (BCX(I),I=1,NBC)
      WRITE(6,112) (BCY(I),I=1,NBC)



      THE AZIMUTH POSITION
      DELTIM=0.75/U
      DELTIM=7.5/RADIAN/ROT
      DO 15 NB=1,NBCSIE
      ZNB=NB
      BCSIED=BCSIE(NB)*RADIAN
```

```
      LOCATE THE BC POINT IN THE BLADE MASH
      DO 20 IBC1=1,NBC1
      WRITE(6,998)
      IBC=IBC1+(NB-1)*NBC1
      ICC=1+(IBC1-1)/NBCRAD
      CHOOSE A BLADE
      DO 16 NBL=1,NBLADE
      IF(NBL.EQ.1) GO TO 16
      ZNBL=FLOAT(NBL)
      SIE=BCSIE(NB)-(ZNBL-1.0)*DSIE
      WRITE(6,114) NB,IBC1,NBL,BCSIED,BCX0(IBC),BCY0(IBC)
      TIM=0.0
      FLAG2=1.0
      IF(NBL.NE.1) GO TO 14
      TIM=BCCHOD(ICC)/(U*SIN(SIE)+ROT*(BCRAD(IBC1)+X1))

      FLAG2=0.0
      FLAGL=1.0
      FLAGU=0.0
      TIML=0.0
      ICOUNT=0
      WRITE(6,120)
11    CONTINUE
      ICOUNT=ICOUNT+1
      BCX(IBC)=BCX0(IBC)-U*TIM
      SIE=BCSIE(NB)-(ZNBL-1.0)*DSIE-ROT*TIM
      SIED=SIE*RADIAN
      BCXD=BCX(IBC)*COS(SIE)+BCY(IBC)*SIN(SIE)
      BCYD=-BCX(IBC)*SIN(SIE)+BCY(IBC)*COS(SIE)
      BCXB=-BCYD+C1
      BCYB=BCXD-RAD/2.0-X1
      WRITE(6,201) IBC,SIED,BCXB,BCYB,TIM

      IF(FLAG2.EQ.0.0) GO TO 27
      CHECK IF ON THE BLADE
      IF((BCXB.GT.0.0).AND.(BCXB.LE.CHORD).AND.(ABS(BCYB).LE.RAD/2.0))
     1GO TO 21

      GO TO 12
21    CONTINUE
      WRITE(6,116) NBL
      FLAG2=0.0
      FLAGL=0.0
27    CONTINUE
      LOWER LIMIT
      IF(FLAGL.NE.0.0) GO TO 23
      IF(ABS(BCXB-CHORD).LE.TOLL) GO TO 24
      IF(ICOUNT.GT.ITER) WRITE(6,202)
      IF(ICOUNT.GT.ITER) GO TO 20
      TIM=TIM-(CHORD-BCXB)/(U*SIN(SIE)+ROT*BCXD)
      GO TO 11
24    CONTINUE
      FLAGL=1.0
      FLAGU=0.0
      TIML=TIM
      ICOUNT=0
      WRITE(6,999)
```

```
 23  CONTINUE
     UPPER LIMIT
     IF(FLAGU.NE.0.0) GO TO 25
     IF(((BCXB.LT.TOLU).AND.(BCXB.GT.0.0)).OR.(ABS(BCYB).GE.RAD/2.0))
    1GO TO 26
     IF(ICOUNT.GT.ITER) WRITE(6,202)
     IF(ICOUNT.GE.ITER) GO TO 26
     TIM=TIM+BCXB/(U*SIN(SIE)+ROT*BCXD)
     GO TO 11
 26  CONTINUE
     FLAGU=1.0
     FLAG2=1.0
     TIMU=TIM
     ICOUNT=0
 25  CONTINUE


     DO 40 INC=1,NLC
     ZINC=INC
     DO 41 INS=1,NLS
     ZINS=INS
     DO 44 L2=1,NLSIF
     ZL2=L2
     L1=INS+(INC-1)*NLS


     DTIM=(TIMU-TIML)/300.0
     TIM1=TIML+DTIM*150.0
     TIM2=TIM1+DTIM*100.0
     TIM3=TIM2+DTIM*40.0
     TIM4=TIM3+DTIM*5.0
     TIM5=TIM4+DTIM*4.0
     TIM6=TIMU
     FLAGCO=1.0
     CALL GG6(TIML,TIM1,WPOS,WINT1)
     CALL GG6(TIM1,TIM2,WPOS,WINT2)
     CALL GG10(TIM2,TIM3,WPOS,WINT3)
     CALL GG10(TIM3,TIM4,WPOS,WINT4)
     CALL GG10(TIM4,TIM5,WPOS,WINT5)
     CALL GG10(TIM5,TIM6,WPOS,WINT6)
     IF(FLAGCO.EQ.0.0) WRITE(6,118)
     IF(FLAGCO.EQ.0.0) GO TO 20
     WP(IPC,L2,L1)=WP(IPC,L2,L1)+ZINC*(WINT1+WINT2+WINT3+WINT4
    1+WINT5+WINT6)

 44  CONTINUE
 41  CONTINUE
 40  CONTINUE
     WRITE(6,999)
     WRITE(6,117)  ((WP(IPC,I,J),J=1,NL),I=1,NLSIF)
     WRITE(6,999)


 12  CONTINUE
     IF(ABS(BCXB).GE.(RAD+X1+C1)) GO TO 13
```

```
      IF(ABS(BCXD).GE.(RAD+X1))  GO TO 13
   14 CONTINUE
      TIM=TIM+DELTIM
      ICOUNT=0
      GO TO 11
   13 CONTINUE
   14 CONTINUE

      WRITE(6,999)
      WRITE(6,110) ((WP(IRC,I,J),J=1,NL),I=1,NLSIF)
      WRITE(7,200) ((WP(IRC,I,J),J=1,NL),I=1,NLSIF)
   20 CONTINUE
   15 CONTINUE

  100 FORMAT(F10.4)
  101 FORMAT(5F10.4)
  102 FORMAT(5F10.4)
  110 FORMAT(10X,5(E15.5,5X)//)
  111 FORMAT(10X,3HBCX,7X,10E8.3)
  112 FORMAT(10X,3HBCY,7X,10E8.3)
  113 FORMAT(10X,F10.4)
  114 FORMAT(//10X,*NB=*,2X,I3,5X,*NRAD=*,2X,I3,5X,*NBLADE=*,2X,I3,
     15X,*SIF=*,2X,E6.1,5X,*BCXB=*,2X,E6.2,5X,*BCYB=*,2X,E6.2//)
  115 FORMAT(10X,*ACOS ARGUMENT GREATER THAN 1.0*)
  116 FORMAT(20X,*TRAJECTORY MEETS THE BLADE*,2X,I3//)
  117 FORMAT(10X,5(E15.2,5X))
  118 FORMAT(12X,*BC*,14X,*SIF*,14X,*BCXB*,15X,*BCYB*,15X,*TIME*)
  200 FORMAT(5E14.8)
  201 FORMAT(10X,I3,10X,E10.2,10X,E10.6,10X,E10.6,10X,E10.6)
  202 FORMAT(//15X,*DOES NOT CONVERGE IN*,2X,I4,2X,*ITERATIONS*)
  208 FORMAT(1H1)
  999 FORMAT(10X,1H )
      STOP
      END
      FUNCTION XPOS(DELTIM)
      DIMENSION FACTOR(10)
      COMMON  U,BOT,DSIF,SIFO,RAD,CHORD,X1,C1
     1,IRC,ZNB,ZINC,ZINS,ZL2,ZNBL,BCSIF(8),FLAGCO
     2,BCXO(72),BCYO(72)


      NB=ZNB
      NBL=IFIX(ZNBL)
      L2=ZL2
      PIF=4.0*ATAN(1.0)
      BCX=BCXO(IRC)-DELTIM*U
      SIF=BCSIF(NB)-(ZNBL-1.0)*DSIF-BOT*DELTIM
      THE LOAD ON THE BLADE
      FACTOR(1)=1.0
      FACTOR(2)=SIN(SIF)
      FACTOR(3)=COS(SIF)
      FACTOR(4)=SIN(2.0*SIF)
      FACTOR(5)=COS(2.0*SIF)
      FACTOR(6)=SIN(3.0*SIF)
      FACTOR(7)=COS(3.0*SIF)
      BCXB=C1-BCYO(IRC)*COS(SIF)+BCX*SIN(SIF)
      BCYB=BCX*COS(SIF)+BCYO(IRC)*SIN(SIF)-RAD/2.0-X1
```

```
      RCXB=ABS(RCXB)
      PHIR=1.0-RCXB*2.0/CHORD
      IF(ABS(PHIR).GE.1.0) FLAGCO=0.0
      IF(FLAGCO.EQ.0.0) RETURN
      PHI=ACOS(PHIR)
      THETA=PIE*(0.5+RCYB/RAD)
      IF(ZINC.EQ.1.0) WPOS=(COS(PHI/2.0)/SIN(PHI/2.0))*
     1SIN(ZINS*THETA)*FACTOR(L2)
      IF(ZINC.NE.1.0) WPOS=(-SIN((ZILC-1.0)*PHI))*
     1SIN(ZINS*THETA)*FACTOR(L2)
      RETURN
      END
      6400 END OF RECORD
```

CD TOT = 0293

COMPUTER PROGRAM LISTING NO. 7

```
      SUBROUTINE BCS(U,ROT,C1,X1,NBCSIE,NBCRAD,NBCCHD)
      COMMON/ROUND/BCSIE(1),BCRAD(20),BCCHOD(1),AC(3),AF(3)
      COMMON/JHA/W(13,5),BC(13)


      PIE=4.0*ATAN(1.0)
      RADIAN=180.0/PIE
      AC(1)=5.0/RADIAN
      AC(2)=0.0
      AC(3)=0.0
      AF(2)=0.0
      AF(3)=0.0


      DO 1 I=1,NBCSIE
      SIE=BCSIE(I)
      THETA=AC(1)+AC(2)*COS(SIE)+AC(3)*SIN(SIE)
      BETAD=-AF(2)*SIN(SIE)+AF(3)*COS(SIE)
      DO 2 J=1,NBCCHD
      CX=BCCHOD(J)-C1
      DO 3 K=1,NBCRAD
      NBC=K+(J-1)*NBCRAD+(I-1)*NBCRAD*NBCCHD
      R=X1+BCRAD(K)
      TAO=ATAN(CX/R)
      UC=ROT*R*COS(TAO)+U*SIN(SIE)
      US=ROT*R*SIN(TAO)+U*COS(SIE)
      V=SQRT(UC*UC+US*US)
      DEL=ATAN(US/UC)
      THETAR=THETA*COS(DEL)
      W=V*TAN(THETAR)
      BC(NBC)=W-BETAD
    3 CONTINUE
    2 CONTINUE
    1 CONTINUE

      WRITE(6,998)
      WRITE(6,10) BC
      NBC1=NBCSIE*NBCRAD*NBCCHD
      WRITE(7,200) (BC(I),I=1,NBC1)
  200 FORMAT(F14.8)
   10 FORMAT(10X,2HBC,5F15.4)
  998 FORMAT(1H1)
      RETURN
      END
```

CD TOT 0045

COMPUTER PROGRAM LISTING NO. 8

```
D
      DIMENSION  GH(30),GX(7),GXSTRT(7),GX1(7),GX2(7),GG(7),GG2(7)
     1,GALPHA(7),GP(7,7),GPY(7),GPE(7),GBIGV(7),GESP(5)
     2,GY(7),GDUM1(7),GDUM2(7)
     3,A(5),CL(15),CM(15),WP(100)
      COMMON/SK4/IPIVOT(90),NPIVOT
      COMMON/BOUND/BCSIE(10),BCRAD(9),BCCHOD(2),AC(3),AE(3)
      COMMON/JHA/ W(90,35),BC(90)
      COMMON/NVARS/NBC,NLT
      COMMON/SK/PIE,RAD,CHORD,NLS,NLC,NL,RO,INB
      COMMON/SK3/ FACTOR(7),NHAR(7),NLSIE
      EXTERNAL XLIFT

C
C     BLADE  LOADING IN FORWARD FLIGHT
C
C
C
C
C     ROTOR DATA
      PIE=ATAN(1.0)*4.0
      RADIAN=180.0/PIE
      FLAGBC=1.0
      FLAGBC=0.0
      FLAGWF=0.0
      FLAGWF=1.0
      ICHECK=0
      ICHECK=1
      RAD=73.5/12.0
      X1=18.0/12.0
      CHORD=14.0/12.0
      C1=CHORD/4.0
      DELTA=3.5/2.0/12.0
      VTIP=0.0
      VTIP=483.0
      VMU=0.29
      U=150.0
      U=VTIP*VMU
      ROT=VTIP/(RAD+X1)
      RPM=60.0*ROT/2.0/PIE
      NBLADE=2
      NBLADE=1
      DSIE=2.0*PIE/FLOAT(NBLADE)
      RO=0.00238

C     B.C. DATA
      NBCSIE=6
      NBCSIE=1
      NBCSIE=7
      NBCSIE=9
      NBCSIE=8
```

```
      NBCSIE=10
      NBCRAD=1
      NBCRAD=5
      NBCRAD=7
      NBCRAD=8
      NBCRAD=9
      NBCCHD=2
      NBCCHD=1
      NBC=NBCSIE*NBCRAD*NBCCHD
C     THE POINTS IN THE ROTOR DISC WHERE BC ARE SATISFIED
      DO 1 I=1,NBCSIE
      READ(5,100) BCSIE(I)
    1 CONTINUE
      READ(5,102) (BCCHOD(I),I=1,NBCCHD)
      READ(5,101) (BCRAD(I),I=1,NBCRAD)
C
C     WRITE THE INPUT DATA
      WRITE(6,130)
      WRITE(6,131) RPM,U,VMU
      WRITE(6,132)
      WRITE(6,134) (BCSIE(I),I=1,NBCSIE)
      WRITE(6,133) (BCCHOD(I),I=1,NBCCHD)
      WRITE(6,135) (BCRAD(I),I=1,NBCRAD)
      DO 30 I=1,NBCCHD
      BCCHOD(I)=BCCHOD(I)/12.0
   30 CONTINUE
      DO 31 I=1,NBCRAD
      BCRAD(I)=BCRAD(I)/12.0
   31 CONTINUE
      DO 32 I=1,NBCSIE
      BCSIE(I)=BCSIE(I)/RADIAN
   32 CONTINUE

      NPIVOT=48
      NPIVOT=45
      NPIVOT=59
      NPIVOT=54
      NPIVOT=61
      NPIVOT=49
      NPIVOT=63
      NPIVOT=40
      NPIVOT=55
      THE PIVOT POINTS ACTUALLY USED
      READ(5,136) (IPIVOT(I),I=1,NPIVOT)
      WRITE(6,140) (IPIVOT(I),I=1,NPIVOT)

C     LOADING DATA
      NLC=2
      NLC=1
      NLS=1
      NLS=5
      NLSIE=3
      NLSIE=1
      NLSIE=5
      NLSIE=7
      NL=NLC*NLS
      NLT=NL*NLSIE
```

```
C
C
C
C
      IF(FLAGBC.EQ.0.0) READ(5,202) (BC(I),I=1,NLT)
      IF(FLAGBC.EQ.0.0) GO TO 44
C
C
C     READ WN
      READ(5,200) ((W(I,J),J=1,NLT),I=1,NBC)
      WRITE(6,998)
      IF(FLAGWF.EQ.0.0) GO TO 50
      WRITE(6,136)
      WRITE(6,999)
      WRITE(6,999)
      WRITE(6,999)
C
C
C     READ THE POSITIVE CONTRIBUTION OF SINGULARITY
      WRITE(6,998)
      WRITE(6,137)
      DO 40 IBC=1,NBC
      READ(5,200) (WB(J),J=1,NLT)
      DO 41 I=1,NLT
      W(IBC,I)=-W(IBC,I)+WB(I)
   41 CONTINUE
   40 CONTINUE
   50 CONTINUE
      WRITE(6,998)
      WRITE(6,108)
      DO 51 IBC=1,NBC
   51 CONTINUE
C
C
C     THE GIVEN BC
      READ(5,201)  (BC(I),I=1,NBC)
      WRITE(6,998)
      WRITE(6,116) (BC(I),I=1,NBC)
      WRITE(6,998)
      DO 46 I=1,NBC
      BC(I)=BC(I)*4.0*PIE/(DELTA*DELTA)
   46 CONTINUE
C
      IF(ICHECK.EQ.0) CALL CHECK
      IF(ICHECK.EQ.0) STOP
C
C
      DO 61 I=1,NPIVOT
      IP=IPIVOT(I)
      BC(I)=BC(IP)
      DO 60 J=1,NLT
      W(I,J)=W(IP,J)
   60 CONTINUE
   61 CONTINUE
C
C
      NLT=5
```

```
      NLT=25
      NLT=15
      NLT=35
      KG=NLT*(NLT+7)/2
      NNLT=NLT+2
      NBC=NPIVOT
      DO 62 IBC=1,NBC
      WRITE(6,999)
      WRITE(6,110) (W(IBC,J),J=1,NLT)
   62 CONTINUE
C
C
      KRG=1
      CALL GRADMT(NLT,GX,GXSTRT,GX2,GX1,GG,GG2,GALPHA,GH,GR,GRY,GRS,
     1GRIGV,GESP,NNLT,GY,GDUM1,GDUM2,KRG)
      KRG=0
      WRITE(6,998)
      DO 43 I=1,NLT
      BC(I)=GX2(I)
      WRITE(6,138) GX(I), GX1(I), GX2(I)
   43 CONTINUE
      WRITE(7,202) (BC(I),I=1,NLT)
      WRITE(7,202) (GX2(I),I=1,NLT)
   44 CONTINUE
C
      GO TO 321
  321 CONTINUE
C
C
C
C     LOAD DISTRIBUTION ON THE BLADE
      DELX=0.5
      NSTAT=RAD/DELX
C
C     HARMONICS CONSIDERED
      NLSIE=5
      NLSIE=3
      NLSIE=7
      NLSIE=1
      NRCSIE=1
      NBCSIE=3
      NRCSIE=8
      NHAR(1)=5
      NHAR(1)=4
      NHAR(1)=2
      NHAR(1)=3
      NHAR(1)=1
      NHAR(2)=2
      NHAR(3)=3
      NHAR(4)=4
      NHAR(5)=5
      NHAR(6)=6
      NHAR(7)=7
      NUMHAR=5
      NUMHAR=1
      NUMHAR=7
      DO 39 JH=1,NUMHAR
```

```
      NHAR(1)=JH
C     VARIOUS POSITIONS OF THE ROTOR BLADES
      DO 37 ISIE=1,NBCSIE
      BCSIED=BCSIE(ISIE)*RADIAN
      WRITE(6,998)
      WRITE(6,119)
      WRITE(6,999)
      WRITE(6,999)
      WRITE(6,122) (NHAR(IH),IH=1,NLSIE)
      WRITE(6,121) BCSIED
      DO 33 NB=1,NBLADE
      INB=NB
      ZNB=NB
      SIE=BCSIE(ISIE)+(ZNB-1.0)*DSIE
      FACTOR(1)=1.0
      FACTOR(2)=SIN(SIE)
      FACTOR(3)=COS(SIE)
      FACTOR(4)=SIN(2.0*SIE)
      FACTOR(5)=COS(2.0*SIE)
      FACTOR(6)=SIN(3.0*SIE)
      FACTOR(7)=COS(3.0*SIE)
      X=0.0
      XL1=0.0
      THRUST=0.0
      DO 34 IX=1,NSTAT
      X=X+DELX
      XL2=X
      US=U+ROT*(X+X1)
      THETA=PIE*X/RAD

      A(1)=0.0
      A(2)=0.0
      DO 35 J=1,NLC
      DO 38 IH=1,NLSIE
      IS=NHAR(IH)
      DO 36 K=1,NLS
      ZK=K
      KK=K+(IS-1)*NLS+(J-1)*NLS*NLSIE
      A(J)=A(J)+SIN(ZK*THETA)*FACTOR(IS)*BC(KK)
   36 CONTINUE
   38 CONTINUE
   35 CONTINUE

      XLOAD=PIE*CHORD*0.5*A(1)*RC
      CM(IX)=-PIE*(-A(2))/16.0
      CL(IX)=XLOAD/(0.5*RC*US*US*CHORD)

      CALL SIM(XL1,XL2,XLIFT,XLL)
      THRUST=THRUST+XLL
      XL1=XL2
      WRITE(6,999)
      XINCH=X*12.0
      XND=(X+X1)/(RAD*X1)
      WRITE(6,119) XINCH,XND,XLOAD,CL(IX)
   34 CONTINUE
      WRITE(6,120) THRUST
   33 CONTINUE
```

```
 37   CONTINUE
 38   CONTINUE
C
 100  FORMAT(F10.4)
 101  FORMAT(5E10.4)
 102  FORMAT(2F10.4)
 108  FORMAT(///10X,*FINAL VALUE OF W*//)
 109  FORMAT(5X,3HNXT,5X,10(E8.2,2X))
 110  FORMAT(10X,5(E10.3,5X))
 113  FORMAT(5X,I1,5X,E8.2,5X,I3,5X,F6.2,5X,F6.2,5X,F6.3,5X,F6.3)
 114  FORMAT(10X,22HTOO FAR FROM THE BLADE)
 115  FORMAT(10X,3HVUC,5X,I3,5X,3HVUS,5X,I3)
 116  FORMAT(10X,4HP.C.,5X,9E10.2///)
 117  FORMAT(10X,14HLOADING COEFF.,2X,5E20.8)
 118  FORMAT(12X,*X-INCH*,10X,*X/R*,18X,*THRUST*,13X,*CL*//)
 119  FORMAT(10X,E10.2,5X,E10.2,10X,E10.2,10X,E10.4)
 120  FORMAT(//20X,*TOTAL THRUST*,5X,E10.2)
 121  FORMAT(15X,*AZIMUTH POSITION OF THE FIRST BLADE*,5X,E10.2///)
 122  FORMAT(15X,*HARMONICS CONSIDERED*,15X,5I10)
 130  FORMAT(1H1,20X,*HARMONICS CONSIDERED*,15X,5I10)
 131  FORMAT(20X,*RPM*,15X,E10.2/,20X,*FORWARD VELOCITY*,2X,E10.2/,
     120X,*ADVANCE RATIO*,5X,E10.2///)
 132  FORMAT(20X,*PIVOT POINTS*/)
 133  FORMAT(20X,*CHORDWISE LOC.*,3X,2E10.2)
 134  FORMAT(20X,*AZIMUTH LOC.*,4X,8E10.2)
 135  FORMAT(20X,*RADIAL LOC.*,4X,8E10.2)
 136  FORMAT(30X,*HW-MATRIX*///)
 137  FORMAT(30X,*HB-MATRIX*//)
 138  FORMAT(10X,*GX  *,E10.2,5X,*GX1  *,E10.2,5X,*GX2  *,E10.2)
 139  FORMAT(16I5)
 140  FORMAT(20X,*PIVOT POINTS USED*,20X,10I5)
 200  FORMAT(5E14.8)
 201  FORMAT(E14.8)
 202  FORMAT(5E16.8)
 998  FORMAT(1H1)
 999  FORMAT(10X,1H )
      STOP
      END


      SUBROUTINE FUNCT(N,X,F,G)
      DIMENSION X(1),G(1)
      CALL FUN(X,F)
      CALL GANALY(X,G)
      RETURN
      END


      SUBROUTINE SUPPLY(X,G)
      DIMENSION X(1),G(1)
      COMMON/NVARS/NBC,NLT
      CALL FUN(X,F)
      DO 10 I=1,NLT
      X(I)=X(I)+1.E-6
      CALL FUN(X,FNEW)
      X(I)=X(I)-1.E-6
```

```
      G(I)=(FNEW-F)/1.E-6
   10 CONTINUE
      RETURN
      END

      SUBROUTINE FUN(X,F)
      DIMENSION X(1)
      COMMON/NVARS/NBC,NLT
      COMMON/JHA/AA(90,35),BC(90)
      SUM2=0.0
      DO 2 J=1,NBC
      SUM1=0.0
      DO 1 I=1,NLT
    1 SUM1=SUM1+AA(J,I)*X(I)
      DIFSQ=(BC(J)-SUM1)**2
      SUM2=SUM2+DIFSQ
    2 CONTINUE
      F=SUM2
      RETURN
      END

      SUBROUTINE GANALY(X,G)
      DIMENSION X(1),G(1)
      COMMON/JHA/ A(90,35),BC(90)
      COMMON/NVARS/NBC,NLT

C
C
      DO 3 K=1,NLT
      G(K)=0.0
      DO 2 J=1,NBC
      SUM1=BC(J)
      DO 1 I=1,NLT
      SUM1=SUM1-A(J,I)*X(I)
    1 CONTINUE
      G(K)=G(K)-2.0*SUM1*A(J,K)
    2 CONTINUE
    3 CONTINUE
      RETURN
      END

      FUNCTION XLIFT(X)
      COMMON/JHA/ A(90,35),BC(90)
      COMMON/SK/PIE,RAD,CHORD,NLS,NLC,NL,RO,INR
      COMMON/SK2/ FACTOR(7),NHAR(7),NLSIF

C
C
      A=0.0
      NL=NLS*NLC
      THETA=PIE*X/RAD
      DO 38 IH=1,NLSIF
      ISIF=NHAR(IH)
      DO 36 K=1,NLS
      ZK=K
```

```
C
      KK=K+(ISIE-1)*NL
      A=A+SIN(ZK*THETA)*FACTOR(ISIE)*BC(KK)
   36 CONTINUE
   38 CONTINUE
      XLIFT=PIE*CHORD*0.5*A*RO
      RETURN
      END


      SUBROUTINE CHECK
      DIMENSION ANS(35)
      COMMON/JHA/W(90,85),BC(90)
      COMMON/NVARS/NBC,NLT
      COMMON/SK4/IPIVOT(90),NPIVOT
C
C
      NLT=25
      READ(5,202)(ANS(I),I=1,NLT)
C
      WRITE(6,30)
      DO 1 IBC=1,NBC
      NBC=0
      DO 3 IP=1,NPIVOT
      IF(IBC.EQ.IPIVOT(IP)) NBC=1
      RHS=0.0
      DO 2 J=1,NLT
      RHS=RHS+ANS(J)*W(IBC,J)
    2 CONTINUE
      ERROR=BC(IBC)-RHS
      ERROR=100.0*ERROR/BC(IBC)
      WRITE(6,31) IBC,NBC,RHS,BC(IBC),ERROR
    1 CONTINUE
   30 FORMAT(1H1,11X,*IBC*,7X,*NBC*,9X,*RHS*,8X,*LHS*,9X,*ERROR*///)
   31 FORMAT(10X,I5,5X,I5,10X,2(F10.2,5X),5X,F10.2)
  202 FORMAT(5E16.8)
      RETURN
      END
```

CD TOT 0063

COMPUTER PROGRAM LISTING NO. 9

```
      DIMENSION BLLOAD(5)
     1,PCSIE(8),XBC(15)
      COMMON  PIE,RADIAN,UU,UV,W,SIE,ROT,RAD,CHORD,X1,BETAD,AT(5),AE(5),
     1RO,BETA,CLD
      EXTERNAL XLIFT

C
C     COMPUTE THE LOAD DISTRIBUTION ON THE BLADES
C     USE THE MOMENTUM THEORY
C

      PIE=4.0*ATAN(1.0)
      RADIAN=180.0/PIE
      RAD=73.5/12.0
      X1=18.0/12.0
      CHORD=14.0/12.0
      C1=CHORD/4.0
      VTIP=483.0
      VMU=0.29
      U=VTIP*VMU
      ALPHA1=11.7/RADIAN
      U=U/COS(ALPHA1)
      ROT=VTIP/(RAD+X1)
      RPM=60.0*ROT/2.0/PIE
      ALPHA=11.7/RADIAN
      ALPHA=0.0
      UU=U*COS(ALPHA)
      UV=U*SIN(ALPHA)
      NBLADE=1
      NBLADE=2
      SIE0=90.0/RADIAN
      DSIE=2.0*PIE/NBLADE
      RO=0.00248
      RO=0.00238
      CLD=2.0*PIE
      CLD=0.1*RADIAN
      ASR=73.5/14.0
      CLD=CLD*ASR/(ASR+2.0)

C
      AT(1)=5.0/RADIAN
      AT(2)=0.0
      AT(3)=-11.7/RADIAN
      AT(3)=0.0
      AE(1)=0.0
      AE(2)=6.5/RADIAN
      AE(2)=0.0
      AE(3)=0.0

C
      NXBC=15
      DO 62 I=1,NXBC
      READ(5,35) XBC(I)
```

```
      XRC(I)=XRC(I)*(RAD+X1)-X1
   62 CONTINUE
      INTEG=6
      ZINTEG=INTEG
      DELXIN=RAD/ZINTEG
      TOL=10.0
      TOL=5.0
      ATD=AT(1)*RADIAN
      WRITE(6,30) RAD,RPM,VMU,NBLADE,U
      RAT1=AT(1)*RADIAN
      RAT2=AT(2)*RADIAN
      RAT3=AT(3)*RADIAN
      RAF1=AF(1)*RADIAN
      RAF2=AF(2)*RADIAN
      RAF3=AF(3)*RADIAN
      WRITE(6,36) RAT1,RAT2,RAT3
      WRITE(6,37) RAF1,RAF2,RAF3
      CLDD=CLD/RADIAN
      ALPHAD=ALPHA*RADIAN
      WRITE(6,38) CLDD,ALPHAD
C
C     THE LOADING AT DIFFERANT POSITIONS OF THE ROTOR BLADES
      NBCSIE=6
      NBCSIE=2
      NBCSIE=8
      NBCSIE=4
      DO 15 ISIE=1,NBCSIE
      READ(5,100) BCSIE(ISIE)
      BCSIE(ISIE)=BCSIE(ISIE)/RADIAN
   15 CONTINUE
C
C
C
      W=0.0
      TOLD=0.0
    2 CONTINUE
      WRITE(6,999)
      WRITE(6,40) W,TOLD
      THRUST=0.0
      DO 16 ISIE=1,NBCSIE
      SIE0=BCSIE(ISIE)
      BCSIED=BCSIE(ISIE)*RADIAN
      WRITE(6,34) BCSIED
      WRITE(6,31)
C     SELECT A BLADE
      DO 9 I=1,NBLADE
      BLLOAD(I)=0.0
    9   CONTINUE
      DO 11 NB=1,NBLADE
      IF(NB.GT.1) WRITE(6,999)
      ZNB=NB
      SIE=SIE0+(ZNB-1.0)*DSIE
      BETAD=-AF(2)*SIN(SIE)+AF(3)*COS(SIE)
      BETAD=BETAD*ROT
      BETA=AF(1)+AF(2)*COS(SIE)+AF(3)*SIN(SIE)
C
C
```

```
C     LOAD DISTRIBUTION ON THE BLADE
      DO 10 I=1,NXBC
      X=XBC(I)
      XINCH=X*12.0
      UT=UU*SIN(SIE)+(X+X1)*ROT
      UP=UV+W+BETAD*(X+X1)
      UP=UP+UU*COS(SIE)*SIN(BETA)
      V=SQRT(UT*UT+UP*UP)
      PHI=ATAN(UP/UT)
      ATTACK=AT(1)+AT(2)*COS(SIN)+AT(3)*SIN(SIE)-PHI
      CL=CLD*ATTACK
      XLOAD=0.5*RO*V*V*CL*CHORD
      WRITE(6,32) NB,XINCH,XLOAD,CL
   10 CONTINUE
C
C     TOTAL THRUST ON THE BLADE
      XL1=0.0
      DO 12 I=1,INTEG
      XL2=XL1+DELXIN
      IF(I.EQ.INTEG) XL2=XL2-0.03*(XL2+X1)
      CALL GG6(XL1,XL2,XLIFT,XL)
      BLLOAD(NB)=BLLOAD(NB)+XL
      XL1=XL2
   12 CONTINUE
      TOTAL THRUST
      THRUST=THRUST+BLLOAD(NB)
   11 CONTINUE
      WRITE(6,33)(BLLOAD(I),I=1,NBLADE)
   16 CONTINUE
      THRUST=THRUST/FLOAT(NBCSIE)
C
C
C     THE INDUCED VELOCITY
      W=THRUST/(2.0*RO*PIE*(X1+RAD)*(X1+RAD)*U)
      IF(ABS(TOLD-THRUST).LT.TOL) GO TO 1
      TOLD=THRUST
      GO TO 2
    1 CONTINUE
   30 FORMAT(40X,*FLIGHT CONDITIONS*,///10X,*RADIUS*,4X,F10.2/,4X,*
     1RPM*,7X,F10.2/,10X,*MU*,8X,F10.2,/10X,*BLADES*,4X,I10,/10X,*
     2*FOR VEL*, 3X,F10.2////)
   31 FORMAT(1H1,10X,*NB*,14X,*X*,17X,*THRUST*,14X,*CL*///)
   32 FORMAT(10X,I2,10X,F10.2,10X,F10.2,10X,F10.4)
   33 FORMAT(////10X,*LOAD ON THE BLADES*,5X,F10.2
     1,10X,F10.2)
   34 FORMAT(////5X,          *AZIMUTH POSITION OF THE FIRST BLADE*,4X
     1,F10.2)
   35 FORMAT(F10.2)
   36 FORMAT(10X,*CYCLIC COE.*, 5X,3F10.2///)
   37 FORMAT(10X,*FLAPP. COE.*, 5X,3F10.2///)
   38 FORMAT(10X,*LIFT SLOPE*,5X,F10.2,//10X,*ALPHA*,10X,F10.2)
   40 FORMAT(///10X,*INDUCED VELOCITY*,5X,F10.2,/10X,*TOTAL THRUST*,6X,
     1F10.2)
  100 FORMAT(F10.4)
  999 FORMAT(1H1)
  999 FORMAT(10X,*  *)
      STOP
```

```
      END
      FUNCTION XLIFT(X)
      COMMON  PIE,RADIAN,UU,UV,W,SIE,ROT,RAD,CHORD,X1,BETAD,AT(5),AE(5),
     1RO,BETA,CLD
C
C
      UT=UU*SIN(SIE)+(X+X1)*ROT
      UP=UV+W+BETAD*(X+X1)
      UP=UP+UU*COS(SIE)*SIN(BETA)
      V=SQRT(UT*UT+UP*UP)
      PHI=ATAN(UP/UT)
      ATTACK=AT(1)+AT(2)*COS(SIN)+AT(3)*SIN(SIE)-PHI
      CL=CLD*ATTACK
      XLOAD=0.5*RO*V*V*CL*CHORD
      XLIFT=XLOAD
      RETURN
      END
```

CD TOT 0187